Clinical pharmacometrics with diagnostic probes

Non-parametric techniques in pharmacokinetic studies

Markus Herberg Hovd

Supervisors:
Hege Christensen
Ida Robertsen
Anders Åsberg
Per Kristian Eide

Department of Pharmacy

Faculty of Mathematics and Natural Sciences

University of Oslo

Dissertation for the degree of Philosophiae Doctor (Ph.D)

Table of Contents

Table of Contents

What we have done for ourselves alone dies with us; what we have done for others and the world remains, and is immortal.
— Albert Pike

Table of Contents

iv

Acknowledgements

Oslo, February 2024

Markus Herberg Hovd

Acknowledgements

List of papers

Paper I   **Hovd M**, Robertsen I, Johnson LK, Krogstad V, Wegler C, Kvitne KE, Kringen MK, Skovlund E, Karlsson C, Andersson S, Artursson P, Sandbu R, Hjelmesæth J, Åsberg A, Jansson-Löfmark R, Christensen H.

Neither Gastric Bypass Surgery Nor Diet-Induced Weight-Loss Affect OATP1B1 Activity as Measured by Rosuvastatin Oral Clearance.

Paper II   **Hovd M**, Mariussen E, Uggerud H, Lashkarivand A, Christensen H, Ringstad G, Eide PK.

Population pharmacokinetic modeling of CSF to blood clearance: prospective tracer study of 161 patients under work-up for CSF disorders.

Paper III   **Hovd M**, Robertsen I, Woillard JB, Åsberg A.

A Method for Evaluating Robustness of Limited Sampling Strategies - Exemplified by Serum Iohexol Clearance for Determination of Measured Glomerular Filtration Rate.

List of papers

Abstract

The observed variability in drug response both between and within individuals remains a challenge in the clinical setting, leading to variable therapeutic outcomes of drug therapy, from lack of efficacy to adverse drug reactions. Probe drugs may be utilized in phenotyping studies to characterize specific pharmacokinetic processes, allowing for greater understanding of the underlying mechanisms behind pharmacokinetic variability. Pharmacometrics provides a tool to describe and predict drug disposition at the individual and population level. This thesis presents the results from three clinical trials employing diagnostic probes.

In the first study, rosuvastatin was used as a probe for OATP1B1 activity in patients with severe obesity scheduled for Roux-en-Y gastric bypass surgery (RYGB) or very-low energy diet for weight loss, as well as a non-obese control group. The overall aim was to disentangle the effect of obesity, RYGB, and weight loss on OATP1B1 activity. The study concluded that neither gastric bypass surgery nor diet-induced weight loss affects the activity of the hepatic uptake transporter OATP1B1 as measured by rosuvastatin oral clearance.

Secondly, the magnetic resonance imaging contrast agent gadobutrol was employed as a surrogate tracer to characterize human cerebrospinal fluid (CSF) clearance to blood in patients with various neurological disorders. A population pharmacokinetic model was developed, and revealed significant inter-individual variability in CSF to blood clearance, both within and between the various disorders. This work may contribute to the understanding of CSF dynamics and the diagnostics of CSF disorders.

Determination of iohexol serum clearance may be used to accurately determine the glomerular filtration rate (mGFR) for assessment of renal function. In the third study, a general method for evaluating the robustness of limited sampling strategies for clearance determination to deviations in sample time was developed. Additionally, the method allows for the estimation of empirical sample windows, providing a range of acceptable sampling times, for different degrees of renal function. This advancement allows for more efficient and accurate monitoring of kidney function in a clinical setting.

Collectively, these studies demonstrate the role of pharmacometrics and diagnostic probes in the clinic. The research contributes to the field by providing population pharmacokinetic models and strategies that aim to improve diagnostic capabilities and therapeutic interventions through personalized dosing.

Abstract

x

Sammendrag

En utfordring innen moderne legemiddelbehandling er den store variasjonen i legemiddelrespons både blant og mellom individer. Dette kan føre til ulike utfall av legemiddelbehandling, fra manglende effekt til bivirkninger. Probelegemidler kan benyttes til å fenotype pasienter for å karakterisere spesifikke farmakokinetiske prosesser, som kan bidra til økt forståelse av mekanismene for slik variasjon. Farmakometri er et klinisk nyttig verktøy som lar oss beskrive og forutsi omsetningen av legemidler i kroppen både for individer og populasjoner. Denne avhandling presenterer resultatene fra tre kliniske studier som benytter seg av probelegemidler.

I den første studien ble rosuvastatin benyttet som en probe for aktivitet i den hepatiske opptakstransportøren OATP1B1 i pasienter med sykelig overvekt med planlagt Roux-en-Y gastrisk bypass (RYGB) eller veldig lav-energi diett for vektnedgang. Pasienter med normal- til overvektig kroppsvekt ble inkludert som en kontrollgruppe. Studien konkluderte med at verken gastrisk bypass eller diett påvirker aktiviteten i OATP1B1, ved å undersøke oral clearance av rosuvastatin.

Den andre studien benyttet seg av gadobutrol, et kontrastmiddel for magnetisk resonans bildetaking, som en surrogat for å karakterisere utskillelsen av cerebrospinalvæske til blod i pasienter med ulike nevrologiske tilstander. En populasjonsfarmakokinetisk modell ble utviklet, og avdekket en betydelig mengde variasjon i evnen til utskillelse av cerebrospinalvæske til blod, både innad og mellom ulike diagnosegrupper.

Ved å måle deplesjon i plasma av røntgenkontrastmiddelet iohexol kan man nøyaktig bestemme nyrefuksjon i pasienter. I den tredje studien ble det utviklet en generell metode for å vurdere robustheten til feil i prøvetidspunkt for begrensede prøvetakingsstrategier for dette formålet. Denne metoden muliggjør å definere utvidede vinduer for prøvetaking, slik at bestemmelsen av nyerefunksjon kan bli mer fleksibel, og kan derfor enklere gjennomføres i en klinisk hverdag.

Samlet demonstrerer disse tre studiene rollen til probelegemidler innen klinisk farmakometri. Denne avhandlingen og tilhørende verk bidrar til et stadig mer relevant felt gjennom bruk populasjonsfarmakokinetiske modeller, og strategier som kan bedre den diagnostiske nytteverdien av prober. Disse resultatene kan således bidra til mer nøyaktig persontilpasning av legemidler, og bedre legemiddelbehandling.

Sammendrag

Glossary

CL Clearance

CL/F Oral clearance

C_0 Pre-dose concentration, or trough

C_{max} Maximum concentration

F Bioavailability

K_a Absorption rate constant

K_e Elimination rate constant

$K_{i,j}$ Transfer rate coefficient from compartment i to j

Q Intercompartmental bloodflow

T_{lag} Lag time (of absorption)

T_{max} Time to maximum concentration

ABCG ATP-binding cassette super-family G

AC Arachnoid cyst

ADME Absorption, Distribution, Metabolism and Elimination

ATP Adenosine triphosphate

AUC Area under the concentration-time curve

BBB Blood-brain barrier

BCRP Breast-cancer resistance protein

BMI Body mass index

CKD Chronic kidney disease

CNS Central nervous system

CSF Cerebrospinal fluid

CYP Cytochrome P450, a superfamily of drug metabolizing enzymes

EDTA Ethylenediamine tetraacetic acid

eGFR Estimated GFR

GCP Good clinical practice

GFR Glomerular filtration rate

HC Hydrocephalus

IIH Idiopathic intracranial hypertension

iNPH Idiophathic normal pressure hydrocephalus

LED Low energy diet

LSS Limited sampling strategy

mGFR Measured GFR

MLR Multiple linear regression

MRI Magnetic resonance imaging

MRP Multidrug resistance protein

MS Mass spectrometry

NADPH Nicotinamide adenine dinucleotide phosphate

NAFLD Non-alcoholic fatty liver disease

NASH Non-alcoholic steatohepatitis

NKCC Sodium-potassium-chloride co-transporter

NLME Non-linear mixed effects

NPAG Non parametric adaptive grid

NRIS Norwegian research infrastructure services

NTCP Sodium taurocholate co-transporter

OATP Organic anion-transporting polypeptide

ODE Ordinary differential equation

P-gp Permeability glycoprotein

PC Pineal cyst

popPK Population pharmacokinetics

RYGB Roux-en-Y gastric bypass

SIH Spontaneous intracranial hypotension

TDM Therapeutic drug monitoring

VLED Very low energy diet

Introduction

Among the main challenges in modern drug therapy is the observed variability in drug response. Following administration of a drug, a given response may vary both between and within individuals, referred to as inter- and intra-individual variability, respectively. Variability in drug response may be attributed to both pharmacodynamic and pharmacokinetic processes. Pharmacodynamics is the study of a drugs interaction with an organism, where the resulting effect is a function of the drug exposure at the site of action, the affinity of the drug to the target, and the properties of the target in question. Conversely, pharmacokinetics is the study of an organism's interaction with the drug, and the disposition of said drug in the organism. In order to understand the underlying mechanisms of pharmacokinetic variability, one must first understand the physiological processes governing drug disposition. These processes may be abstracted to the mass transfer of drug, for which pharmacometrics provides one of many tools for describing and predicting such processes.

1.1   Pharmacokinetic variability

As stated, pharmacokinetic variability is recognized as one of the main challenges in modern drug therapy. Following administration, the disposition of drugs is determined by the interplay of pharmacokinetic processes. These processes may be categorized into four distinct, but highly interconnected phases: absorption, distribution, metabolism, and excretion, the four of which are referred to by their abbreviation, ADME. A simple visualization is provided in Figure 1.1 below.
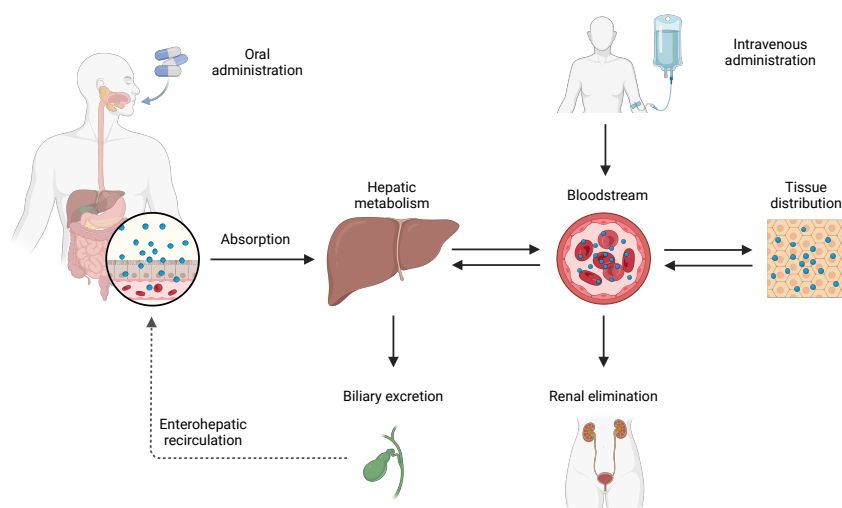
Figure 1.1: A simple visualization of pharmacokinetic processes following oral or intravenous administration of a drug. Following oral administration, and possibly dissolution, the drug is absorbed in the gastrointestinal tractus. Then, hepatic metabolism may occur before the drug is distributed to and from the bloodstream, from which it may further be subject to renal or hepatic elimination. Created with BioRender.com

Absorption

When a drug is not injected intravenously, it must first be absorbed from the site of administration. Following oral administration, drugs must pass multiple barriers, both physical and chemical, in order to reach the systemic circulation from which it can distribute to its pharmacodynamic target. The acidity of the gastric juices poses a chemical barrier, and is known to affect the chemical stability of drugs and bioavailability of drugs.[1] Only few drugs are absorbed through the epithelial lining of the stomach. Rather, the majority requires gastric emptying to relay the contents to the small intestine, which boasts a greater surface area and perfusion to facilitate uptake of drugs and nutrients alike. Gastric emptying has been found to vary even in healthy individuals, and is thought to be affected by factors such as age, sex, and obesity.[2] Throughout absorption, various fractions of the drug may be lost, and the fraction reaching systemic circulation is termed bioavailability. This fraction, symbolically represented as F, is considered the product of the fraction of drug absorbed in the lumen (F_A), the fraction escaping metabolism by the gut-wall (F_G) and liver (F_H), respectively. As drug exposure is limited by bioavailability, interindividual differences in gastrointestinal physiology is a significant contributor to overall pharmacokinetic variability.[3]

Distribution

Immediately after administration, drugs distribute from the site of administration. While there is no clear distinction between absorption and distribution, the latter usually refers to distribution of drugs to and from systemic circulation, while the former relates to distribution from the site of administration. Overall distribution

is considered the sum of passive diffusion and active transportation. The degree of passive diffusion across tissue barriers such as the intestinal wall is governed by the physiochemical properties of the drug, the permeability of the membrane, and tissue surface area. Active transportation, whether influx or efflux, requires energy, either from energy sources such as adenosine triphosphate (ATP) or nicotinamide adenine dinucleotide phosphate (NADPH), or from concentration gradients of e.g. hydrogen ions.[4] While influx transporters facilitate uptake of drugs and nutrients, efflux transporters provide protection against xenobiotics, reducing exposure. The intestine is rich in such transporters, such as permeability glycoprotein (P-gp), multidrug resistance-associated proteins (MRPs), and more.[5, 6] However, such efflux transporters are also abundant in the liver, kidney, and the blood-brain barrier.[7, 8] Additionally, most drugs exhibit some affinity for plasma and interstitial proteins, such as albumin or α-1 acid glycoprotein, forming a (usually) reversible protein-drug complex. Such binding can greatly alter the disposition drugs, as the complex constitutes a reservoir of drug, increasing the apparent volume of distribution, and prolonging the biological half-life. Only the free fraction of the drug, that which is unbound, is able to distribute freely. With some exceptions, bound drug is sterically hindered from interaction with most targets. As such, as a rule of thumb, only unbound drug may exert a pharmacologic effect.

Metabolism

In the context of pharmacokinetics, metabolism refers to the biotransformation of drugs, and may be categorized into two distinct phases[I], I and II. During phase I metabolism, drugs are subject to oxidation, reduction, or hydrolysis. In contrast, phase II metabolism refers to processes where a hydrophilic group is added to, or conjugated with, the drug, such as methylation, glucuronidation, acetylation, sulfation, or conjugation.[9] In both cases, drugs are made more hydrophilic, reinforcing renal elimination. Of great interest is the cytochrome P450 (CYP) superfamily of enzymes, which is known to metabolize approximately 75% of clinically used drugs.[10] Due to the high abundance in human liver, but also the small intestine, they limit drug bioavailability through first-pass metabolism. However, inter-individual variability in both expression and function of CYP enzymes, due to intrinsic and acquired factors, contribute to high variability in drug bioavailability and clearance, and as such drug exposure.[11] Age, disease, foodstuffs and drug-drug interactions are well known modulators of CYP expression and activity. Furthermore, several microorganisms are capable of similar drug biotransformation, and drug-microbiota interactions are considered a potential source of interindividual variability.[12] This is especially true in the case of mycophenolic acid, an immunosuppressant commonly used in solid organ transplantation, where the microbiome cleaves the biliary excreted glucuronide metabolite, facilitating enterohepatic recirculation of the parent drug, accounting for approximately 40% of total systemic exposure.[13, 14, 15] In some cases, drugs are administered in their less active or inactive form, and are activated by

---

[I]This term is one of many misnomers in pharmacology as both phases may occur simultaneously, or sequentially in any order. A more fitting description would be "category".

biotransformation, so-called prodrugs. As such, metabolism is not synonymous with inactivation.

Excretion

Several processes facilitate the removal of drug from the body, preventing buildup of possibly toxic substances. Among the main organs responsible for excretion are the kidney, liver, and lungs. The kidneys are essential for elimination of both endogenous and exogenous substances, and many drugs and/or their metabolites exhibits at least some renal elimination, especially following biotransformation. The process of renal elimination is considered the sum of glomerular filtration, tubular secretion, and reabsorption. The former is the result of filtration through a capillary network in the glomerulus, where unbound small-molecular substances such as water, salts, sugars, and creatinine diffuse to the lumen of the proximal tubule. Tubular secretion and reabsorption are mostly active processes, mediated by the many transporters found in the kidney.[8] The resulting urine, and the solutes not reabsorbed, are eliminated following their passage down the ureter to the bladder, from which it is expelled. Renal elimination can vary greatly between individuals, and is known to decrease with age. In contrast, hepatic elimination is mediated by the hepatobiliary system. Following hepatic uptake of drugs, by passive diffusion or hepatic uptake transporters such as the organic anion transporting polypeptide 1B1 (OATP1B1) and more, drug may transfer to the bile canaliculus.[16] This transfer is mediated by several drug transporters, including multidrug resistance-associated protein 2 (MRP2), breast-cancer resistance protein (BCRP), and more.[17] Bile is collected in the gallbladder, with a capacity of approximately 40-70 mL, and emptied in the intestinal lumen.[18] The concentration of drug in bile may be much greater than that in plasma, as a result of selective transport and subsequent enrichment.[19] Drug in bile may further be repeat absorbed in a process referred to as enterohepatic recirculation.[18] On the other hand, pulmonary excretion is primarily observed for volatile, small-molecular substances, such as anesthetics. While such substances are able to diffuse across lung epithelial cells, the lungs are also rich in efflux transporters such as P-gp, BCRP, and MRPs.[20, 21] Following entry into the alveolar space, they may be exhaled and as such eliminated from the body. Reduced excretion of any kind may lead to potentially toxic buildups of both endo- and exogenous substances, and constitutes as such an important aspect of pharmacokinetics.

1.2 Pharmacokinetic challenges in select patient populations

The aforementioned pharmacokinetic processes facilitate mass transfer, biotransformation, or excretion of drugs. Several diseases and conditions are known to affect such processes, and a select panel of such patient populations are introduced below.

1.2.1 Patients with severe obesity

The prevalence of obesity is of epidemic proportion — across more than 70 countries, the prevalence has more than doubled from 1980 to 2015.[22] In Norway, the prevalence of adult obesity is estimated to 25%.[23, 24] Characterized by an excessive accumulation of adipose tissue, it is most commonly categorized using the body mass index (BMI), relating total body weight to height (Table 1.1). However, BMI alone has been scrutinized as an imperfect classification aid, as it does not assess body fat, among other reasons[25, 26]. This is substantiated by the fact that all-cause mortality was found to be similar across a wide range of BMI categories, but still greatly increased for BMI $\geq$ 30 kg m^{-2}.[27]

Table 1.1: Classification of body mass index (BMI).

Classification	BMI (kg m^{-2})
Underweight	< 18.5
Normal weight	18.5-24.9
Overweight	≥ 25
Obesity	≥ 30
Severe obesity	$\geq 40^{\dagger}$

†Or BMI $\geq$ 35 kg m^{-2} with obesity-related complications.

Still, obesity has been identified as a risk factor for several detrimental comorbidities, such as diabetes mellitus type II, cardiovascular disease, cancer, and chronic kidney disease.[22] Additionally, obesity is associated with increased prevalence of non-alcoholic fatty liver disease (NAFLD) and non-alcoholic steatohepatitis (NASH).[28, 29] Such disease of the liver is known to affect the expression and activity of several drug metabolizing enzymes, further contributing to inter-individual variability.[30] Similar alteration has been shown for drug transporters in both rodent models and humans.[31] As such, physiological changes associated with obesity are a source of pharmacokinetic variability. Compared to a normal weight population, several aspects of drug disposition have been shown to be altered in patients with obesity, and predicting these effects has proven a difficult task.[32] The volume of distribution, especially for lipophilic drugs, is expected to increase proportionally with increased fatty mass. However, the direction of change in volume of distribution, when adjusted for body weight, is bidirectional.[33] Additionally, activity in drug-metabolizing enzymes for a range of substrates have been found to significantly vary between individuals with and without obesity.[34] Allometric scaling has been suggested as a method to predict changes in drug disposition, where e.g. clearance is scaled with total body weight (TBW), such as in Equation 1.1 below, demonstrated in Figure 1.2.[35]

$$CL_{\text{obese}} = CL_{\text{reference}} \cdot \left(\frac{\text{TBW}}{70} \right)^{0.75} \tag{1.1}$$

An example of the effect of allometric scaling is shown in Figure 1.2 below.
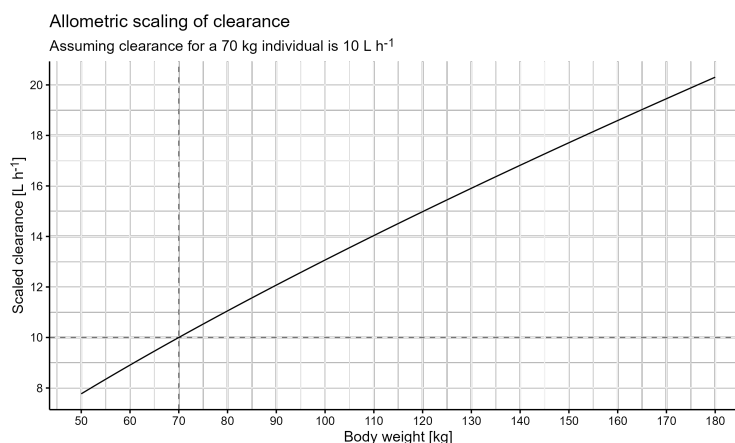
Figure 1.2: An example of allometric scaling of clearance, where the reference value is 10 L h^{-1} for a 70 kg individual.

A typical value of P varies between 0.75 to 1, so-called fixed exponent scaling. The value of P may also be fitted, e.g. using ordinary least-squares regression. For a range of drugs with varying lipophilicity, fixed-exponent allometric scaling was shown to be inferior for predicting clearance, but not volume of distribution, when compared with a fitted exponent.[35] Furthermore, body weight is often normalized to 70 kg, or a "standard man", the existence of which has been called into question.[36] Alternatively, the mean or median of the reference population may be used.

The main treatment for obesity is weight loss, effectuated by a reduced caloric intake, increased physical activity, pharmacological therapy, or bariatric surgery. Of these, bariatric surgeries, such as the Roux-en-Y gastric bypass (RYGB) procedure has shown superior long-term effects both in terms of sustained weight loss and remission of type 2 diabetes.[37, 38] During the procedure, the proximal stomach is reduced to a small, gastric pouch of approximately 35-50 mL, directly anastomosed to the distal jejunum, thus bypassing approximately one meter of the distal small intestine, as shown in Figure 1.3.[37, 39] This gastrointestinal rearrangement leads to malabsorption and subsequent weight loss. However, the extent to which RYGB and/or weight loss affect the disposition of drugs remains to be fully characterized and is vital for safe and precise dosing of drugs following RYGB and/or weight loss. While the impact of such intervention has been somewhat studied for drug metabolizing enzymes, drug transporters has received less focus.[40] A transporter of interest is the hepatic uptake transporter organic anion transporting polypeptide (OATP) 1B1, or OATP1B1 for short.[41] The transporter is exclusively expressed in hepatocytes, and mediates uptake of both exogenous and endogenous compounds from blood, such as bile acids, statins, antibiotics, immunosuppressants, anti-cancer drugs and more.[42, 41, 43] Several sequence variants have been identified in SLCO1B1, the gene coding for OATP1B1, with clinical implications. One of the most prevalent and studied is the c.521T>C (rs4149056) reduced function variant, which is associated with increased risk of adverse drug reactions in patients treated with simvastatin and

rosuvastatin.[44]
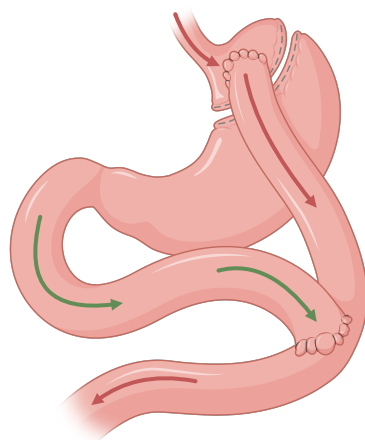
Figure 1.3: A simplified, anatomical overview of the gastrointestinal tractus following Roux-en-Y gastric bypass surgery. Red arrow signifies flow of foodstuffs, while the green arrow signifies flow of gastric juices. Created with BioRender.com

Rosuvastatin is an established and preferred probe for assessing OATP1B1 activity, owing to its sparse metabolism and low degree of diffusion into tissue.[45] In fact, OATP1B1 contributes to 49-86% of rosuvastatin hepatic uptake, with some contribution from sodium taurocholate co-transporting polypeptide (NTCP).[46, 47, 45, 48] Approximately 70% of rosuvastatin total clearance is hepatic, and predominantly through biliary excretion mediated by canalicular transporters such as breast cancer resistance protein (BCRP) and permeability-glycoprotein (P-gp).[49, 50] The excreted drug may in turn be reabsorbed in a process referred to as enterohepatic recirculation, which has been readily described in the case of rosuvastatin.[19, 50]

1.2.2 Patients with cerebrospinal fluid disorders

The brain is the central organ of the nervous system (CNS), and is enveloped in cerebrospinal fluid (CSF), providing necessary buoyancy and fluid homeostasis. CSF is produced at the choroid plexuses, a vascularized structure which protrudes into the four ventricles of the brain.[51] For completeness, the general anatomy of the brain is depicted in Figure 1.4. While previously thought to be an ultrafiltrate of plasma, it is now known that CSF production is the result of active fluid secretion, mediated by Na^+/K^+-ATP-ase, sodium-potassium-chloride co-transporter-1 (NKCC1) and HCO_3-transporters.[52] However, despite its importance in brain homeostasis and role in neurological disease, there is still much dispute regarding both CSF production and turnover.[53, 54]

Drug access to the CNS and CSF is limited, due to the protective capabilities of the blood-brain barrier (BBB). The BBB is not a physical barrier, but the result of endothelial cells with tight junctions lining the cerebral capillaries and spinal cord, limiting passive diffusion.[55, 56] For drugs to passively cross the (healthy and
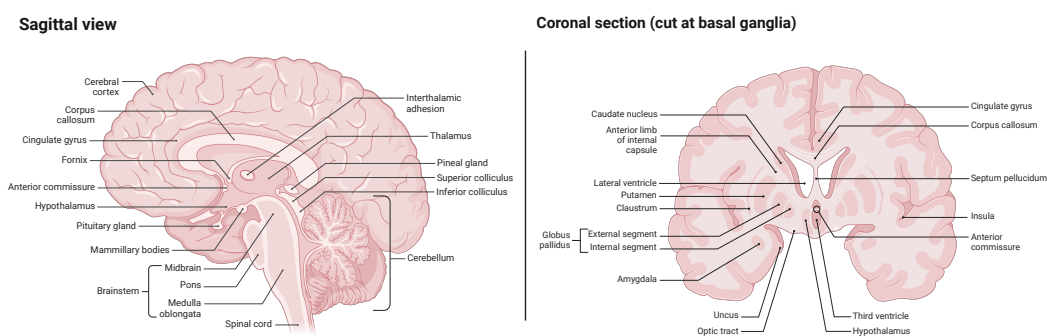
Figure 1.4: An anatomical overview of the brain from the saggital (left) and coronal (right) plane. The coronal plane is cut at the basal ganglia. Created with BioRender.com

intact) BBB, an upper limit in molecular mass of approximately 400-600 Daltons has been suggested, in combination with a high degree of lipophilicity (log P < 5).[57, 58] Additionally, the BBB is rich in efflux transporters such as P-gp, BCRP, and other multidrug resistance-associated proteins (MRPs), further limiting the CNS availability of orally and intravenously administered drugs.[59, 60] When direct access to the CNS is required, alternative strategies for administration must be considered. Intrathecal injection provides direct access to CSF in the subarachnoid space, which communicates with the CNS. While several drugs are administered intrathecally, for example for treatment of chronic pain, there is limited knowledge on CNS drug disposition, especially clearance, following such administration in humans.[61]

Recent research provides evidence of a glia-lymphatic (glymphatic) system for CSF egress, which was first considered in 2012, using a two-photon imaging approach to investigate CSF flow in rodent brain.[62] It is believed that impaired glymphatic function plays an important role in the pathogenesis of neurological disorders such as Alzheimer's and Parkinson's disease.[63] Through increased formation or reduced elimination, an abundance of CSF may increase the intracranial pressure, leading to hydrocephalus, characterized by active distension of brain ventricles.[64] Reduced elimination may also lead to a build-up of possibly neurodegenerative metabolites and byproducts. Thus, individual measurements of CSF clearance may provide additional insight into the etiology and diagnostics of CSF disturbances.

A gold standard for the measurement of glymphatic clearance has not been established. However, off-label intrathecal injection of the magnetic resonance imaging (MRI) contrast agent gadobutrol has shown promise.[65] Gadobutrol is a macrocyclic, gadolinium-based contrast agent, and is considered a second-generation tracer. The pharmacokinetics of intravenously administered gadobutrol has been well researched — it exhibits no metabolism, but is excreted unchanged in the kidneys, with no relevant extrarenal elimination.[66] Deposition and retention of gadolinium in the brain has been a concern. However, following intrathecal administration of 0.5 mmol of gadobutrol, no retention was found in the brain stem or cerebellum.[67] As such, intrathecal injection of up to 0.5 mmol is considered

safe.[68] In contrast, when administered intravenously, a dose of 0.1 mmol kg^{-1} is recommended. In a large single-center study, the rate of adverse events in patients receiving gadobutrol was relatively low, approximately 20 per 10 000 injections, or 0.2%.[69]

In a pilot study evaluating the clinical applicability of intrathecally administered gadobutrol, a preliminary population pharmacokinetic model was developed.[65] In brief, the predicted whole blood pharmacokinetic profiles of gadobutrol varied significantly between disease groups, possibly providing additional insight into the pathophysiology of CSF disorders. As such, additional research into the variability and mechanisms of glymphatic clearance is warranted.

1.2.3 Patients with impaired renal function

Through injury, disease, or age-related decline, the kidneys' ability to filter may be compromised, either acutely or chronically.[70] The kidneys are imperative for the excretion of both endogenous and exogenous substances, including drugs. Directly, renal impairment may lead to accumulation and potential toxicity of drugs as a result of reduced elimination. This is especially challenging for drugs exhibiting mostly renal elimination, and are associated with nephrotoxic effects, such as the antibiotic vancomycin.[71] Additionally, the accompanying buildup of uremic toxins is known to indirectly affect several aspects of drug disposition, including absorption, distribution, and metabolism.[72, 73] The most common index of kidney function is the glomerular filtration rate (GFR), which is used both for dose adjustment of drugs and diagnostics alike. Based on the GFR, patients may be categorized into various stages of chronic kidney disease (CKD). CKD is mainly defined by a sustained (> 3 months) reduced filtration capacity of the kidneys, or presence of kidney damage markers (Table 1.2).[74] A global meta-analysis from 2016 estimated that the prevalence of CKD stage 1-5 was 13.4%, and 10.6% for stages 3-5, and is expected to increase along an aging population.[75]

Table 1.2: Classification of chronic kidney disease (CKD) according to the 2012 KDIGO guidelines.[76]

Stage	Description	GFR (mL min^{-1} 1.73 m^{-2})
1	Normal or high	$\geq 90^{\dagger}$
2	Mildly decreased	$60\text{-}89^{\dagger}$
3a	Mildly to moderately decreased	45-59
3b	Moderately to severely decreased	30-44
4	Severely decreased	15-29
5	Kidney failure	< 15

†Only in the presence of kidney damage markers.

Several methods have been suggested to determine either an estimated (eGFR) or measured (mGFR) GFR. Methods for eGFR rely on multiple linear regression (MLR) involving an endogenous biomarker, such as serum creatinine (S_{CR}), and demographic variables such as age, sex, body weight, and more. Examples of

equations for eGFR using Cockroft & Gault (Equation 1.2) and the 2021 version of CKD-EPI (Equation 1.3) is provided below, where age is in years, weight in kilograms, and serum creatinine (S_{CR}) is in mg dL^{-1}.[77, 78]

$$
\begin{aligned}
\text{eGFR} &= \frac{(140 - \text{Age}) \cdot \text{Weight}}{72 \cdot \text{S}_{\text{CR}}} \cdot \beta_{\text{sex}} \\
\beta_{\text{sex}} &= \begin{cases} 0.85 & \text{if Female} \\ 1 & \text{if Male} \end{cases}
\end{aligned}
\tag{1.2}
$$

$$
\begin{aligned}
\text{eGFR} &= 142 \cdot \min\left(\frac{\text{Scr}}{\kappa}, 1\right)^{\alpha} \cdot \max\left(\frac{\text{Scr}}{\kappa}, 1\right)^{-1.2} \cdot 0.9938^{\text{Age}} \cdot 1.012 \\
\kappa &= \begin{cases} 0.7 & \text{if Female} \\ 0.9 & \text{if Male} \end{cases}, \quad \alpha = \begin{cases} -0.241 & \text{if Female} \\ -0.302 & \text{if Male} \end{cases}
\end{aligned}
\tag{1.3}
$$

However, these represent only a fraction of the more than 70 equations previously proposed to estimate eGFR.[79] Despite the many variations of, and the increasingly larger datasets they are developed on, MLR based approaches to estimate GFR are still considered inaccurate.[80, 79] This is unsurprising from a pharmacometric perspective — population point estimates generally perform worse than individual predictions. Still, such models are considered clinically useful for gauging renal function.

When additional accuracy is desired, the measured GFR (mGFR) may be determined, by measuring the renal clearance of an exogenous tracer, either through urine collection (renal clearance) or by measuring plasma depletion (plasma clearance). The ideal tracer should be freely filtered by the glomeruli, exhibit no active secretion or reabsorption, and have little to no plasma protein binding. Several tracers are commercially available, such as inulin, iohexol and iothalamate, and the radioactive tracers ^{51}Cr-EDTA, $^{99\text{m}}$Tc-DTPA. Inulin possesses all the properties of an ideal tracer, and its urinary clearance is considered the gold standard for determination of GFR.[81] However, its measurement is both expensive and time-consuming, and is as such not ideal for routine use in the clinical setting.[82] The alternative choice of tracer is not arbitrary, but when compared to inulin clearance measured under continuous infusion with urine collection, renal clearance of ^{51}Cr-EDTA and iothalamate, as well as plasma clearance of ^{51}Cr-EDTA and iohexol, were found to be accurate.[83] Importantly, when used for the determination of mGFR, iohexol demonstrates an excellent safety profile.[84] Additionally, it can be reliably and accurately measured at low cost.[85]

Population pharmacokinetic methods provides a framework for measuring plasma clearance of tracers, and several models for plasma iohexol clearance has been developed.[86, 87, 88] However, such methods usually rely on several blood samples over an extended period of time for accurate parameter estimation. Limited sampling strategies (LSS) aim to reduce the number of samples required, and the time window during which they are collected. For iohexol plasma clearance,

such strategies have been shown to accurately determine GFR using as few as four samples within five hours.[86]

1.3 Fundamental principles of pharmacometrics

Pharmacometrics is a multidisciplinary field, integrating mathematical and statistical modelling with pharmacology, clinical pharmacokinetics, and pharmacodynamics. The main objective is to quantitatively describe and/or predict drug disposition at the population or individual level. This requires three components: a structural model ($\mathbf{M}$), description of dose input ($\mathbf{D}$), and model parameters (θ).[89] For a given model, the response ($\mathbf{Y}$) may be summarized as in Equation 1.4 below.

$$\underbrace{y(t)}_{\mathbf{Y}} = \underbrace{f(x(t), \overbrace{d(t)}^{\mathbf{D}}, \theta) + \epsilon}_{\mathbf{M}} \tag{1.4}$$

In this example, the response of interest, $y(t)$, is the predicted drug concentration over time, which itself is a function of the current amount of drug over time, $x(t)$, the dosing input, $d(t)$, and the model parameters, θ. An error term, ϵ, is included to account for residual variability. These elements are elaborated on in the following sections.

1.3.1 Pharmacokinetic models

In its essence, a model is a simplified representation of a system. In the context of pharmacokinetics, such models aim to represent drug disposition in a finite number of compartments, where a compartment is an abstraction of a bodily space, e.g. plasma or peripheral tissue.[90] In population pharmacokinetics (popPK), models are typically restricted to a low number of compartments, usually three or less. By employing ordinary differential equations (ODEs), it is possible to describe the rate of change in each compartment. There is no inherent limitation on how these rates are modelled, but such processes are often modelled as zero-order (constant), first-order (proportional), or Michaelis-Menten kinetics (parameterized over K_m and V_{max}).[91] A simple example of a one-compartmental[II] model is provided below in Equation 1.5.

$$\frac{dA_1}{dt} = -K_a \cdot A_1$$
$$\tag{1.5}$$
$$\frac{dA_2}{dt} = K_a \cdot A_1 - K_e \cdot A_2$$

[II]In this example, "one-compartmental" is a misnomer, as the model technically consist of two compartments. However, the absorptive compartment is usually not included in the tally.

Here, A_1 and A_2 represents the amount of drug in the absorptive compartment and plasma, respectively. The model is visualized in Figure 1.5 below.
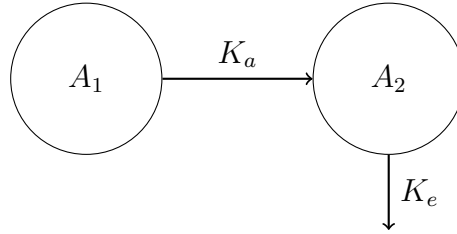
Figure 1.5: Visualization of a one-compartmental model, with first-order absorption from A_1 to A_2, and first-order elimination from A_2

Simple models such as the one in Equation 1.5 may be solved by integration to provide an analytical solution. Assuming the initial conditions $t = 0$, $A_1 = D$, and $A_2 = 0$, we obtain Equation 1.6 below.

$$X_1(t) = D \cdot e^{-K_a \cdot t}$$

$$X_2(t) = \frac{D \cdot K_a}{K_e - K_a} \cdot \left(e^{-K_a \cdot t} - e^{-K_e \cdot t}\right)$$

$$(1.6)$$

However, as the number of compartments grow, these analytical solutions may become unwieldly or be undefined. More complex models may be solved by e.g. Laplace transformations, but this will not be covered in this section.[92] Note that we model the amount of drug, and not the concentration. For this, another parameter, the apparent volume of distribution[III], abbreviated V_d, is required. The output equation thus becomes Equation 1.7.

$$C_{plasma}(t) = \frac{A_2}{V_d} \qquad (1.7)$$

For the example values of $K_a = 1.2\,\mathrm{h}^{-1}$, $K_e = 0.8\,\mathrm{h}^{-1}$, $V_d = 10\,\mathrm{L}$, and $D = 100\,\mathrm{mg}$, the plasma concentration over time is shown in Figure 1.6.

[III]Given its non-physiological properties, V_d may be considered a scaling parameter.
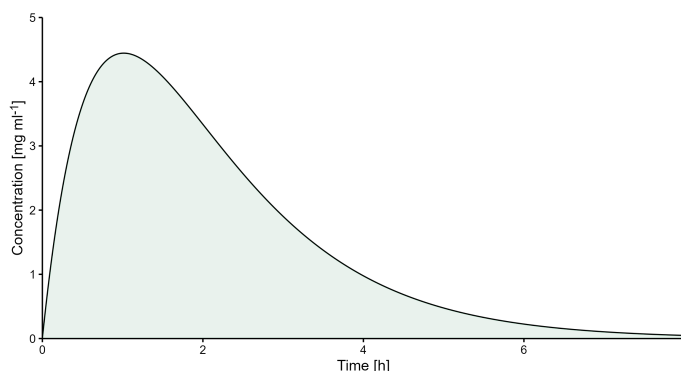
Figure 1.6: Example output from a one-compartmental pharmacokinetic model, showing plasma concentration over time.

It is important to reiterate that no model can fully and truly mirror a biological system. Models are approximative in nature, and should first and foremost be judged by their usefulness rather than correctness. Still, model development should be guided by the underlying pharmacokinetic principles.

1.3.2 Pharmacokinetic data

The term "pharmacokinetic data" is appreciably ubiquitous but refers in this context to data from which pharmacokinetic information may be derived. Over the last couple of decades, major advances in the field of analytical chemistry have increased the availability and cost-effectiveness of drug quantification, allowing for richer sampling with greater precision and accuracy. Nevertheless, there is an inherent error in all observations, which must be considered during model development, and especially for parameter estimation.[90] For further argumentation, a formal definition of such observations is required. Let $\mathbf{Y}$ be the vector of observed data, where y_i is the ith observation at time t_i. We assume that the observations in $\mathbf{Y}$ are independently, but not necessarily identically, sampled. When this distribution is Gaussian, the noisy measurement is considered as in Equation 1.8 below.

$$y_i = \mu_i + \sigma_i \cdot n_i \tag{1.8}$$

Here, n_i is considered a zero-mean Gaussian distribution, i.e. $n_i \sim \mathcal{N}(0, 1)$, and scaled by σ_i to the desired level of uncertainty. This is important, as the measurement uncertainty is not necessarily the same across all ranges, especially as the measurement approaches the upper or lower limit of quantification. One approach to estimating σ_i is to model the measurement assay uncertainty, usually at the level of the calibrators used, as the true concentration is known, and they are repeatedly sampled across multiple batches. In the modelling software Pmetrics, this is achieved by modelling the uncertainty as an error polynomial, outlined in

Equation 1.9, where σ is the standard deviation of a given observation (y_i).[93] As such, it is possible to weight each observation by their uncertainty, usually by the reciprocal of the squared error $(1/\sigma^2)$.

$$\sigma = C_0 + C_1 \cdot y + C_2 \cdot y^2 + C_3 \cdot y^3 \tag{1.9}$$

The representation of data is a crucial element in pharmacokinetic modelling, especially for repeated measurements, possibly at multiple occasions. There are several methods for adjusting for, or estimating the effect of, intraindividual variability, which in turn affect parameter estimation. While the methods for parameter estimation will be introduced later, assume that the estimated parameters for the ith individual is $\hat{\theta}_i$, which is a function of the vector of observations $\mathbf{Y}$, where $\mathbf{Y_{i,j}}$ represents the observations for the ith individual at the jth occasion, and model $\mathbf{M}$

$$\hat{\theta}_i = \begin{cases} \theta_i = f(M, Y_{i,1}, Y_{i,2}, \ldots, Y_{i,n}) \\ \theta_{i,j} = f(M, Y_{i,j}) \end{cases} \tag{1.10}$$

Evidently, $\hat{\theta}_i$ will depend on the choice of handling inter-occasion variability — determining if all observations for that individual be considered, providing a common estimate, or if the estimate be produced for the pseudo-individual, coded by the occasion. Notably, occasion may also be modelled as a covariate effect, which is considered in the following section.

1.3.3 Pharmacokinetic parameter estimation

Given a structural model $\mathbf{M}$ and a set of observations $\mathbf{Y}$ following input $\mathbf{D}$, the task of estimating the most likely parameters follows. Depending on the assumptions regarding the distribution of parameters θ, two different, but similar approaches are considered: parametric and non-parametric. An expert discussion on their differences has been conducted by Goutelle, Woillard et al. (2022), and as such their differences will be introduced, but not contrasted, in this section.[94] Briefly, parametric approaches assume that the distribution of parameters follows known distributions, such as the normal or log-normal distribution.[95] This assumption is embodied in Equation 1.11 below for the normal and log-normal distribution.

$$\begin{aligned} \theta_i &= \theta + \eta_i \\ \ln \theta_i &= \ln(\theta + \eta_i) \quad \text{or} \quad \theta_i = \theta \cdot e^{\eta_i} \end{aligned} \tag{1.11}$$

Where the parameter value for the ith individual is considered the sum of a fixed effect, i.e. θ, representing the population mean, and a random, individual effect, η_i, representing the deviation from the mean. The element η is assumed Gaussian with a mean of zero and variance equal to ω^2. This approach to population pharmacokinetic modelling is referred to as mixed effects modelling, and because

the change in response is non-linear to changes in θ, it is referred to as non-linear mixed effects (NLME).

In contrast to parametric approaches, non-parametric methods make no assumptions regarding the underlying distribution of parameters. A common motivation for the non-parametric approach is paraphrased as follows; assume that by some method, the parameter value(s) for a population is precisely known — then, the distribution which best describes the population is the empirical distribution of the exact parameters.[96] Rather than estimating a single mean and variance for each parameter, the distribution consists of discrete, possibly multidimensional, support points. The location and weight of the support points themselves provide the joint parameter distribution. Importantly, this assumption limits the maximum number of support points to the number of individuals. An example of a parametric and non-parametric distribution for a one-compartment model parameterized by K_e and V_d is provided in Figure 1.7 below.
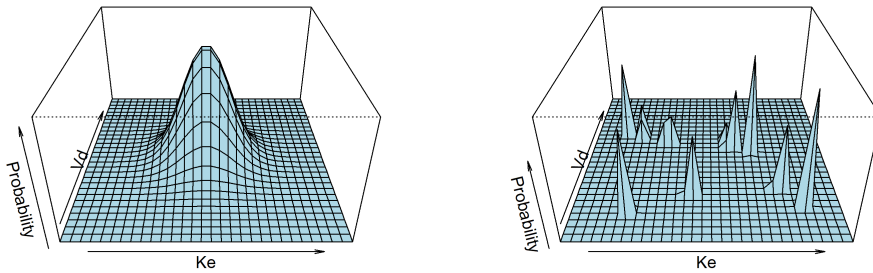
Figure 1.7: Example of a parametric (left) and non-parametric (right) distribution of parameters K_e and V_d.

Both approaches may also utilize information on covariates, demographic variables providing information at the individual level. The covariate model depends on the properties of the covariate in question. Continuous variables may be modelled similar to the allometric scaling suggested in Equation 1.1. Categorical variables may be one-hot encoded, as demonstrated in Equation 1.12 for modelling the influence of biological sex on CL, where values are restricted to male or female[IV].

$$CL = CL_{\text{BASE}} + CL_{\text{SEX}} \cdot \beta$$
$$\beta = \begin{cases} 1 & \text{if Male} \\ 0 & \text{if Female} \end{cases} \tag{1.12}$$

[IV]Such encoding is also possible for categorical variables with more than two levels, but necessitates a coefficient for each level, increasing the dimensionality.

This model implies a population average, CL_{BASE}, and an additional, estimated effect for sex, CL_{SEX}, which is only present when the covariate codes for male. Similar approaches may be used for modelling inter-occasion variability, either through a continuous effect or one-hot encoding for each occasion, being aware of the added dimensionality. It is important to be aware that the inclusion of covariates will affect the distribution of the covariate-influenced parameter, and possibly others. As such, covariates must be carefully selected in order to avoid potential bias.[97] Covariate inclusion should thus be considered only after the structural model has been determined.[98] Furthermore, decision rules for covariate inclusion should primarily be based on domain knowledge, but may in exploratory studies use methods such as forward and backwards selection.[99] It has been suggested, but ultimately not shown, that covariates may be more useful in parametric approaches compared to non-parametric.[94]

Given the brief differentiation of parametric and non-parametric approaches, the mathematical methods for parameter estimation itself will not be introduced further, due to the vast heterogeneity in such methods, ranging from ordinary least squares, expectation maximization, maximum likelihood estimation, and even stochastic variants of those.[100] However, due to its relevance in this work, the non-parametric adaptive grid (NPAG) algorithm will be presented in the following section.

1.3.4 The non-parametric adaptive grid (NPAG) algorithm

The NPAG algorithm was developed and is maintained by the Laboratory of Applied Pharmacokinetics and Bioinformatics, Los Angeles, USA.[93] As this work relies heavily on this algorithm, it will be briefly introduced, based on the description provided by Yamada, Neely et al. (2021).[96] Given a structural model, often defined as a set of ordinary differential equations, the set of bounded parameters $\theta_1, \theta_2, \ldots, \theta_n$ is assumed to be members of the compact subset Θ, and have a common, but unknown distribution F. The objective is to find F, the parameter distribution for all elements of Θ which best fits the observed data. Here, F is expressed as a set of support points $\Phi = \Phi_1, \Phi_2, \ldots, \Phi_K$ where K is equal to or less than the number of subjects, N, with weights $\lambda_1, \lambda_2, \ldots, \lambda_K$.

Estimation of F is performed using an iterative, two-stage approach; first, given a set of support points, determine the optimal weights. This is achieved using a primal-dual interior point method, which is common in convex optimization theory. Second, given the updated weights, find a better set of support points. This is done through an adaptive grid, where for each point in Φ, bounded by Θ, up to twice the number of dimensions in Θ is produced, respecting the bounds of θ and a minimum distance to the original point. An example is shown in Figure 1.8.

The distance at which expansion occurs is given by $(\theta_{\text{upper}} - \theta_{\text{lower}}) \cdot \epsilon$, with an initial value $\epsilon = 20\%$. For each iteration, ϵ is reduced by a factor of two. Next, the number of points is pruned to conform to $K \leq N$, keeping the unique support points with the overall greatest contribution with respect to describing the observed data.
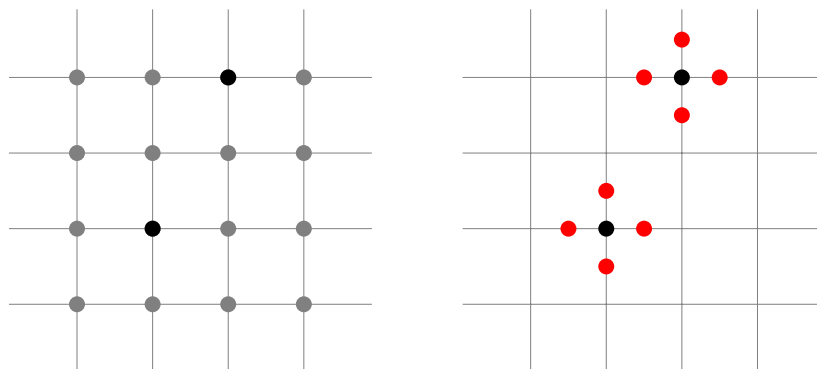
Figure 1.8: Example of a grid expansion in two dimensions. The left grid represents the original grid, where the gray points are pruned, leaving the black points. The right grid represents expansion from those points to the surrounding red points. This iteration is then repeated.

This iteration is repeated until both the change in improvement is negligible, and ϵ is below a given criterion.

In addition to the uncertainty in observations modelled by assay error, previously outlined in Equation 1.9, the NPAG algorithm utilizes an additional element for the total observation error, either additively (λ, Equation 1.13) or proportionally (γ, Equation 1.14). The values of λ or γ may be estimated by the algorithm, or fixated to a given value. The terms represent additional process noise, such as misspecification of dose and observation times.

$$\text{Error} = \sqrt{\text{SD}^2 + \lambda^2} \tag{1.13}$$

$$\text{Error} = \text{SD} \cdot \gamma \tag{1.14}$$

A major limitation of this non-parametric approach is the imposed boundaries on Θ. For an infinitely or sufficiently large parameter space, the probability for a given support point, obtained by normalizing the likelihood, approaches zero. While both the boundaries of, and the number of initial grid points in, the parameter space, are likely to affect parameter estimation, NPAG has been shown to be a consistent estimator when the number of subjects is large.[101] As such, it has been suggested to first employ a parametric approach for estimating initial values or boundaries, followed by non-parametric analysis, to facilitate model development.[102]

1.4 Clinical application of pharmacometrics

Pharmacometrics has been proven to be a valuable tool for describing and predicting drug disposition. As such, it has been implemented in several areas of clinical pharmacology and practice.

1.4.1 Pharmacokinetic simulation

Through pharmacokinetic simulation it is possible to evaluate scenarios outside the original dataset, such as different dose regimens, covariate effects, and more.[103] Simulation can also be used to evaluate drug-drug interactions.[104] However, depending on the approach used for parameter estimation, methods for simulation vary greatly. Simulating from a parametric parameter distribution is straightforward, as the distribution itself is known. In the case of multiple parameters, the covariance between parameters must be known, as some parameters may be correlated. For a two-parameter, one-compartmental model given by Equation 1.15 below

$$\frac{dA_1}{dt} = -A_1 \cdot K_e$$

$$C(t) = \frac{A_1}{V_d} \tag{1.15}$$

The covariance matrix Σ is given by Equation 1.16.

$$\Sigma = \begin{bmatrix} Var(K_e) & Cov(K_e, V_d) \\ Cov(K_e, V_d) & Var(V_d) \end{bmatrix} \tag{1.16}$$

Where diagonal elements represent the variance of each parameter, and the off-diagonal elements represent the covariance between them. As the probability density function for the multivariate normal distribution is well described, sampling is as mentioned straightforward. It is important to note that for parametric approaches, the covariance matrix is itself estimated, as opposed to non-parametric approaches where the support point location itself convey the relationship between parameters.[91]

However, simulation from non-parametric distributions is more complex. In their review of non-parametric methods in population pharmacokinetics, Goutelle, Woillard et al. (2022) suggest three methods for simulation: 1) sampling the support points directly, 2) sampling from the summary statistics, i.e. mean and variance of the parameters, and 3) semi-parametrically, sampling from the Gaussian distribution around each support point.[105] However, the choice of method will greatly impact the resulting parameter distributions, a discussion on which is provided later.

1.4.2 Limited sampling strategies

Accurate estimation of pharmacokinetic parameters often relies on numerous observations. From a practical perspective, this poses multiple challenges. First and foremost, there is a cost associated with quantifying the concentration of a drug. Secondly, there is temporal aspect to consider in order to sample during the absorption, distribution, and elimination phases of the drug. This requires

that both the patient and health care personnel is available, inconveniencing the patient and locking up health care personnel. The latter may be remedied by patient-driven micro sampling, allowing the patient to perform the sampling. The feasibility of such sampling has been readily demonstrated in the clinic.[106, 107] In order to reduce the burden associated with frequent sampling, limited sampling strategies (LSS) may be developed to reduce the cost and/or time associated with pharmacokinetic investigations. The aim is to reduce the number of samples while maintaining accurate parameter estimates. This introduces the concepts of information and optimality — some samples provide more information than others. One such measure is the separation distance between two responses at a given time. Still, strategies for LSS development vary, ranging from simple methods such as multiple linear regression, to more complex methods based on the Fisher information matrix or maximum a posteriori Bayesian estimation.[108, 109]

1.4.3 Therapeutic drug monitoring

Several classes of drugs, such as immunosuppressants, antibiotics, and anticancer drugs demonstrate a narrow therapeutic window, and require monitoring for safe and efficient therapy. A hallmark example is the immunosuppressive drug tacrolimus, a calcineurin inhibitor used to prevent rejection in solid organ transplantation. Its pharmacokinetic-pharmacodynamic relationship is well described, but not fully understood.[110] With insufficient exposure the patient risks organ rejection, and conversely, when exposure is too great the risk of adverse effects increases. This is especially challenging for drugs with known interindividual pharmacokinetic variability. In the TDM setting, an additional challenge is in the sparsity of available data, often limited to the pre-dose (trough; C_0) concentration. However, Bayesian statistics provides a framework for updating the beliefs of the population parameter distribution (prior) when presented with new data, allowing for accurate estimates of the individual, posterior distribution of pharmacokinetic parameters. Pharmacometrics may thus be employed to optimize individual drug therapy, by estimating and optimizing indices of exposure, such as C_0, dose-interval AUC, or their ratio.[111] Several algorithms has been developed for this use, and computerized dosing has previously been found to outperform conventional dosing by experienced physicians.[112, 113]

Aims of the present studies

This work aims to highlight the application of pharmacometrics and probe drugs in order to predict and describe drug disposition at the individual and population level. To achieve this, pharmacokinetic analyses has been performed on various patient populations with different perspectives.

Paper I   To evaluate and disentangle the effect of diet- and surgery induced weight loss on the activity of hepatic uptake transporter OATP1B1, using rosuvastatin as a probe drug.

Paper II   To develop a population pharmacokinetic model in order to estimate the individual cerebrospinal fluid (CSF) to blood clearance of intrathecally administered gadobutrol, as a possible diagnostic aid for CSF disorders by comparison of the group-wise differences in clearance between patients with various CSF disorders.

Paper III   To evaluate the robustness of a limited sampling strategy using Bayesian estimates based on a previously developed population pharmacokinetic model, and quantify the effect of deviation in sample time on the resulting estimate of measured glomerular filtration rate using iohexol serum clearance.

Chapter 2.   Aims of the present studies

Methods

3.1 Study designs and patient populations

Paper I

This work was based on the COCKTAIL study, an open, non-randomized, three-armed study performed at the Morbid Obesity Centre at Vestfold Hospital Trust, Norway.[114] The study included patients with severe obesity (BMI $\geq$ 35 kg m^{-2} in combination with comorbidity or BMI $\geq$ 40 kg m^{-2}) scheduled for elective weight-reducing intervention, either by Roux-en-Y gastric bypass (RYGB) or strict diet. Additionally, a cross-sectional normal- to overweight (BMI 18.5 - 29.9 kg m^{-2}) control group of patients scheduled for cholecystectomy were included. A complete list of inclusion and exclusion criteria is provided in the associated protocol paper.[114] The intervention groups first underwent a three-week low energy diet (<1200 kcal day^{-1}; LED), followed by either RYGB or very-low energy diet (VLED), restricting energy intake to <800 kcal day^{-1}. This continued until two years following start of LED. A graphical overview of the study protocol is provided in Figure 3.9 below.
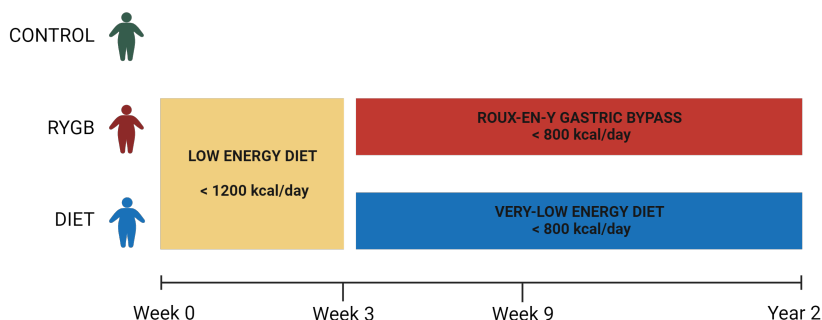
Figure 3.9: A simplified graphical overview of the COCKTAIL study protocol. Created with BioRender.com

Pharmacokinetic investigations were conducted at baseline (week 0), after LED (week 3), six weeks after RYGB and VLED (week 9), and at year 2. At each investigation, a cocktail of probe drugs consisting of rosuvastatin (OATP1B1), midazolam (CYP3A), digoxin (P-gp), omeprazole (CYP2C19), losartan (CYP2C9), and caffeine (CYP1A2) were investigated. All patients were genotyped for, among others, SLCO1B1 c.521T>C (rs4149056) and ABCG2 variants V12M (rs2231137) and Q141K (rs2231142). During RYGB and cholecystectomy, jejunal and hepatic biopsies were obtained, which were subject to proteomic analysis using a total protein approach.[115]

Paper II

The present paper included patients referred to the Department of Neurosurgery, Oslo University Hospital — Rikshospitalet, Oslo, Norway, in whom intrathecal contrast enhanced MRI was indicated for clinical reasons as part of their diagnostic workup. Exclusion criteria included previous hypersensitivity to contrast media agents, severe allergic reactions in general, evidence of renal dysfunction (eGFR < 30 mL min^{-1}), below 18 or above 80 years of age, pregnancy, or breastfeeding. Patients were categorized according to their tentative diagnosis prior to MRI. Patients with no apparent evidence of CSF disturbances were denoted reference (REF), but should not be considered healthy individuals. The following diagnoses were included; spontaneous intracranial hypotension (SIH), idiopathic intracranial hypertension (IIH), pineal cysts (PC), arachnoid cysts (AC), and idiopathic normal pressure hydrocephalus (iNPH). For the latter, the Japanese guidelines for Definite iNPH were used.[116]

The MRI contrast agent gadobutrol was administered intrathecally by an experienced radiologist, and correct entrance to the subarachnoid space was verified by CSF backflow. A 1 mmol mL^{-1} solution of gadobutrol was administered in volumes of 0.10, 0.25, or 0.50 mL over 10 seconds, for a total dose of 0.10, 0.25, or 0.50 mmol, respectively. The first 80 patients received 0.50 mmol only, and later patients alternatingly received 0.10 or 0.25 mmol. Following administration, venous blood samples were obtained at empirically determined regular time points up to 48 hours. Additionally, MRI was performed regularly and in conjunction with blood sampling. The protocol is briefly outlined in Figure 3.10 below.
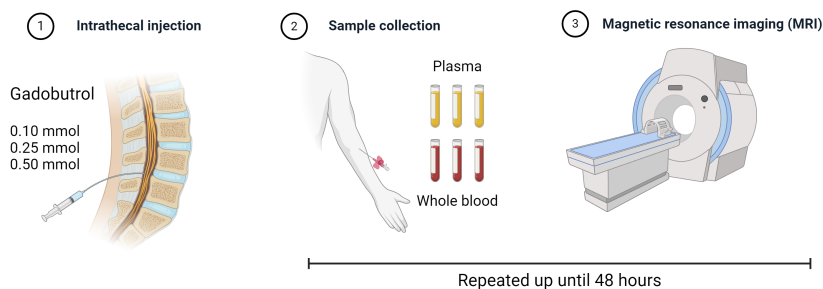

Figure 3.10: A simplified graphical overview of the sampling protocol in Paper II. Created with BioRender.com

Paper III

This simulation-based study was based on a previously developed population pharmacokinetic model for iohexol serum clearance.[86] The purpose of the model was to determine the measured glomerular filtration rate (mGFR) following intravenous administration of iohexol by plasma depletion. The two-compartmental model was parameterized in terms of clearance and volume of distribution, and included body weight as a covariate on both clearance and volume of distribution. A semi-parametric approach was used for simulating new pharmacokinetic profiles from the discrete support points of the original model. Conceptually, a Gaussian distribution is assumed around each support point, where the standard deviation is optimized so that the resulting Gaussian mixing distribution best fits the target parameter distribution. Parameter density overlap was evaluated using the overlap index for empirical distributions.[117]

As stated in the aim, the chief objective was to estimate the robustness of the limited sampling strategy. To this end, two methods were used to sample around the prescribed sample schedule of 10 minutes, 30 minutes, 2 hours, and 5 hours. First, a zero-mean Gaussian error was assumed around each optimal sample time, with incremental relative standard deviation. Sample times were truncated to prevent overlap. This approach introduced deviation in all sample point simultaneously, which can be expected in a clinical, real-life setting. The second method evaluated an empirical amount, e.g. 5-, 10-, and 15-minutes error for one sample point at a time. This allowed for evaluating which sample points are most critical, in essence evaluating the optimality of the sampling schedule. These metrics were further used to define optimal windows for sampling, both for the overall population and stratified by CKD stage according to the true, simulated GFR.

3.2 Bioanalytical methods

In **Paper I**, bioanalytical quantification of rosuvastatin was performed by a third-party, Covance Laboratories.[118] Buffered plasma samples were stored at -80 °C, and were extracted by supported liquid extraction, and evaporated. Following reconstitution, the samples were analyzed with liquid chromatography (LC) tandem mass spectrometry (MS), using a C18-column. The mobile phase consisted of acetonitrile and 0.1% formic acid using a gradient. Rosuvastatin was detected by monitoring the m/z 482.2-258.2 transition. The standard curve ranged from 0.04 to 40 ng/mL, using a human plasma sample volume of 0.1 mL. The assay variation coefficients of the rosuvastatin analysis were 7.1%, 4.4% and 4.5% at 0.12 ng mL^{-1}, 2 ng mL^{-1}, and 20 ng mL^{-1} (n = 130), respectively.

In **Paper II**, venous whole blood and plasma samples were stored at -80 °C, and quantified for the gadolinium-based contrast agent gadobutrol at the Norwegian Institute for Air Research.[65] Samples were homogenized and subjected to nitric acid-based digestion with deionized water in a closed-vessel microwave technique system. Digestion was performed according to a 60-minute stepwise heating

program, reaching a maximum temperature of 250 °C, maintained for 15 minutes. Following dilution, gadolinium was quantified by inductively coupled plasma mass spectrometry using indium (0.1 μg L^{-1}) as internal standard. Samples were corrected for procedural blank values, with a detection limit of 0.009 μg L^{-1}. Assay coefficients of variation were 3.2%, 2.6%, 1.6%, 1.0%, and 0.01% at 0.01 ng mL^{-1}, 0.05 ng mL^{-1}, 0.1 ng mL^{-1}, 1.0 ng mL^{-1}, and 10.0 ng mL^{-1}, respectively. Measured gadolinium was recalculated to concentrations of gadobutrol. Linear regression was used to interpolate whole blood gadobutrol to plasma concentrations for pharmacokinetic analysis.

The underlying population pharmacokinetic model used in **Paper III** was developed on serum samples of iohexol. These concentrations were quantified for iohexol using high-performance liquid chromatography using an ultraviolet light detector at the respective hospital laboratories. The validated lower level of detection and quantification was 20 mg/L, and the linear range was validated between 20 and 1100 mg L^{-1}, with a coefficient of variation of 6%.

3.3 Population pharmacokinetics

In **Papers I-III**, population pharmacokinetic modelling was performed using Pmetrics, a software package for R.[93] All models employed the previously introduced NPAG-algorithm for parameter estimation. In general, model development and selection were guided by comparison of the relative root mean square predictive error (RMSE, %) calculated from the relative prediction error, as well as the linear regression slope, R^2-values of the observed versus predicted plot, and to a lesser extent the Akaike and Bayesian information criteria. For all evaluations, the individual predicted, mean posterior concentrations were used. Transfer rate coefficients are provided on the form of $K_{i,j}$, denoting the transfer from the ith to the jth compartment, where $j = 0$ implies elimination.

Paper I

The mammillary three-compartmental model used in **Paper I** included two transit compartments for absorption, with individual lag-times (T$_{lag}$), in order to accommodate the multiple peaks in concentration of rosuvastatin over time. These transit compartments, as well as the direct absorption route, employed a modified Heaviside equation as noted in Equation 3.1 for the absorption coefficients. Elimination was modeled as a first-order process from the central compartment only. The response surface for $K_{i,j}$ for the example values of $K_a = 5$ and $T_{lag,i} = 2$ is dependent on the slope parameter lambda, L.

$$K_{i,j}(t) = K_a \cdot \left[\frac{1}{2} \cdot \left(1 + \tan^{-1}\left(L \cdot (t - T_{\mathrm{lag},i}) \right) \cdot \frac{2}{\pi} \right) \right] \tag{3.1}$$

This is visualized below for various values of L in Figure 3.11.
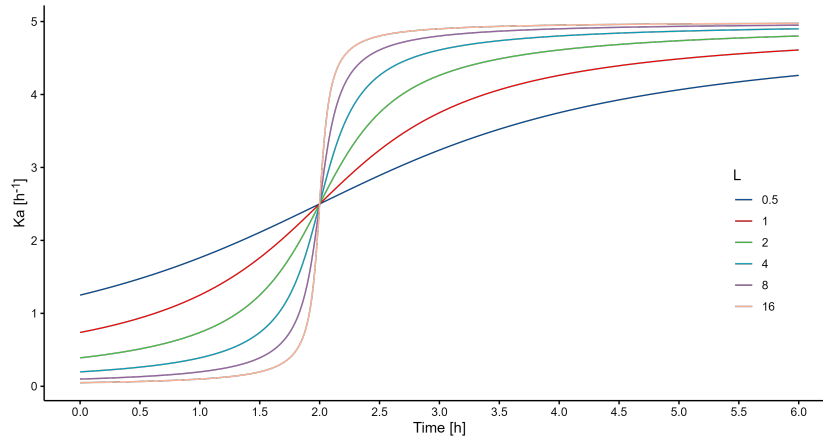
Figure 3.11: The response surface for the modified Heaviside equation for various values of L.

The full, structural model, including a bioavailability term (F), is provided in Equation 3.2 below.

$$
\begin{aligned}
\frac{dA_1}{dt} &= -A_1 \cdot (K_{12} + K_{15} + K_{16}) \\
\frac{dA_2}{dt} &= K_{12} \cdot A_1 - (K_{20} + K_{23} + K_{24}) \cdot A_2 \\
&\quad + K_{32} \cdot A_3 + K_{42} \cdot A_4 + K_{52} \cdot A_5 + K_{62} \cdot A_6 \\
\frac{dA_3}{dt} &= K_{23} \cdot A_2 - K_{32} \cdot A_3 \\
\frac{dA_4}{dt} &= K_{24} \cdot A_2 - K_{42} \cdot A_4 \\
\frac{dA_5}{dt} &= K_{15} \cdot A_1 - K_{52} \cdot A_5 \\
\frac{dA_6}{dt} &= K_{16} \cdot A_1 - K_{62} \cdot A_6 \\
C(t) &= \frac{A_2}{V_d} \quad ; \quad A_1(0) = F \cdot Dose
\end{aligned}
\tag{3.2}
$$

The model is subsequently visualized in Figure 3.12.
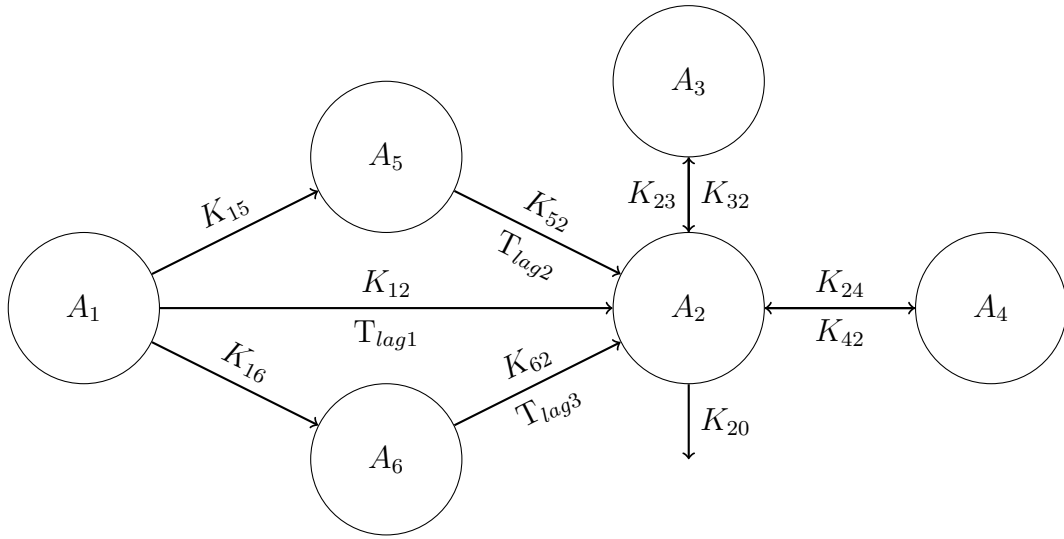
Figure 3.12: Visual representation of the pharmacokinetic model for rosuvastatin

The transfer rate coefficients $K_{1,2}$, $K_{5,2}$ and $K_{6,2}$ are functions of the modified Heaviside equation outlined in Equation 3.1. An additive error model, as previously shown in Equation 1.13, was used. As a longitudinal study, **Paper I** included up to four investigations for each patient. Rather than attempting to model changes within and between intervention groups directly with the pharmacokinetic model, a pseudo-individual approach was used, disconnecting the individual from the repeated measurements. Longitudinal changes were evaluated using the methods outlined in 3.4.

Due to memory limitations in the current implementation of NPAG, the Fortran routines were modified to allow for 64-bit precision and memory allocations above 2 gigabytes. This effort was part of an Advanced User Support provided by the Norwegian research infrastructure services (NRIS) through Sigma2.[119]

Paper II

In **Paper II**, the final population pharmacokinetic model comprised of a two-compartmental model with first-order absorption to, and first-order elimination from, the central compartment. Additionally, the model included a lag term to account for individual differences in neuraxial flow of CSF. The model is provided in Equation 3.3 below.

$$
\begin{aligned}
\frac{dA_1}{dt} &= -A_1 \cdot K_{12} \\
\frac{dA_2}{dt} &= A_1 \cdot K_{12} + K_{32} \cdot A_3 - (K_{20} + K_{23}) \cdot A_2 \\
\frac{dA_3}{dt} &= A_2 \cdot K_{23} - K_{32} \cdot A_3 \\
C(t) &= \frac{A_2}{V_d} \quad ; \quad A_1(0) = \text{Dose}
\end{aligned}
\tag{3.3}
$$

The model is subsequently visualized in Figure 3.13.
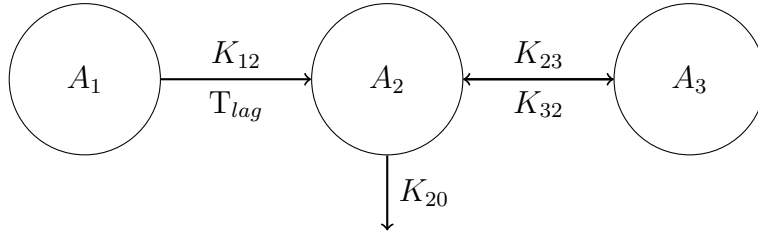
Figure 3.13: Visual representation of the pharmacokinetic model for gadobutrol

An additive error model was used, as outlined in Equation 1.14.

Paper III

The population pharmacokinetic model employed in **Paper III** was based on a previously published model.[86] However, as the intended method for simulation was not amenable to inclusion of covariates, a covariate-free version was developed on the same data, and subsequently used. The model included two compartments, and was parameterized in terms of clearance from the central volume (CL), volume of central V_{CENT} and peripheral V_{PERI} compartments, and inter-compartmental blood flow (Q). The structural model is provided in Equation 3.4.

$$\frac{dA_1}{dt} = -K_{12} \cdot A_1 + K_{21} \cdot A_2 - K_{10} \cdot A_1$$
$$\frac{dA_2}{dt} = K_{12} \cdot A_1 - K_{21} \cdot A_2 \tag{3.4}$$
$$C(t) = \frac{A_2}{V_{\text{CENT}}} \quad ; \quad A_1(0) = \text{Dose}$$

Parameterization was performed according to Equation 3.5 below.

$$K_{10} = \frac{CL}{V_{\text{CENT}}} \quad ; \quad K_{12} = \frac{Q}{V_{\text{CENT}}} \quad ; \quad K_{21} = \frac{Q}{V_{\text{PERI}}} \tag{3.5}$$

The model is visualized in Figure 3.14.
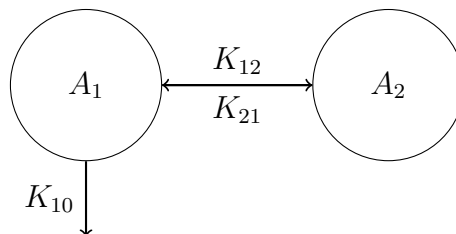
Figure 3.14: Visual representation of the pharmacokinetic model for iohexol

The model employed a multiplicative error model, as outlined in Equation 1.14.

3.4 Statistics

In **Paper I**, statistical analysis was conducted using linear mixed effects models. Such models excel in cases of repeated measurements and dependent data. By treating intervention group and study visit, as well as their interaction, as fixed effects, their respective mean effects were calculated. To allow for dependence in the data, random effects on the intercept were considered for each individual. Model residuals were evaluated for normality, and the dependent variable was logarithmically transformed when appropriate. In such cases, the model was adjusted for the (theoretically) introduced bias. Estimated marginal means and corresponding contrasts were used for primary analysis. Cross-sectional analysis comparing the control- and intervention groups were performed using Welch's two-sample t-test. Associations were evaluated using Pearson's correlation coefficient unless otherwise specified.

In **Paper II**, groupwise comparisons were performed using a two-tailed t-test for continuous variables, and Fishers exact test for categorical variables. To account for differences in the administered dose of gadobutrol, the exposure parameters $C_{\max}$ and AUC were normalized by dose prior to analysis.

The main objective in **Paper III** was to evaluate the robustness of a limited sampling strategy. Deviation was evaluated by calculating the mean prediction error in mGFR, and the proportion of individuals with relative prediction error greater than 15% (P15), where a P15 less than 15% was considered acceptable.

All statistical analyses were performed in R.[120]

3.5 Ethics

In this work, whenever human research was conducted, prior independent review board approval and informed consent was obtained. All studies followed good clinical practice (GCP) and complied with the Helsinki declaration. **Paper I** was approved by the Regional Committee for Medical and Health Research Ethics (2013/2379), and pre-registered on ClinicalTrials.gov (NCT02386917). **Paper II** was approved by the Regional Committee for Medical and Health Research Ethics (2015/96), the Institutional Review Board of Oslo University Hospital (2015/1868) and the National Medicines Agency of Norway (15/04932-7). **Paper III** did not involve collection of new human data, but was based on a previously published study, which was approved by the Regional Committee for Medical and Health Research Ethics (2014/2180).

Summary of papers

Paper I

Neither Gastric Bypass Surgery Nor Diet-Induced Weight-Loss Affect OATP1B1 Activity as Measured by Rosuvastatin Oral Clearance

In this work, we aimed to disentangle the effect of Roux-en-Y gastric bypass (RYGB) surgery and diet-induced weight loss on the activity of the hepatic uptake transporter OATP1B1. A total of 80 patients with severe obesity were included, and subjected to either RYGB (n = 40) or very-low energy diet (VLED; n = 40). A normal-to-overweight control group of patients scheduled for cholecystectomy (n = 18) were also included, but did not receive dietary intervention. The intervention groups first underwent a three-week low-energy diet (LED; <1200 kcal day^{-1}), followed by either RYGB or VLED, restricting energy intake to <800 kcal day^{-1}. Pharmacokinetic investigations were performed at baseline (week 0), after LED (week 3), six weeks after RYGB or VLED (week 9) and at long-term follow-up (year 2).

The initial low energy diet (LED; < 1200 kcal day-1) introduced a similar (mean ± standard deviation) weight loss in the RYGB (5±2%) and diet (5±2%) group. Total weight loss at week 9 was 13±3% and 11±4%, respectively. While the RYGB-group maintained a total weight loss of 29±9% at year 2, the diet group mostly returned to their baseline weight, for a total weight loss of 3±6%. The final population pharmacokinetic model included a total of 3630 samples, from 197 18-point and 111 9-point 24-hour pharmacokinetic profiles from 98 individuals, and was used to describe individual changes in pharmacokinetics of rosuvastatin. Following LED, oral clearance (CL/F) of rosuvastatin decreased in both the RYGB- (16%) and diet- (23%) group. However, no additional change in CL/F was observed 6 weeks after RYGB or VLED. At year 2, the RYGB-group demonstrated a total increase in CL/F of 21% compared with baseline, while the diet group returned to baseline values. There were no differences in short- or long-term change in oral clearance in patients with reduced-function variants of *SLCO1B1* when compared with wildtype.

In conclusion, while weight loss appeared to affect oral clearance of rosuvastatin,

these effects were not mediated by change in activity of OATP1B1. This was substantiated by the lack of differences in change in patients with wildtype and reduced-function variants of OATP1B1. As rosuvastatin demonstrates a high hepatic extraction ratio (0.63), it may be susceptible to altered hepatic blood flow. It has previously been shown that LED may induce a decrease in liver size in patients with severe obesity, and that hepatic blood flow is increased following bariatric surgery.[121, 122] A transient increase in portal vein blood flow could thus lead to an increased bioavailability, effectively decreasing oral clearance. Additional studies of hepatic hemodynamics following weight loss is warranted to confirm this hypothesis. Overall, the changes in oral clearance of rosuvastatin were clinically negligible, and as such, no dose adjustments of rosuvastatin appears necessary following RYGB or weight loss in patients with severe obesity.

Paper II

Population pharmacokinetic modeling of CSF to blood clearance: prospective tracer study of 161 patients under work-up for CSF disorders

The primary objective of this work was to investigate the mechanisms of, and variability in, the cerebrospinal fluid (CSF) to blood clearance between individuals. The study included 161 patients under work-up for various disturbances of CSF, such as pineal (PC, n = 13) and arachnoid cysts (AC, n = 14, spontaneous intracranial hypotension (SIH, n = 14), idiopathic intracranial hypertension (IIH, n = 15), communicating (cHC, n = 11) and non-communicating (ncHC, n = 3), as well as idiopathic normal pressure hydrocephalus (iNPH, n = 63). Patients without evidence of CSF disorders were retrospectively included as a reference cohort (n = 28), but should not be considered healthy.

The magnetic resonance imaging (MRI) contrast agent gadobutrol was used as a surrogate marker for clearance of e.g., brain metabolites or drugs from the CSF to blood. Extensive clearance is thought to be due to CSF leakage or increased intracranial pressure, while reduced clearance is hypothesized to contribute to neurodegenerative disease. Following intrathecal administration of 0.10, 0.25 or 0.5 mmol gadobutrol, the patients underwent frequent venous blood sampling in combination with MRI investigations over the course of 72 hours.

The population pharmacokinetic model was developed based on 1140 blood samples from 161 individuals. The two-compartmental model included first-order absorption from the subarachnoid space with first-order elimination from the central compartment. The predicted plasma disposition of tracer revealed a significant level of pharmacokinetic variability, both between and within disease categories. This was also true for the primary parameter of interest, CSF to blood clearance, which was associated with a coefficient of variation of more than 70% even in the reference cohort. Additionally, in this group, age was negatively associated with C_{max} $(r = -0.5)$, but positively so with T_{max} $(r = 0.42)$.

Overall, the observed variability suggests that measurements of CSF to blood

clearance of gadobutrol may be useful in the assessment of CSF disorders as a diagnostic aid. Disposition of intrathecal gadobutrol appeared linear with increasing dose, and the predictive performance of the model was similar between the different doses, and as such a low dose of 0.10 appears adequate for such measurements.

Paper III

A Method for Evaluating Robustness of Limited Sampling Strategies — Exemplified by Serum Iohexol Clearance for Determination of Measured Glomerular Filtration Rate

This work was a simulation-based study, based on a previously developed population pharmacokinetic model for determination of measured glomerular filtration rate (mGFR) using serum iohexol clearance. A total of 400 pharmacokinetic profiles were simulated from a prior, discrete set of support points representing the population parameter distribution by employing a semi-parametric approach. Of these, 61 profiles were excluded as the simulated GFR was outside the validated range of 15-115 mL min^{-1} However, this approach was not amenable to inclusion of covariates, and as such a modified, covariate-free model was used, developed on the original dataset. Semi-parametric simulation with optimized variance terms yielded satisfactory overlap for all parameter densities, with 91%, 92%, 90% and 86% overlap for the parameters CL, Q, V, and V_p, respectively, when comparing the simulated to the original distribution.

The original limited sampling strategy demonstrated a mean absolute and relative error of 1.5 ± 2.2 mL min^{-1} and 4.1 ± 5.5%, respectively. Overall, the limited sampling strategy proved robust to errors in sampling time, for all empirical deviations, mean and median absolute error was below 4 mL min^{-1} and 2.5 mL min^{-1}, respectively. However, it was evident that this effect differed based on individual clearance, i.e. the strategy was less robust when the simulated clearance was very low.

An estimate of appropriate sampling windows was obtained by defining a treshold for acceptable error. In this, it was possible to (individually) perform the 10-minute sample between 6-16 minutes, the 30-minute sample between 20-45 minutes, the 2-hour sample between 1.5-3 hours, and the 5-hour sample between 4.75-12 hours, all while maintaing a mean prediction error below 2 mL min^{-1}. Conversely, a different approach for estimating sampling windows was through the 90% confidence interval around the sample time for a relative standard deviaton of 25%, which was associated with a mean P15 of 8.3%. This approach suggested to perform the 10-minute sample between 6-12 minutes, the 30-minute sample between 18-42 minutes, the 2-hour sample between 1-3 hours, and the 5-hour sample between 2.5-7.4 hours. With either approach, sampling windows are likely to have great practical value, as it provides additional insight into which patients groups require additional diligence during sample collection.

Chapter 4. Summary of papers

Discussion

Pharmacokinetic modelling and simulation have proven to be invaluable tools in several areas, such as dose optimization, therapeutic drug monitoring (TDM), predicting drug-drug interactions, and diagnostics. Each of **Paper I-III** introduces or evaluates a concept in pharmacometrics, using a probe or tracer, which may contribute to enhanced application of pharmacokinetic modelling and simulation.

5.1 Time-varying parameters and alternative absorption strategies

As previously mentioned, the population pharmacokinetic model for rosuvastatin employed in **Paper I** included a time-varying coefficient of absorption, modelled by a modified Heaviside equation. Time-dependent model parameters allow for increased flexibility in the response space, at the cost of additional dimensionality in the parameter space. Such time-dependency is not new in pharmacometric literature, but has been readily applied for a variety of drugs and parameters. In one of the simpler cases, for the monoclonal antibody teclistamab, Miao, Wu et al. (2023) modelled clearance as the sum of a fixed and exponential time-dependent term.[123] Similarly, Niazi (1976) suggests modelling the volume of distribution as a linear function of time from an initial to its maximum value.[124] The use of statistical distributions for pharmacokinetic parameters have also been applied previously, with the advantage of their well described moments, such as the mean, variance, and skewness. The gamma function has been applied both to model parameters, for example by Wesolowski, Wesolowski et al. (2016) for describing the half-life and volume of distribution of ^{169}Yb-DTPA, but also for the response itself in the case of cyclosporin by Debord, Risco et al. (2001)[125, 126]. In the same study population of patients with severe obesity in **Paper I**, a modified Weibull distribution was applied to the absorption of digoxin, as first-order absorption inadequately captured the absorption phase.[127]

The paradigm shifts from constant, first-order rate coefficients to more complex functions for mass transfers introduces new possibilities in pharmacometrics, but

at a price, as interpretation of time-dependent parameters can be difficult. First-order absorption models are easily summarized, but may not adequately model the underlying processes. Implicitly, they assume that the maximum absorption occurs immediately after administration, ignoring the requisite drug dissolution and dispersion before absorption can take place.[128] This is sometimes, but not always, alleviated by a lag-term. In the case of the approach used in **Paper I**, one could (erroneously) argue that the modified Heaviside equation models the varying dissolution and absorption along the intestinal tract. However, such claims must be backed by supporting data, such as in vitro dissolution assays. Still, in the case of rosuvastatin in **Paper I**, traditional model approaches were unable to adequately capture both the irregular absorption phase and multiple peaks due to enterohepatic recirculation. The use of population pharmacokinetic models to investigate rosuvastatin disposition is sparse in literature. Tzeng, Schneck et al. (2008) employed a two-compartmental model with simultaneous zero- and first-order absorption with separate lag terms for each absorption pathway.[129] Park, Jang et al. (2016) built on this model, but replaced zero-order absorption with an Erlang absorption model.[130] Erlang models, which uses a fixed number of linear transit compartments, provides a gamma-like, asymmetric absorption profile.[131] While statistical distributions such as the Gamma and Weibull has been shown to improve model fit, as previously described, and the statistical moments of such distributions are well known, they are not always amenable to pharmacokinetic interpretation. As such, models incorporating statistical distributions on parameters are to a greater extent reliant on the summary statistics of the response, such as AUC, $C_{\max}$, and $T_{\max}$. In **Paper I**, oral clearance was calculated by dividing the dose by AUC, which showed poor correlation with model-estimated clearance (data not shown). Thus, further importance is placed on the usefulness of the model, pertaining to its intended purpose, which is expanded on below.

5.2 Impact of obesity and RYGB on rosuvastatin oral clearance

In **Paper I**, the overall aim was to disentangle the effect of obesity, RYGB, and weight loss on OATP1B1 activity, as measured by rosuvastatin oral clearance. As previously mentioned, rosuvastatin is an established probe for OATP1B1 activity.[46, 47, 45, 48] In the context of severe obesity, only one study has previously evaluated the pharmacokinetics and -dynamics of rosuvastatin following gastric bypass surgery.[132] However, the work by El-Zailik, Cheung et al. (2019) reported the (single) molar concentration normalized to dose per kilogram bodyweight, sampled at a wide range of times post-dose.[132] As such, the results are not comparable to those in **Paper I**, which is the first to prospectively evaluate the longitudinal pharmacokinetics of rosuvastatin in patients with severe obesity.

As the RYGB- and diet group achieved a similar weight loss during the initial LED, but also following RYGB and VLED, it was possible to directly compare change in oral clearance between the groups. However, a decrease of approximately

20% was observed following LED only, with no additional change after RYGB or VLED. As all patients were genotyped for mutations in *SLCO1B1*, we observed that this reduction was evident also in patients with the reduced function variant, suggesting that the observed change was not due to change in OATP1B1 activity *per se.* Liver size has been found to decrease, and composition especially with regards to sugars and fats has been found to change, following caloric restriction.[133] Additionally, hepatic blood flow has previously been shown to increase following bariatric surgery.[121, 122] This is especially important for a drug like rosuvastatin, which is associated with a high hepatic extration ratio of 0.63, for which an increase in blood flow may lead to an increased bioavailability.[49] While this may explain the reduced oral clearance following LED, further research of hepatic hemodynamics is warranted to confirm. With regards to hepatic composition, change in oral clearance was not associated with predicted liver fat, nor different in patients with predicted NAFLD-scores above and below diagnostic cut-offs, suggesting that liver composition alone does not explain our findings. A similar result was found in a cross-sectional analysis of patients with- and without MRI-confirmed NAFLD, revealing no differences in rosuvastatin pharmacokinetics.[134]

At year 2, the diet group had mostly returned to their baseline weights, and rosuvastatin pharmacokinetics were normalized as well. This is in contrast to the RYGB-group, for which oral clearance increased by approximately 21%. While there is no apparent explanation for this increase, it was postulated to be due to a surgery-specific effect that was not evident in the short-term, possibly due a reduced absorption due to anatomical alterations. While a semi-simultaneous administration of intravenous and oral rosuvastatin, similar to that performed for midazolam in the same patient population could illuminate the underlying mechanisms, this was not available or feasibile to accomplish for rosuvastatin in this study, and constitutes a weakness of the present work.[135] Additionally, the validity of the control group consisting of patients scheduled for cholecystectomy is uncertain, given the dependence of bile transport on rosuvastatin disposition and enterohepatic recirculation. The major strengths of this work is the large number of patients, the matched weight loss between intervention groups, and the accurate determination of oral clearance using population pharmacokinetic methods. Overall, there were no differences in rosuvastatin pharmacokinetics in patients with obesity when compared with a normal- to overweight control group, and longitudinal change in oral clearance, both short- and long-term following LED, RYGB or VLED. As such, no dose adjustments of rosuvastatin is warranted.

5.3 Gadobutrol as a tracer for estimating glymphatic clearance

Paper II presents a population pharmacokinetic model approach to estimate the clearance of intrathecally administered drugs using gadobutrol as a tracer. The two-compartmental model utilized first-order absorption and elimination to and from the central plasma compartment, respectively. In this context, the absorption of tracer to blood from CSF, or conversely, the elimination of tracer from CSF to

blood, was of primary interest. As such, the half-life of absorption was used as a surrogate marker for CSF to blood clearance, which is defined by Equation 5.1 below

$$t_{1/2,\text{absorption}} = \frac{\ln(2)}{K_a} \tag{5.1}$$

However, the appropriateness of such an index should be discussed. First, while half-life is proportional to, it does not equal clearance, which is defined as $CL = K_e \cdot V_d$. The apparent volume of distribution of tracer in CSF may be affected by patient variables, such as ventricular volume, height (as an index for spinal canal length), and total CSF volume. Some CSF disturbances, such as iNPH, is characterized by increased ventricle size.[136] While it was not included in **Paper II**, it is possible to evaluate the volume of the ventricles using MRI, which may provide additional information.[137] Second, the model-estimated value of K_a provides a measure of absorption to plasma only, which may not capture total clearance. The current glymphatic theory considers CSF egress through lymphatic vessels, from which absorption to blood may occur.[54] This is perhaps the greatest limitation of quantification in plasma only. However, the use of gadobutrol as the tracer of choice allows for additional quantitative insight into the brain-wide distribution of tracer. As a paramagnetic contrast agent, gadobutrol leads to a shortened T_1 and T_2 relaxation time of surrounding water protons, enhancing MRI signal intensity MRI.[138] The contrast-enhanced signal intensity may be converted to tracer concentration by measuring the T1 relaxation time prior to, and following, intrathecal injection of gadobutrol.[139] This allows for mathematical modelling of not only global, but regional diffusion of tracer.[140] In the work by Vinje, Zapf et al. (2023), estimated half-life along paravascular pathways was numerically similar to that reported in **Paper II**.[140] Such methods may also be coupled with population pharmacokinetic modelling, allowing for individual optimization of target-site exposure. One such work is currently in development by our research group, and preliminary results suggest significant interindividual variability in not only regional exposure in various compartments of the brain (lateral ventricles, cisterna magna, basal ganglia), but also the ratio of exposure between them (unpublished data).

Nevertheless, the key finding in **Paper II** remains the significant inter-individual variability in plasma disposition of gadobutrol, an index of glymphatic clearance, which was evident not only between the different CSF disorders, but also within. This is especially interesting for the iNPH-group, a disease with known heterogeneity, but equally so for the reference group.[136] In the reference group however, no association with age, height, or weight was found for the half-life of absorption. However, age correlated positively with time to maximum concentration in blood, which may be an indicator of neuraxial movement of CSF. Still, while no signs of CSF disturbances were found in the reference cohort, they should not be considered healthy. Due to the excessive strain on the patient in such investigations, glymphatic function has not been extensively studied in healthy volunteers. Still, smaller cohorts of healthy has been studied in literature;

Verma, Hesterman et al. (2020) employed a similar approach, using intrathecally administered ^{99m}Tc-DTPA in a cohort of 15 healthy volunteers, providing rough estimates of cranial CSF exposure.[141]

During the pilot study, samples collected and quantified for gadobutrol were in whole blood.[65] Later, and in **Paper II**, plasma samples were predominantly used. To utilize the full amount of available data, whole blood concentrations were interpolated to plasma concentrations using linear regression; a factor of 1.8 was found to adequately describe the relationship between the two matrixes. This factor indicates that gadobutrol has little to no association with red blood cells. While hematocrit was not reported in this patient cohort, the factor numerically aligns with its average value in healthy, adult individuals in the Nordic countries (35-50%).[142] This is further supported by the fact that gadobutrol has previously been established as having a very low degree of plasma-protein binding.[143, 144] This provides practical value, as venous sampling is considerably easier and cheaper compared with MRI. Should CSF to blood clearance prove to be clinically correlated in future works, limited sampling strategies may further alleviate the sampling burden by requiring fewer samples. Interfaces to limited sampling strategies have previously been developed for e.g. plasma iohexol clearance for determining mGFR, providing additional clinical applicability without the need for a professional trained in pharmacometrics.[145]

Further motivation is provided by the possibility of optimizing drug therapy of intrathecally administered drugs, such as methotrexate, used prophylactically in patients with acute lymphoblastic leukemia, which may induce severe myelopathy and neurotoxicity.[146, 147, 148] While some effort has been placed in monitoring CSF concentration of methotrexate, model-guided dosing remains to be used clinically.[149] Overall, pharmacometric analysis of intrathecally administered gadobutrol may provide clinically useful information in the diagnostics of CSF disorders, possibly alleviating the current reliance on magnetic resonance imaging techniques.

5.4 Semi-parametric simulation from discrete support points

For Paper III, simulation of new pharmacokinetic profiles played a crucial role. However, the current simulation engine implemented in Pmetrics for R is limited to a maximum of 30 support points, which was unable to capture the original distribution. As such, a manual implementation was required, which is discussed further. While simulation from parametric distributions is trivial, simulation from non-parametric distributions is more complex. In their review of non-parametric methods in population pharmacokinetics Goutelle, Woillard et al. (2022), present three known methods for simulation; A) sampling from the support points directly, B) sampling from the mean/median of the support points, and lastly, C) considering a normal distribution around each support point.[105] The first method alone should not be considered in any case where the desired number

of unique profiles per dose regimen extends beyond the number of support points. The second method relies on summary statistics such as the mean and standard deviation, which is not expected to fully capture a non-parametric distribution, especially in the case of multimodality. The third method assumes a Gaussian distribution around each support point, transforming the discrete distribution to a continuous one, modelled by a Gaussian mixture distribution. By taking advantage of this approach, it is possible to take advantage of parametric methods for sampling from an otherwise non-parametric distribution. The method is roughly visualized in Figure 5.15 below.
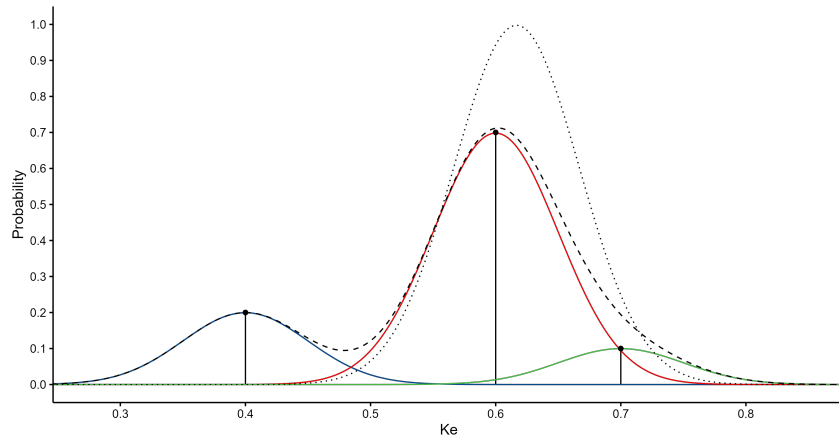
Figure 5.15: A three-support point example of semi-parametric simulation, where a Gaussian distribution is drawn around each support point, shown as solid lines. The resulting mixture distribution is represented as the dashed line. For comparison, the dotted line represents the Gaussian distribution for the weighted mean.

The multivariate Gaussian mixing distribution is the weighted sum of the probability density functions for each of the mixture components, with probability density function as shown in Equation 5.2 below

$$f(x) = \sum_{k=1}^{K} \phi_k \cdot \mathcal{N}(x; \mu_k, \Sigma_k) \quad \text{subject to} \quad \sum_{k=1}^{K} \phi_k = 1 \qquad (5.2)$$

Here, μ_k and Σ_k is the mean and the covariance matrix for the kth mixture, respectively, with weighting (or probability) ϕ_k. While μ_k is readily obtained from each support point, there is no obvious choice of Σ_k when simulating from discrete support points. As previously mentioned, the diagonal elements of a covariance matrix represent the variance of each parameter, while the off-diagonal elements represent the covariances between parameters. Mechanistically, in the non-parametric setting, an argument can be made for ignoring the covariance terms in Σ, i.e. $\sigma_{i \neq j} = 0$.

An argument for this will be presented for an example model parameterized over K_e (with bimodal distribution) and V (with unimodal distribution), adapted from Neely, van Guilder et al. (2012).[93] In Figure 5.16 below, the (Pearson's) correlation coefficient, which may be considered a scaled version of covariance, is shown for

different discrete regions of the joint parameter space. While the regions are roughly divided, it is clear that the correlation between these two parameters are non-constant throughout the parameter space, and not represented by the overall (Pearson's) correlation of $r = 0.08$. Improper off-diagonal elements in the covariance matrix introduces the risk of improper sampling. As such, in **Paper III**, they were set to zero, leaving the diagonal elements.
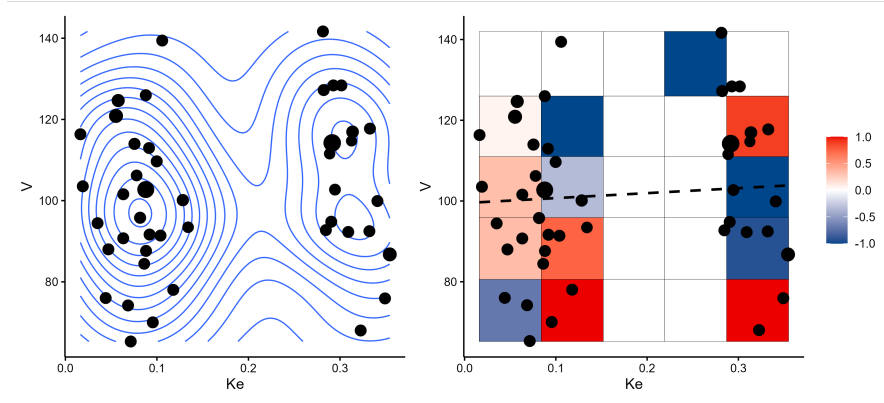
Figure 5.16: The two-dimensional density (left) and the windowed Pearson correlation (right) for an example, discrete distribution of support points, adapted from Neely, van Guilder et al. (2012).[93]

The choice of variance terms in Σ is not readily apparent, and several approaches were evaluated during method development in **Paper III**, and a brief summary of each is provided. First, the total variance was evaluated, but the magnitude of this value proved too large, flattening the Gaussian. Secondly, a windowing approach was used, where the local variance of the K-nearest neighboring support points was used, but this too degenerated the distribution around each support point. For both approaches, normalization by the support point probability did not improve distribution similarity, further discussed below. Finally, the variance was optimized to minimize the squared distance between the (unweighted) kernel density estimates of the individual posterior parameter distribution and the simulated. Still, a closed-form solution for the variance of multivariate mixing distributions would be preferrable, but has so far eluded current efforts .

Independent of the method chosen for simulation, it is important to define a metric for evaluating to which degree the simulated distribution represents the original distribution. Summary statistics alone, such as mean, variance, median, and interquartile range, are unlikely to adequately describe the possible multimodality of non-parametric distributions. Rather, the distributions themselves may be compared. One such measure is the overlap index, defined in Equation 5.3 below

$$\text{Overlap} \in [0, 1] = \int_{-\infty}^{-\infty} \min(f(x), g(x))dx \tag{5.3}$$

Where f(x) and g(x) are the probability density functions of the distributions to be compared. However, in order to apply this to non-parametric distributions,

a distribution-free overlapping index was used in **Paper III**.[117] Ideally, this or similar measures should be reported in all work relying on simulation. Other measures of distribution similarity exist, such as the Bhattacharyya and Hellinger distance, but remain to be evaluated in this context.[150, 151]

A major limitation of the method for simulation employed in **Paper III** was the exclusion of covariates from simulation. Initial attempts at augmenting the covariance matrix with the calculated variance and covariance between parameters was unsuccessful, and a mechanistic relationship between the covariate values and the support points could not be established. An interesting approach would be to consider the individual covariates as random variables, and fit them along the observed concentrations, and as such directly embed the covariates in the support points. As such, this approach should be investigated in a future work. Overall, the semi-parametric method for simulating from discrete support points proved effective, when using an optimized variance term for each individual parameter.

5.5   Robustness of limited sampling strategies

In **Paper III**, the main aim was to evaluate the robustness of a previously developed limited sampling strategy through simulation. This was accomplished by introducing random or empirical deviation in sample time for a large set of simulated pharmacokinetic profiles. Previous evaluations of robustness have been performed for strategies based on multiple linear regression and parametric pharmacokinetic models only.[152, 153, 154, 155] As such, **Paper III** seems the first to evaluate robustness in the non-parametric setting. Methodologically, evaluation of robustness in **Paper III** was carried out similar to aforementioned works. By introducing an empirical or random amount of deviation in sample time in simulated profiles, where the true value of interest is known through simulation, the resulting error can be evaluated, analogous to sensitivity analysis. As such, the main difference between the parametric and non-parametric approaches lies in the simulation, which was discussed previously.

A likely useful quantity that may be derived from robustness evaluation is an empirical sample window, i.e. a range of times for which a sample may be collected and still provide an average, acceptable error, or error rate. In **Paper III**, such windows were calculated with a cutoff of 2 mL min^{-1}, producing the following truncated sample windows for (individual) deviation in sample time: 10 [6-16] minutes, 30 (20-45) minutes, 2 (1.5-3) hours, and 5 (4.75-12) hours. However, this boldly assumes that the remaining samples were collected at their optimal sample times. Bayard and Neely (2017) have previously introduced a multiple model optimal experimental design approach for development of limited sampling strategies, by minimizing Bayes risk.[156] An advantage of this approach is that it also considers the noise in each response, which could theoretically be leveraged to estimate not only optimal sample times, but also sample windows, by transformation of noisy measurement, $y_i = \mu_i + \mathcal{N}(0, \sigma_i)$, to noise in sample time, by finding the coinciding time(s) t where $y(t) \approx y_i$ However, the feasibility of such a strategy must be confirmed in a future work.

Another important observation in **Paper III** was the sensitivity to deviation in sample time across simulated profiles with varying clearance. Patients with (simulated) GFR between 15-29 mL min^{-1} (Stage 4 CKD) and 30-44 mL min^{-1} (Stage 3b CKD) were especially affected, demonstrating an overall increase in median prediction error. In this clinical setting where mGFR is measured in routine visits, it is possible to use the eGFR based on the last serum creatinine to guide sample diligence. Possibly, separate limited sampling strategies should be developed for each stratum, but this could be difficult to implement in the clinical setting.

5.6 New tools for pharmacometric analyses

The work presented in this thesis relied heavily on Pmetrics for population pharmacokinetic modelling and simulation.[93] While the library and underlying Fortran routines are well established, several limitations were uncovered during method development. For large datasets with high-dimensional parameter spaces, such as in **Paper I**, the Fortran routines required modification to allow for the necessary memory allocations. Furthermore, in **Paper III**, it was revealed that the simulation engine was limited to the 30 most probable support points, and thus (possibly) unsuitable for simulation from 30 or more support points. While Fortran is computationally efficient, it lacks modern features and memory safety offered by newer programming languages.

As such, considerable efforts have been made to develop a new framework for non-parametric pharmacometric modelling in Rust, a memory-safe programming language boasting improved speed and concurrency. The library, PMcore, aims to primarily implement both NPAG and new non-parametric algorithms for pharmacokinetic modelling, such as simulated annealing, optimal design, and more.[157, 158] However, parametric algorithms will also be made available. Currently, only NPAG is implemented, and preliminary results indicates an overall 10-fold reduction in computation time, without the previously mentioned memory limitations (data not shown). Furthermore, the library aims to implement the simulation method detailed in **Paper III**, not limited to the 30 most probable support points. Already the library is implemented in, and available for use through, the development branch of Pmetrics. The project[I], for which the author is a maintainer and contributor, is publicly available and provided as open-source software under the GPL 3-0 license.[159]

Overall, the library aims to facilitate the development of new non-parametric algorithms, and provide Pmetrics and other software with a more powerful engine for parameter estimation and simulation.

[I]Available at **github.com/LAPKB/PMcore/**

Chapter 5. Discussion

Conclusion

The overall aim of this thesis was to apply pharmacometric analyses to diagnostic probes, utilizing population pharmacokinetics with a non-parametric approach. The utility of such analysis has been readily discussed, and the results from which are summarized below.

In **Paper I**, a study including patients with severe obesity undergoing Roux-en-Y gastric bypass surgery (RYGB) or strict diet, we found that neither body weight, weight loss, nor RYGB itself seem to affect activity in the hepatic uptake transporter OATP1B1 using rosuvastatin as a probe drug. Both the RYGB and diet led to a matched weight loss between the study groups, and the accompanying pharmacogenomic and proteomic analyses further illuminated determinants of rosuvastatin pharmacokinetics in patients with severe obesity, compared to a normal-to-overweight control group of patients undergoing cholecystectomy. Overall, the observed changes in rosuvastatin pharmacokinetics, accurately determined using a population pharmacokinetic model, following RYGB, diet, and the subsequent weight loss does not appear to be clinically relevant.

Paper II focused on patients with cerebrospinal fluid (CSF) disorders receiving intrathecally administered gadobutrol, a magnetic resonance imaging contrast agent. Through population pharmacokinetic modelling of plasma gadobutrol, we revealed significant variability in the CSF to blood clearance of gadobutrol, as an index of CSF egress. The variability was evident not only within, but also between, various CSF disorders. Pharmacometric analysis of intrathecal gadobutrol may as such provide a clinically valuable tool in the workup of and research in such disorders, given the role of CSF disposition in neurological disorders.

Finally, in **Paper III**, we evaluated the robustness of a previously published limited sampling strategy based on Bayesian estimates, for the determination of measured glomerular filtration rate (GFR) using iohexol serum clearance. Through semi-parametric simulation from a discrete population parameter distribution, two methods were used to evaluate robustness to deviation in sample time: by introducing an empirical amount of deviation for each individual sample point, or a normally distributed error across all sample points. Overall, the population pharmacokinetic model and limited sampling strategy proved robust to errors in sample time, which importantly with simulated GFR. For a given error threshold,

optimal sampling windows were estimated, providing additional flexibility in a clinical setting, possibly stratified by the stage of chronic kidney disease (CKD).

References

1. Kataoka M, Fukahori M, Ikemura A, Kubota A, Higashino H, Sakuma S, and Yamashita S. Effects of gastric pH on oral drug absorption: In vitro assessment using a dissolution/permeation system reflecting the gastric dissolution process. European Journal of Pharmaceutics and Biopharmaceutics. 2016 Apr; 101:103–11. DOI: 10.1016/j.ejpb.2016.02.002. Available from: https://www.ncbi.nlm.nih.gov/pubmed/26873006

2. Hellmig S, Von Schöning F, Gadow C, Katsoulis S, Hedderich J, Fölsch UR, and Stüber E. Gastric emptying time of fluids and solids in healthy subjects determined by 13C breath tests: influence of age, sex and body mass index. Journal of Gastroenterology and Hepatology. 2006 Oct; 21:1832–8. DOI: 10.1111/j.1440-1746.2006.04449.x. Available from: https://www.ncbi.nlm.nih.gov/pubmed/17074022

3. Vinarov Z, Abdallah M, Agundez JA, Allegaert K, Basit AW, Braeckmans M, Ceulemans J, Corsetti M, Griffin BT, Grimm M, Keszthelyi D, Koziolek M, Madla CM, Matthys C, McCoubrey LE, Mitra A, Reppas C, Stappaerts J, Steenackers N, Trevaskis NL, Vanuytsel T, Vertzoni M, Weitschies W, Wilson C, and Augustijns P. Impact of gastrointestinal tract variability on oral drug absorption and pharmacokinetics: An UNGAP review. European Journal of Pharmaceutical Sciences. 2021 Jul; 162:105812. DOI: 10.1016/j.ejps.2021.105812. Available from: https://www.ncbi.nlm.nih.gov/pubmed/33753215

4. Roberts AG. The Structure and Mechanism of Drug Transporters. Yeast Genetic Networks: Methods and Protocols. 2021; 2342:193–234. DOI: 10.1007/978-1-0716-1554-6_8. Available from: https://www.ncbi.nlm.nih.gov/pubmed/34272696

5. Borst P, Evers R, Kool M, and Wijnholds J. A Family of Drug Transporters: the Multidrug Resistance-Associated Proteins. JNCI Journal of the National Cancer Institute. 2000 Aug; 92:1295–302. DOI: 10.1093/jnci/92.16.1295. Available from: https://www.ncbi.nlm.nih.gov/pubmed/10944550

6. Lin JH and Yamazaki M. Role of P-Glycoprotein in Pharmacokinetics: Clinical Implications. Clinical Pharmacokinetics. 2003; 42:59–98. DOI: 10.2165/00003088-200342010-00003. Available from: https://www.ncbi.nlm.nih.gov/pubmed/12489979

7. Kusuhara H and Sugiyama Y. Role of transporters in the tissue-selective distribution and elimination of drugs: transporters in the liver, small intestine, brain and kidney. Journal of Controlled Release. 2002 Jan; 78:43–54. DOI: 10.1016/s0168-3659(01)00480-1. Available from: https://www.ncbi.nlm.nih.gov/pubmed/11772448

8. Lapczuk-Romanska J, Drozdzik M, Oswald S, and Drozdzik M. Kidney Drug Transporters in Pharmacotherapy. International Journal of Molecular Sciences. 2023 Feb; 24:2856. DOI: 10.3390/ijms24032856. Available from: https://www.ncbi.nlm.nih.gov/pubmed/36769175

9. Järvinen E, Deng F, Kiander W, Sinokki A, Kidron H, and Sjöstedt N. The Role of Uptake and Efflux Transporters in the Disposition of Glucuronide and Sulfate Conjugates. Frontiers in Pharmacology. 2022 Jan; 12:802539. DOI: 10.3389/fphar.2021.802539. Available from: https://www.ncbi.nlm.nih.gov/pubmed/35095509

10. Rendic S and Guengerich FP. Survey of Human Oxidoreductases and Cytochrome P450 Enzymes Involved in the Metabolism of Xenobiotic and Natural Chemicals. Chemical Research in Toxicology. 2014 Dec; 28:38–42. DOI: 10.1021/tx500444e. Available from: https://www.ncbi.nlm.nih.gov/pubmed/25485457

11. Tracy TS, Chaudhry AS, Prasad B, Thummel KE, Schuetz EG, Zhong XB, Tien YC, Jeong H, Pan X, Shireman LM, Tay-Sontheimer J, and Lin YS. Interindividual Variability in Cytochrome P450-Mediated Drug Metabolism. Drug Metabolism and Disposition. 2015 Dec; 44:343–51. DOI: 10.1124/dmd.115.067900. Available from: https://www.ncbi.nlm.nih.gov/pubmed/26681736

12. Tsunoda SM, Gonzales C, Jarmusch AK, Momper JD, and Ma JD. Contribution of the Gut Microbiome to Drug Disposition, Pharmacokinetic and Pharmacodynamic Variability. Clinical Pharmacokinetics. 2021 May; 60:971–84. DOI: 10.1007/s40262-021-01032-y. Available from: https://www.ncbi.nlm.nih.gov/pubmed/33959897

13. Bullingham RE, Nicholls AJ, and Kamm BR. Clinical Pharmacokinetics of Mycophenolate Mofetil. Clinical Pharmacokinetics. 1998; 34:429–55. DOI: 10.2165/00003088-199834060-00002. Available from: https://www.ncbi.nlm.nih.gov/pubmed/9646007

14. Staatz CE and Tett SE. Clinical Pharmacokinetics and Pharmacodynamics of Mycophenolate in Solid Organ Transplant Recipients. Clinical Pharmacokinetics. 2007; 46:13–58. DOI: 10.2165/00003088-200746010-00002. Available from: https://www.ncbi.nlm.nih.gov/pubmed/17201457

15. Manes A, Di Renzo T, Dodani L, Reale A, Gautiero C, Di Lauro M, Nasti G, Manco F, Muscariello E, Guida B, Tarantino G, and Cataldi M. Pharmacomicrobiomics of Classical Immunosuppressant Drugs: A Systematic Review. Biomedicines. 2023 Sep; 11:2562. DOI: 10.3390/biomedicines11092562. Available from: https://www.ncbi.nlm.nih.gov/pubmed/37761003

16. Ghibellini G, Leslie EM, and Brouwer KLR. Methods To Evaluate Biliary Excretion of Drugs in Humans: An Updated Review. Molecular Pharmaceutics. 2006 Apr; 3:198–211. DOI: 10.1021/mp060011k. Available from: https://www.ncbi.nlm.nih.gov/pubmed/16749853

17. Kitamura S, Maeda K, Wang Y, and Sugiyama Y. Involvement of Multiple Transporters in the Hepatobiliary Transport of Rosuvastatin. Drug Metabolism and Disposition. 2008 Jul; 36:2014–23. DOI: 10.1124/dmd.108.021410. Available from: https://www.ncbi.nlm.nih.gov/pubmed/18617601

18. Roberts MS, Magnusson BM, Burczynski FJ, and Weiss M. Enterohepatic Circulation: Physiological, Pharmacokinetic and Clinical Implications. Clinical Pharmacokinetics. 2002; 41:751–90. DOI: 10.2165/00003088-200241100-00005. Available from: https://www.ncbi.nlm.nih.gov/pubmed/12162761

19. Bergman E, Forsell P, Tevell A, Persson EM, Hedeland M, Bondesson U, Knutson L, and Lennernäs H. Biliary secretion of rosuvastatin and bile acids in humans during the absorption phase. European Journal of Pharmaceutical Sciences. 2006 Nov; 29:205–14. DOI: 10.1016/j.ejps.2006.04.015. Available from: https://www.ncbi.nlm.nih.gov/pubmed/16806856

20. Lehmann T, Kohler C, Weidauer E, Taege C, and Foth H. Expression of MRP1 and related transporters in human lung cells in culture. Toxicology. 2001 Oct; 167:59–72. DOI: 10.1016/s0300-483x(01)00458-9. Available from: https://www.ncbi.nlm.nih.gov/pubmed/11557130

21. Deen M van der, Vries EG de, Timens W, Scheper RJ, Timmer-Bosscha H, and Postma DS. ATP-binding cassette (ABC) transporters in normal and pathological lung. Respiratory Research. 2005 Jun; 6:59. DOI: 10.1186/1465-9921-6-59. Available from: https://www.ncbi.nlm.nih.gov/pubmed/15967026

22. Collaborators GBDO et al. Health Effects of Overweight and Obesity in 195 Countries over 25 Years. New England Journal of Medicine. 2017 Jul; 377:13–27. DOI: 10.1056/nejmoa1614362. Available from: https://www.ncbi.nlm.nih.gov/pubmed/28604169

23. Midthjell K, Lee CMY, Langhammer A, Krokstad S, Holmen TL, Hveem K, Colagiuri S, and Holmen J. Trends in overweight and obesity over 22 years in a large adult population: the HUNT Study, Norway. Clinical Obesity. 2013 Feb; 3:12–20. DOI: 10.1111/cob.12009. Available from: https://www.ncbi.nlm.nih.gov/pubmed/23935708

24. Løvsletten O, Jacobsen BK, Grimsgaard S, Njølstad I, Wilsgaard T, Løchen ML, Eggen AE, and Hopstock LA. Prevalence of general and abdominal obesity in 2015–2016 and 8-year longitudinal weight and waist circumference changes in adults and elderly: the Tromsø Study. BMJ Open. 2020 Nov; 10:e038465. DOI: 10.1136/bmjopen-2020-038465. Available from: https://www.ncbi.nlm.nih.gov/pubmed/33154051

25. Müller MJ, Braun W, Enderle J, and Bosy-Westphal A. Beyond BMI: Conceptual Issues Related to Overweight and Obese Patients. Obesity Facts. 2016; 9:193–205. DOI: 10.1159/000445380. Available from: https://www.ncbi.nlm.nih.gov/pubmed/27286962

26. Ruder K. Mounting Evidence Suggests That BMI Isn't the Only Measure Needed to Predict Mortality Risk. JAMA. 2023 Aug; 330:490. DOI: 10.1001/jama.2023.13602. Available from: https://www.ncbi.nlm.nih.gov/pubmed/37466937

27. Visaria A and Setoguchi S. Body mass index and all-cause mortality in a 21st century U.S. population: A National Health Interview Survey analysis. PLOS ONE. 2023 Jul; 18. Ed. by Ehrlich SF:e0287218. DOI: 10.1371/journal.pone.0287218. Available from: https://www.ncbi.nlm.nih.gov/pubmed/37405977

28. Fabbrini E, Sullivan S, and Klein S. Obesity and nonalcoholic fatty liver disease: Biochemical, metabolic, and clinical implications. Hepatology. 2009 Sep; 51:679–89. DOI: 10.1002/hep.23280. Available from: https://www.ncbi.nlm.nih.gov/pubmed/20041406

29. Quek J, Chan KE, Wong ZY, Tan C, Tan B, Lim WH, Tan DJH, Tang ASP, Tay P, Xiao J, Yong JN, Zeng RW, Chew NWS, Nah B, Kulkarni A, Siddiqui MS, Dan YY, Wong VWS, Sanyal AJ, Noureddin M, Muthiah M, and Ng CH. Global prevalence of non-alcoholic fatty liver disease and non-alcoholic steatohepatitis in the overweight and obese population: a systematic review and meta-analysis. The Lancet Gastroenterology and Hepatology. 2023 Jan; 8:20–30. DOI: 10.1016/s2468-1253(22)00317-x. Available from: https://www.ncbi.nlm.nih.gov/pubmed/36400097

30. Jamwal R and Barlock BJ. Nonalcoholic Fatty Liver Disease (NAFLD) and Hepatic Cytochrome P450 (CYP) Enzymes. Pharmaceuticals. 2020 Aug; 13:222. DOI: 10.3390/ph13090222. Available from: https://www.ncbi.nlm.nih.gov/pubmed/32872474

31. Dietrich CG, Rau M, Jahn D, and Geier A. Changes in drug transport and metabolism and their clinical implications in non-alcoholic fatty liver disease. Expert Opinion on Drug Metabolism and Toxicology. 2017 Apr; 13:625–40. DOI: 10.1080/17425255.2017.1314461. Available from: https://www.ncbi.nlm.nih.gov/pubmed/28359183

32. Knibbe CAJ, Brill MJE, Rongen A van, Diepstraten J, Graaf PH van der, and Danhof M. Drug Disposition in Obesity: Toward Evidence-Based Dosing. Annual Review of Pharmacology and Toxicology. 2015 Jan; 55:149–67. DOI: 10.1146/annurev-pharmtox-010814-124354. Available from: https://www.ncbi.nlm.nih.gov/pubmed/25340929

33. Cypess AM. Reassessing Human Adipose Tissue. New England Journal of Medicine. 2022 Feb; 386. Ed. by Ingelfinger JR:768–79. DOI: 10.1056/nejmra2032804. Available from: https://www.ncbi.nlm.nih.gov/pubmed/35196429

34. Brill MJ, Diepstraten J, Rongen A van, Kralingen S van, Anker JN van den, and Knibbe CA. Impact of Obesity on Drug Metabolism and Elimination in Adults and Children. Clinical Pharmacokinetics. 2012 May; 51:277–304. DOI: 10.2165/11599410-000000000-00000. Available from: https://www.ncbi.nlm.nih.gov/pubmed/22448619

35. Mahmood I. Prediction of Clearance and Volume of Distribution in the Obese from Normal Weight Subjects: An Allometric Approach. Clinical Pharmacokinetics. 2012 Aug; 51:527–42. DOI: 10.1007/bf03261929. Available from: https://www.ncbi.nlm.nih.gov/pubmed/22671778

36. Ashar BH. In Search of the 70-kg Man. Medical Clinics of North America. 2018 Jan; 102:xv–xvi. DOI: 10.1016/j.mcna.2017.09.004. Available from: https://www.ncbi.nlm.nih.gov/pubmed/29156190

37. Schauer PR, Bhatt DL, Kirwan JP, Wolski K, Brethauer SA, Navaneethan SD, Aminian A, Pothier CE, Kim ES, Nissen SE, and Kashyap SR. Bariatric Surgery versus Intensive Medical Therapy for Diabetes — 3-Year Outcomes. New England Journal of Medicine. 2014 May; 370:2002–13. DOI: 10.1056/nejmoa1401329. Available from: https://www.ncbi.nlm.nih.gov/pubmed/24679060

38. Courcoulas AP, Belle SH, Neiberg RH, Pierson SK, Eagleton JK, Kalarchian MA, DeLany JP, Lang W, and Jakicic JM. Three-Year Outcomes of Bariatric Surgery vs Lifestyle Intervention for Type 2 Diabetes Mellitus Treatment: A Randomized Clinical Trial. JAMA Surgery. 2015 Oct; 150:931. DOI: 10.1001/jamasurg.2015.1534. Available from: https://www.ncbi.nlm.nih.gov/pubmed/26132586

39. Pucci A and Batterham RL. Mechanisms underlying the weight loss effects of RYGB and SG: similar, yet different. Journal of Endocrinological Investigation. 2018 May; 42:117–28. DOI: 10.1007/s40618-018-0892-2. Available from: https://www.ncbi.nlm.nih.gov/pubmed/29730732

40. Angeles PC, Robertsen I, Seeberg LT, Krogstad V, Skattebu J, Sandbu R, Åsberg A, and Hjelmesæth J. The influence of bariatric surgery on oral drug bioavailability in patients with obesity: A systematic review. Obesity Reviews. 2019 Jun; 20:1299–311. DOI: 10.1111/obr.12869. Available from: https://www.ncbi.nlm.nih.gov/pubmed/31232513

41. Niemi M, Pasanen MK, and Neuvonen PJ. Organic Anion Transporting Polypeptide 1B1: a Genetically Polymorphic Transporter of Major Importance for Hepatic Drug Uptake. Pharmacological Reviews. 2011 Jan; 63. Ed. by Koulu M:157–81. DOI: 10.1124/pr.110.002857. Available from: https://www.ncbi.nlm.nih.gov/pubmed/21245207

42. Kalliokoski A and Niemi M. Impact of OATP transporters on pharmacokinetics. British Journal of Pharmacology. 2009 Oct; 158:693–705. DOI: 10.1111/j.1476-5381.2009.00430.x. Available from: https://www.ncbi.nlm.nih.gov/pubmed/19785645

References

43. Yamaguchi H, Takeuchi T, Okada M, Kobayashi M, Unno M, Abe T, Goto J, Hishinuma T, Shimada M, and Mano N. Screening of Antibiotics That Interact with Organic Anion-Transporting Polypeptides 1B1 and 1B3 Using Fluorescent Probes. Biological and Pharmaceutical Bulletin. 2011; 34:389–95. DOI: 10.1248/bpb.34.389. Available from: https://www.ncbi.nlm.nih.gov/pubmed/21372390

44. Mercep I, Radman I, Trkulja V, Bozina T, Simicevic L, Budimir E, Ganoci L, and Bozina N. Loss of function polymorphisms in SLCO1B1 (c.521T>C, rs4149056) and ABCG2 (c.421C>A, rs2231142) genes are associated with adverse events of rosuvastatin: a case-control study. European Journal of Clinical Pharmacology. 2021 Oct; 78:227–36. DOI: 10.1007/s00228-021-03233-7. Available from: https://www.ncbi.nlm.nih.gov/pubmed/34668025

45. McFeely SJ, Ritchie TK, Yu J, Nordmark A, Levy RH, and Ragueneau-Majlessi I. Identification and Evaluation of Clinical Substrates of Organic Anion Transporting Polypeptides 1B1 and 1B3. Clinical and Translational Science. 2019 Mar; 12:379–87. DOI: 10.1111/cts.12623. Available from: https://www.ncbi.nlm.nih.gov/pubmed/30706983

46. Chapman M and McTaggart F. Optimizing the pharmacology of statins: characteristics of rosuvastatin. Atherosclerosis Supplements. 2002 Apr; 2:33–7. DOI: 10.1016/s1567-5688(01)00016-2. Available from: https://www.ncbi.nlm.nih.gov/pubmed/11976075

47. Shitara Y, Maeda K, Ikejiri K, Yoshida K, Horie T, and Sugiyama Y. Clinical significance of organic anion transporting polypeptides (OATPs) in drug disposition: their roles in hepatic clearance and intestinal absorption. Biopharmaceutics and Drug Disposition. 2013 Jan; 34:45–78. DOI: 10.1002/bdd.1823. Available from: https://www.ncbi.nlm.nih.gov/pubmed/23115084

48. Zhang D, Ding Y, Wang X, Xin W, Du W, Chen W, Zhang X, and Li P. Effects of ABCG2 and SLCO1B1 gene variants on inflammation markers in patients with hypercholesterolemia and diabetes mellitus treated with rosuvastatin. European Journal of Clinical Pharmacology. 2020 May; 76:939–46. DOI: 10.1007/s00228-020-02882-4. Available from: https://www.ncbi.nlm.nih.gov/pubmed/32361904

49. Martin PD, Warwick MJ, Dane AL, Hill SJ, Giles PB, Phillips PJ, and Lenz E. Metabolism, excretion, and pharmacokinetics of rosuvastatin in healthy adult male volunteers. Clinical Therapeutics. 2003 Nov; 25:2822–35. DOI: 10.1016/s0149-2918(03)80336-3. Available from: https://www.ncbi.nlm.nih.gov/pubmed/14693307

50. Bergman E, Lundahl A, Fridblom P, Hedeland M, Bondesson U, Knutson L, and Lennernäs H. Enterohepatic Disposition of Rosuvastatin in Pigs and the Impact of Concomitant Dosing with Cyclosporine and Gemfibrozil. Drug Metabolism and Disposition. 2009 Sep; 37:2349–58. DOI: 10.1124/dmd.109.029363. Available from: https://www.ncbi.nlm.nih.gov/pubmed/19773540

51. MacAulay N and Toft-Bertelsen TL. Dual function of the choroid plexus: Cerebrospinal fluid production and control of brain ion homeostasis. Cell Calcium. 2023 Dec; 116:102797. DOI: 10.1016/j.ceca.2023.102797. Available from: https://www.ncbi.nlm.nih.gov/pubmed/37801806

52. MacAulay N, Keep RF, and Zeuthen T. Cerebrospinal fluid production by the choroid plexus: a century of barrier research revisited. Fluids and Barriers of the CNS. 2022 Mar; 19:26. DOI: 10.1186/s12987-022-00323-1. Available from: https://www.ncbi.nlm.nih.gov/pubmed/35317823

53. Hladky SB and Barrand MA. The glymphatic hypothesis: the theory and the evidence. Fluids and Barriers of the CNS. 2022 Feb; 19:9. DOI: 10.1186/s12987-021-00282-z. Available from: https://www.ncbi.nlm.nih.gov/pubmed/35115036

54. Rasmussen MK, Mestre H, and Nedergaard M. Fluid transport in the brain. Physiological Reviews. 2022 Apr; 102:1025–151. DOI: 10.1152/physrev.00031.2020. Available from: https://www.ncbi.nlm.nih.gov/pubmed/33949874

55. Abbott NJ. Dynamics of CNS Barriers: Evolution, Differentiation, and Modulation. Cellular and Molecular Neurobiology. 2005 Feb; 25:5–23. DOI: 10.1007/s10571-004-1374-y. Available from: https://www.ncbi.nlm.nih.gov/pubmed/15962506

56. Kadry H, Noorani B, and Cucullo L. A blood–brain barrier overview on structure, function, impairment, and biomarkers of integrity. Fluids and Barriers of the CNS. 2020 Nov; 17:69. DOI: 10.1186/s12987-020-00230-3. Available from: https://www.ncbi.nlm.nih.gov/pubmed/33208141

57. Lipinski CA, Lombardo F, Dominy BW, and Feeney PJ. Experimental and computational approaches to estimate solubility and permeability in drug discovery and development settings. Advanced Drug Delivery Reviews. 2001 Mar; 46:3–26. DOI: 10.1016/s0169-409x(00)00129-0. Available from: https://www.ncbi.nlm.nih.gov/pubmed/11259830

58. Henderson J and Piquette-Miller M. Blood–brain barrier: An impediment to neuropharmaceuticals. Clinical Pharmacology and Therapeutics. 2015 Feb; 97:308–13. DOI: 10.1002/cpt.77. Available from: https://www.ncbi.nlm.nih.gov/pubmed/25670372

59. Pardridge WM. The blood-brain barrier: Bottleneck in brain drug development. NeuroRX. 2005 Jan; 2:3–14. DOI: 10.1602/neurorx.2.1.3. Available from: https://www.ncbi.nlm.nih.gov/pubmed/15717053

60. Raaphorst R, Windhorst A, Elsinga P, Colabufo N, Lammertsma A, and Luurtsema G. Radiopharmaceuticals for assessing ABC transporters at the blood–brain barrier. Clinical Pharmacology and Therapeutics. 2015 Feb; 97:362–71. DOI: 10.1002/cpt.73. Available from: https://www.ncbi.nlm.nih.gov/pubmed/25669763

61. De Andres J, Hayek S, Perruchoud C, Lawrence MM, Reina MA, De Andres-Serrano C, Rubio-Haro R, Hunt M, and Yaksh TL. Intrathecal Drug Delivery: Advances and Applications in the Management of Chronic Pain Patient. Frontiers in Pain Research. 2022 Jun; 3:900566. DOI: 10.3389/fpain.2022.900566. Available from: https://www.ncbi.nlm.nih.gov/pubmed/35782225

62. Iliff JJ, Wang M, Liao Y, Plogg BA, Peng W, Gundersen GA, Benveniste H, Vates GE, Deane R, Goldman SA, Nagelhus EA, and Nedergaard M. A Paravascular Pathway Facilitates CSF Flow Through the Brain Parenchyma and the Clearance of Interstitial Solutes, Including Amyloid β. Science Translational Medicine. 2012 Aug; 4:147ra111. DOI: 10.1126/scitranslmed.3003748. Available from: https://www.ncbi.nlm.nih.gov/pubmed/22896675

63. Buccellato FR, D'Anca M, Serpente M, Arighi A, and Galimberti D. The Role of Glymphatic System in Alzheimer's and Parkinson's Disease Pathogenesis. Biomedicines. 2022 Sep; 10:2261. DOI: 10.3390/biomedicines10092261. Available from: https://www.ncbi.nlm.nih.gov/pubmed/36140362

64. Rekate HL. A Contemporary Definition and Classification of Hydrocephalus. Seminars in Pediatric Neurology. 2009 Mar; 16:9–15. DOI: 10.1016/j.spen.2009.01.002. Available from: https://www.ncbi.nlm.nih.gov/pubmed/19410151

65. Eide PK, Mariussen E, Uggerud H, Pripp AH, Lashkarivand A, Hassel B, Christensen H, Hovd MH, and Ringstad G. Clinical application of intrathecal gadobutrol for assessment of cerebrospinal fluid tracer clearance to blood. JCI Insight. 2021 May; 6. DOI: 10.1172/jci.insight.147063. Available from: https://www.ncbi.nlm.nih.gov/pubmed/33822769

66. Hahn G, Sorge I, Gruhn B, Glutig K, Hirsch W, Bhargava R, Furtner J, Born M, Schröder C, Ahlström H, Kaiser S, Moritz JD, Kunze CW, Shroff M, Stokland E, Trnkova ZJ, Schultze-Mosgau M, Reif S, Bacher-Stier C, and Mentzel HJ. Pharmacokinetics and Safety of Gadobutrol-Enhanced Magnetic Resonance Imaging in Pediatric Patients. Investigative Radiology. 2009 Dec; 44:776–83. DOI: 10.1097/rli.0b013e3181bfe2d2. Available from: https://www.ncbi.nlm.nih.gov/pubmed/19858730

67. Ringstad G, Valnes LM, Vatnehol SAS, Pripp AH, and Eide PK. Prospective T1 mapping to assess gadolinium retention in brain after intrathecal gadobutrol. Neuroradiology. 2023 Jul; 65:1321–31. DOI: 10.1007/s00234-023-03198-7. Available from: https://www.ncbi.nlm.nih.gov/pubmed/37479768

68. Sperre A, Karsrud I, Rodum A, Lashkarivand A, Valnes L, Ringstad G, and Eide P. Prospective Safety Study of Intrathecal Gadobutrol in Different Doses. American Journal of Neuroradiology. 2023 Apr; 44:511–6. DOI: 10.3174/ajnr.a7841. Available from: https://www.ncbi.nlm.nih.gov/pubmed/37024308

69. McDonald JS, Hunt CH, Kolbe AB, Schmitz JJ, Hartman RP, Maddox DE, Kallmes DF, and McDonald RJ. Acute Adverse Events Following Gadolinium-based Contrast Agent Administration: A Single-Center Retrospective Study of 281 945 Injections. Radiology. 2019 Sep; 292:620–7. DOI: 10.1148/radiol.2019182834. Available from: https://www.ncbi.nlm.nih.gov/pubmed/31264948

70. D'Agati VD, Chagnac A, Vries AP de, Levi M, Porrini E, Herman-Edelstein M, and Praga M. Obesity-related glomerulopathy: clinical and pathologic characteristics and pathogenesis. Nature Reviews Nephrology. 2016 Jun; 12:453–71. DOI: 10.1038/nrneph.2016.75. Available from: https://www.ncbi.nlm.nih.gov/pubmed/27263398

71. Filippone E, Kraft W, and Farber J. The Nephrotoxicity of Vancomycin. Clinical Pharmacology and Therapeutics. 2017 Jun; 102:459–69. DOI: 10.1002/cpt.726. Available from: https://www.ncbi.nlm.nih.gov/pubmed/28474732

72. Lalande L, Charpiat B, Leboucher G, and Tod M. Consequences of Renal Failure on Non-Renal Clearance of Drugs. Clinical Pharmacokinetics. 2014 May; 53:521–32. DOI: 10.1007/s40262-014-0146-1. Available from: https://www.ncbi.nlm.nih.gov/pubmed/24861189

73. Nolin TD. A Synopsis of Clinical Pharmacokinetic Alterations in Advanced <scp>CKD</scp>. Seminars in Dialysis. 2015 Apr; 28:325–9. DOI: 10.1111/sdi.12374. Available from: https://www.ncbi.nlm.nih.gov/pubmed/25855244

74. Webster AC, Nagler EV, Morton RL, and Masson P. Chronic Kidney Disease. The Lancet. 2017 Mar; 389:1238–52. DOI: 10.1016/s0140-6736(16)32064-5. Available from: https://www.ncbi.nlm.nih.gov/pubmed/27887750

75. Hill NR, Fatoba ST, Oke JL, Hirst JA, O'Callaghan CA, Lasserson DS, and Hobbs FDR. Global Prevalence of Chronic Kidney Disease – A Systematic Review and Meta-Analysis. PLOS ONE. 2016 Jul; 11. Ed. by Remuzzi G:e0158765. DOI: 10.1371/journal.pone.0158765. Available from: https://www.ncbi.nlm.nih.gov/pubmed/27383068

76. Group KUW. KDIGO 2017. Clinical Practice Guideline Update for the Diagnosis, Evaluation, Prevention, and Treatment of Chronic Kidney Disease — Mineral and Bone Disorder (CKD-MBD). Kidney International Supplements. 2021 Sep; 3. KDIGO 2012 Clinical Practice Guideline for the Evaluation and Management of Chronic Kidney Disease:149–54. DOI: 10.22141/2307-1257.6.3.2017.109030. Available from: https://www.sciencedirect.com/science/article/pii/S2157171615311011

77. Cockcroft DW and Gault H. Prediction of Creatinine Clearance from Serum Creatinine. Nephron. 1976; 16:31–41. DOI: 10.1159/000180580. Available from: https://www.ncbi.nlm.nih.gov/pubmed/1244564

78. Inker LA, Eneanya ND, Coresh J, Tighiouart H, Wang D, Sang Y, Crews DC, Doria A, Estrella MM, Froissart M, Grams ME, Greene T, Grubb A, Gudnason V, Gutiérrez OM, Kalil R, Karger AB, Mauer M, Navis G, Nelson RG, Poggio ED, Rodby R, Rossing P, Rule AD, Selvin E, Seegmiller JC, Shlipak MG, Torres VE, Yang W, Ballew SH, Couture SJ, Powe NR, and Levey AS. New Creatinine- and Cystatin C–Based Equations to Estimate GFR without Race. New England Journal of Medicine. 2021 Nov; 385:1737–49. DOI: 10.1056/nejmoa2102953. Available from: https://www.ncbi.nlm.nih.gov/pubmed/34554658

79. Porrini E, Ruggenenti P, Luis-Lima S, Carrara F, Jiménez A, Vries APJ de, Torres A, Gaspari F, and Remuzzi G. Estimated GFR: time for a critical appraisal. Nature Reviews Nephrology. 2018 Dec; 15:177–90. DOI: 10.1038/s41581-018-0080-9. Available from: https://www.ncbi.nlm.nih.gov/pubmed/30518813

80. Luis-Lima S and Porrini E. An Overview of Errors and Flaws of Estimated GFR versus True GFR in Patients with Diabetes Mellitus. Nephron. 2016 Dec; 136:287–91. DOI: 10.1159/000453531. Available from: https://www.ncbi.nlm.nih.gov/pubmed/27978513

81. Levey AS. Measurement of renal function in chronic renal disease. Kidney International. 1990 Jul; 38:167–84. DOI: 10.1038/ki.1990.182. Available from: https://www.ncbi.nlm.nih.gov/pubmed/2200925

82. Levey A and Inker L. Assessment of Glomerular Filtration Rate in Health and Disease: A State of the Art Review. Clinical Pharmacology and Therapeutics. 2017 Jun; 102:405–19. DOI: 10.1002/cpt.729. Available from: https://www.ncbi.nlm.nih.gov/pubmed/28474735

83. Soveri I, Berg UB, Björk J, Elinder CG, Grubb A, Mejare I, Sterner G, and Bäck SE. Measuring GFR: A Systematic Review. American Journal of Kidney Diseases. 2014 Sep; 64:411–24. DOI: 10.1053/j.ajkd.2014.04.010. Available from: https://www.ncbi.nlm.nih.gov/pubmed/24840668

84. Gaspari F, Thakar S, Carrara F, Perna A, Trillini M, Aparicio MC, Diadei O, Ferrari S, Cannata A, Stucchi N, Ruggenenti P, Remuzzi G, and Perico N. Safety of Iohexol Administration to Measure Glomerular Filtration Rate in Different Patient Populations: A 25-Year Experience. Nephron. 2018; 140:1–8. DOI: 10.1159/000489898. Available from: https://www.ncbi.nlm.nih.gov/pubmed/29772565

85. Nordin G, Ekvall S, Kristoffersson C, Jonsson AS, Bäck SE, Rollborn N, and Larsson A. Accuracy of determination of the glomerular filtration marker iohexol by European laboratories as monitored by external quality assessment. Clinical Chemistry and Laboratory Medicine. 2019 May; 57:1006–11. DOI: 10.1515/cclm-2018-1175. Available from: https://www.ncbi.nlm.nih.gov/pubmed/31075079

86. Åsberg A, Bjerre A, Almaas R, Luis-Lima S, Robertsen I, Salvador CL, Porrini E, Schwartz GJ, Hartmann A, and Bergan S. Measured GFR by Utilizing Population Pharmacokinetic Methods to Determine Iohexol Clearance. Kidney International Reports. 2020 Feb; 5:189–98. DOI: 10.1016/j.ekir.2019.11.012. Available from: https://www.ncbi.nlm.nih.gov/pubmed/32043033

87. Taubert M, Schaeffner E, Martus P, Giet M van der, Fuhr U, Lösment A, and Ebert N. Advancement of pharmacokinetic models of iohexol in patients aged 70 years or older with impaired kidney function. Scientific Reports. 2021 Nov; 11:22656. DOI: 10.1038/s41598-021-01892-1. Available from: https://www.ncbi.nlm.nih.gov/pubmed/34811403

88. Destere A, Salmon Gandonnière C, Åsberg A, Loustaud-Ratti V, Carrier P, Ehrmann S, Barin-Le Guellec C, Marquet P, and Woillard JB. A single Bayesian estimator for iohexol clearance estimation in ICU, liver failure and renal transplant patients. British Journal of Clinical Pharmacology. 2022 Jan; 88:2793–801. DOI: 10.1111/bcp.15197. Available from: https://www.ncbi.nlm.nih.gov/pubmed/34951499

89. Bonate PL. Pharmacokinetic-Pharmacodynamic Modeling and Simulation. New York, NY: Springer US, 2011 :xii, 387 p. DOI: 10.1007/978-1-4419-9485-1

90. Mould D and Upton R. Basic Concepts in Population Modeling, Simulation, and Model-Based Drug Development. CPT: Pharmacometrics and Systems Pharmacology. 2012 Sep; 1:1–14. DOI: 10.1038/psp.2012.4

91. Mould D and Upton R. Basic Concepts in Population Modeling, Simulation, and Model-Based Drug Development—Part 2: Introduction to Pharmacokinetic Modeling Methods. CPT: Pharmacometrics and Systems Pharmacology. 2013 Apr; 2:1–14. DOI: 10.1038/psp.2013.14

92. Abuhelwa AY, Foster DJ, and Upton RN. ADVAN-style analytical solutions for common pharmacokinetic models. Journal of Pharmacological and Toxicological Methods. 2015 May; 73:42–8. DOI: 10.1016/j.vascn.2015.03.004. ppublish

93. Neely MN, Guilder MG van, Yamada WM, Schumitzky A, and Jelliffe RW. Accurate detection of outliers and subpopulations with Pmetrics, a nonparametric and parametric pharmacometric modeling and simulation package for R. Therapeutic Drug Monitoring. 2012; 34:467–76. DOI: 10.1097/FTD.0b013e31825c4ba6. Available from: https://www.ncbi.nlm.nih.gov/pubmed/22722776

94. Goutelle S, Woillard JB, Buclin T, Bourguignon L, Yamada W, Csajka C, Neely M, and Guidi M. Parametric and Nonparametric Methods in Population Pharmacokinetics: Experts' Discussion on Use, Strengths, and Limitations. The Journal of Clinical Pharmacology. 2021 Dec; 62:158–70. DOI: 10.1002/jcph.1993. Available from: https://www.ncbi.nlm.nih.gov/pubmed/34713491

95. Guidi M, Csajka C, and Buclin T. Parametric Approaches in Population Pharmacokinetics. The Journal of Clinical Pharmacology. 2020 Oct; 62:125–41. DOI: 10.1002/jcph.1633. Available from: https://www.ncbi.nlm.nih.gov/pubmed/33103774

96. Yamada WM, Neely MN, Bartroff J, Bayard DS, Burke JV, Guilder M van, Jelliffe RW, Kryshchenko A, Leary R, Tatarinova T, and Schumitzky A. An Algorithm for Nonparametric Estimation of a Multivariate Mixing Distribution with Applications to Population Pharmacokinetics. Pharmaceutics. 2021; 13:42. Available from: https://www.mdpi.com/1999-4923/13/1/42

97. Ribbing J and Niclas Jonsson E. Power, Selection Bias and Predictive Performance of the Population Pharmacokinetic Covariate Model. Journal of Pharmacokinetics and Pharmacodynamics. 2004 Apr; 31:109–34. DOI: 10.1023/b:jopa.0000034404.86036.72. Available from: https://www.ncbi.nlm.nih.gov/pubmed/15379381

98. Wade JR, Beal SL, and Sambol NC. Interaction between structural, statistical, and covariate models in population pharmacokinetic analysis. Journal of Pharmacokinetics and Biopharmaceutics. 1994 Apr; 22:165–77. DOI: 10.1007/bf02353542. Available from: https://www.ncbi.nlm.nih.gov/pubmed/7815312

99. Amann LF and Wicha SG. Operational characteristics of full random effects modelling ('frem') compared to stepwise covariate modelling ('scm'). Journal of Pharmacokinetics and Pharmacodynamics. 2023 Apr; 50:315–26. DOI: 10.1007/s10928-023-09856-w. Available from: https://www.ncbi.nlm.nih.gov/pubmed/37083930

100. Lavielle M and Mbogning C. An improved SAEM algorithm for maximum likelihood estimation in mixtures of non linear mixed effects models. Statistics and Computing. 2013 Apr; 24:693–707. DOI: 10.1007/s11222-013-9396-2

101. Kiefer J and Wolfowitz J. Consistency of the Maximum Likelihood Estimator in the Presence of Infinitely Many Incidental Parameters. The Annals of Mathematical Statistics. 1956 Dec; 27:887–906. DOI: 10.1214/aoms/1177728066

102. Bustad A, Terziivanov D, Leary R, Port R, Schumitzky A, and Jelliffe R. Parametric and Nonparametric Population Methods: Their Comparative Performance in Analysing a Clinical Dataset and Two Monte Carlo Simulation Studies. Clinical Pharmacokinetics. 2006; 45:365–83. DOI: 10.2165/00003088-200645040-00003. Available from: https://www.ncbi.nlm.nih.gov/pubmed/16584284

103. Bonate PL. Clinical trial simulation in drug development. Pharmaceutical Research. 2000; 17:252–6. DOI: 10.1023/a:1007548719885. Available from: https://www.ncbi.nlm.nih.gov/pubmed/10801212

104. Wang DD, Yu Y, Kassir N, Zhu M, Hanley WD, Earp JC, Chow AT, Gupta M, and Hu C. The Utility of a Population Approach in Drug–Drug Interaction Assessments: A Simulation Evaluation. The Journal of Clinical Pharmacology. 2017 May; 57:1268–78. DOI: 10.1002/jcph.921. Available from: https://www.ncbi.nlm.nih.gov/pubmed/28513856

105. Goutelle S, Woillard JB, Neely M, Yamada W, and Bourguignon L. Nonparametric Methods in Population Pharmacokinetics. The Journal of Clinical Pharmacology. 2020 Oct; 62:142–57. DOI: 10.1002/jcph.1650. Available from: https://www.ncbi.nlm.nih.gov/pubmed/33103785

106. Vethe NT, Gustavsen MT, Midtvedt K, Lauritsen ME, Andersen AM, Åsberg A, and Bergan S. Tacrolimus Can Be Reliably Measured With Volumetric Absorptive Capillary Microsampling Throughout the Dose Interval in Renal Transplant Recipients. Therapeutic Drug Monitoring. 2019 Oct; 41:607–14. DOI: 10.1097/ftd.0000000000000655. Available from: https://www.ncbi.nlm.nih.gov/pubmed/31584926

107. Morgan PE. Microsampling Devices for Routine Therapeutic Drug Monitoring—Are We There Yet? Therapeutic Drug Monitoring. 2021 Jun; 43:322–34. DOI: 10.1097/ftd.0000000000000884. Available from: https://www.ncbi.nlm.nih.gov/pubmed/33675301

108. D'Argenio DZ. Optimal sampling times for pharmacokinetic experiments. Journal of Pharmacokinetics and Biopharmaceutics. 1981 Dec; 9:739–56. DOI: 10.1007/bf01070904. Available from: https://www.ncbi.nlm.nih.gov/pubmed/7341758

109. Meer AF van der, Marcus MAE, Touw DJ, Proost JH, and Neef C. Optimal Sampling Strategy Development Methodology Using Maximum A Posteriori Bayesian Estimation. Therapeutic Drug Monitoring. 2011 Apr; 33:133–46. DOI: 10.1097/ftd.0b013e31820f40f8. Available from: https://www.ncbi.nlm.nih.gov/pubmed/21383653

110. Brunet M, Gelder T van, Åsberg A, Haufroid V, Hesselink DA, Langman L, Lemaitre F, Marquet P, Seger C, Shipkova M, Vinks A, Wallemacq P, Wieland E, Woillard JB, Barten MJ, Budde K, Colom H, Dieterlen MT, Elens L, Johnson-Davis KL, Kunicki PK, MacPhee I, Masuda S, Mathew BS, Millán O, Mizuno T, Moes DJAR, Monchaud C, Noceti O, Pawinski T, Picard N, Schaik R van, Sommerer C, Vethe NT, Winter B de, Christians U, and Bergan S. Therapeutic Drug Monitoring of Tacrolimus-Personalized Therapy: Second Consensus Report. Therapeutic Drug Monitoring. 2019 Jun; 41:261–307. DOI: 10.1097/ftd.0000000000000640. Available from: https://www.ncbi.nlm.nih.gov/pubmed/31045868

111. Marquet P, Albano L, Woillard JB, Rostaing L, Kamar N, Sakarovitch C, Gatault P, Buchler M, Charpentier B, Thervet E, and Cassuto E. Comparative clinical trial of the variability factors of the exposure indices used for the drug monitoring of two tacrolimus formulations in kidney transplant recipients. Pharmacological Research. 2018 Mar; 129:84–94.

DOI: 10.1016/j.phrs.2017.12.005. Available from: https://www.ncbi.nlm.nih.gov/pubmed/29229354

112. Størset E, Åsberg A, Skauby M, Neely M, Bergan S, Bremer S, and Midtvedt K. Improved Tacrolimus Target Concentration Achievement Using Computerized Dosing in Renal Transplant Recipients—A Prospective, Randomized Study. Transplantation. 2015 Oct; 99:2158–66. DOI: 10.1097/tp.0000000000000708. Available from: https://www.ncbi.nlm.nih.gov/pubmed/25886918

113. Goutelle S, Alloux C, Bourguignon L, Van Guilder M, Neely M, and Maire P. To Estimate or to Forecast? Lessons From a Comparative Analysis of Four Bayesian Fitting Methods Based on Nonparametric Models. Therapeutic Drug Monitoring. 2021 Aug; 43:461–71. DOI: 10.1097/ftd.0000000000000879. Available from: https://www.ncbi.nlm.nih.gov/pubmed/34250963

114. Hjelmesæth J, Åsberg A, Andersson S, Sandbu R, Robertsen I, Johnson LK, Angeles PC, Hertel JK, Skovlund E, Heijer M, Ek AL, Krogstad V, Karlsen TI, Christensen H, Andersson TB, and Karlsson C. Impact of body weight, low energy diet and gastric bypass on drug bioavailability, cardiovascular risk factors and metabolic biomarkers: protocol for an open, non-randomised, three-armed single centre study (COCKTAIL). BMJ Open. 2018 May; 8:e021878. DOI: 10.1136/bmjopen-2018-021878. Available from: https://www.ncbi.nlm.nih.gov/pubmed/29844102

115. Wiśniewski JR and Rakus D. Multi-enzyme digestion FASP and the 'Total Protein Approach'-based absolute quantification of the Escherichia coli proteome. Journal of Proteomics. 2014 Sep; 109:322–31. DOI: 10.1016/j.jprot.2014.07.012. Available from: https://www.ncbi.nlm.nih.gov/pubmed/25063446

116. Mori E, Ishikawa M, Kato T, Kazui H, Miyake H, Miyajima M, Nakajima M, Hashimoto M, Kuriyama N, Tokuda T, Ishii K, Kaijima M, Hirata Y, Saito M, Arai H, and Japanese Society of Normal Pressure H. Guidelines for Management of Idiopathic Normal Pressure Hydrocephalus: Second Edition. Neurologia Medico-Chirurgica. 2012; 52:775–809. DOI: 10.2176/nmc.52.775. Available from: https://www.ncbi.nlm.nih.gov/pubmed/23183074

117. Pastore M and Calcagnì A. Measuring Distribution Similarities Between Samples: A Distribution-Free Overlapping Index. Frontiers in Psychology. 2019 May; 10:1089. DOI: 10.3389/fpsyg.2019.01089. Available from: https://www.ncbi.nlm.nih.gov/pubmed/31231264

118. Braamskamp MJ, Langslet G, McCrindle BW, Cassiman D, Francis GA, Gagné C, Gaudet D, Morrison KM, Wiegman A, Turner T, Kusters DM, Miller E, Raichlen JS, Wissmar J, Martin PD, Stein EA, and Kastelein JJ. Efficacy and safety of rosuvastatin therapy in children and adolescents with familial hypercholesterolemia: Results from the CHARON study. Journal of Clinical Lipidology. 2015 Nov; 9:741–50. DOI: 10.1016/j.jacl.2015.07.011. Available from: https://www.ncbi.nlm.nih.gov/pubmed/26687694

119. Razick S. Strømsvåg F and Hovd M. Optimization of PMetrics. Report. 2020 May. Available from: https://www.sigma2.no/sites/default/files/imce/AUS/Pmetrics_AUS_report.pdf

120. R Core Team. R: A Language and Environment for Statistical Computing. Computer Program. 2023. Available from: https://www.R-project.org/

121. Honka H, Koffert J, Kauhanen S, Kudomi N, Hurme S, Mari A, Lindqvist A, Wierup N, Parkkola R, Groop L, and Nuutila P. Liver blood dynamics after bariatric surgery: the effects of mixed-meal test and incretin infusions. Endocrine Connections. 2018 Jul; 7:888–96. DOI: 10.1530/ec-18-0234. Available from: https://www.ncbi.nlm.nih.gov/pubmed/29941634

122. Immonen H, Hannukainen JC, Kudomi N, Pihlajamäki J, Saunavaara V, Laine J, Salminen P, Lehtimäki T, Pham T, Iozzo P, and Nuutila P. Increased Liver Fatty Acid Uptake Is Partly Reversed and Liver Fat Content Normalized After Bariatric Surgery. Diabetes Care. 2017 Nov; 41:368–71. DOI: 10.2337/dc17-0738. Available from: https://www.ncbi.nlm.nih.gov/pubmed/29158250

123. Miao X, Wu LS, Lin SXW, Xu Y, Chen Y, Iwaki Y, Kobos R, Stephenson T, Kemmerer K, Uhlar CM, Banerjee A, Goldberg JD, Trancucci D, Apte A, Verona R, Pei L, Desai R, Hickey K, Su Y, Ouellet D, Samtani MN, Guo Y, Garfall AL, Krishnan A, Usmani SZ, Zhou H, and Girgis S. Population Pharmacokinetics and Exposure–Response with Teclistamab in Patients With Relapsed/Refractory Multiple Myeloma: Results From MajesTEC-1. Targeted Oncology. 2023 Sep; 18:667–84. DOI: 10.1007/s11523-023-00989-z. Available from: https://www.ncbi.nlm.nih.gov/pubmed/37713090

124. Niazi S. Volume of Distribution as a Function of Time. Journal of Pharmaceutical Sciences. 1976 Mar; 65:452–4. DOI: 10.1002/jps.2600650339. Available from: https://www.ncbi.nlm.nih.gov/pubmed/1263103

125. Debord J, Risco E, Harel M, Le Meur Y, Buchler M, Lachatre G, Le Guellec C, and Marquet P. Application of a Gamma Model of Absorption to Oral Cyclosporin. Clinical Pharmacokinetics. 2001; 40:375–82. DOI: 10.2165/00003088-200140050-00004. Available from: https://www.ncbi.nlm.nih.gov/pubmed/11432538

126. Wesolowski CA, Wesolowski MJ, Babyn PS, and Wanasundara SN. Time Varying Apparent Volume of Distribution and Drug Half-Lives Following Intravenous Bolus Injections. PLOS ONE. 2016 Jul; 11. Ed. by Janigro D:e0158798. DOI: 10.1371/journal.pone.0158798. Available from: https://www.ncbi.nlm.nih.gov/pubmed/27403663

127. Kvitne KE, Hovd M, Johnson LK, Wegler C, Karlsson C, Artursson P, Andersson S, Sandbu R, Hjelmesæth J, Skovlund E, Jansson-Löfmark R, Christensen H, Åsberg A, and Robertsen I. Digoxin Pharmacokinetics in Patients with Obesity Before and After a Gastric Bypass or a Strict Diet Compared with Normal Weight Individuals. Clinical Pharmacokinetics. 2023 Nov; 63:109–20. DOI: 10.1007/s40262-023-01320-9. Available from: https://www.ncbi.nlm.nih.gov/pubmed/37993699

128. Jaber MM, Al-Kofahi M, Sarafoglou K, and Brundage RC. Individualized Absorption Models in Population Pharmacokinetic Analyses. CPT: Pharmacometrics and Systems Pharmacology. 2020 May; 9:307–9. DOI: 10.1002/psp4.12513. Available from: https://www.ncbi.nlm.nih.gov/pubmed/32437056

129. Tzeng TB, Schneck DW, Birmingham BK, Mitchell PD, Zhang H, Martin PD, and Kung LP. Population pharmacokinetics of rosuvastatin: implications of renal impairment, race, and dyslipidaemia. Current Medical Research and Opinion. 2008 Jul; 24:2575–85. DOI: 10.1185/03007990802312807. Available from: https://www.ncbi.nlm.nih.gov/pubmed/18674408

130. Park WS, Jang D, Han S, and Yim DS. Mixed–effects analysis of increased rosuvastatin absorption by coadministered telmisartan. Translational and Clinical Pharmacology. 2016; 24:55. DOI: 10.12793/tcp.2016.24.1.55. Available from: https://tcpharm.org/Synapse/Data/PDFData/1179TCP/tcp-24-55.pdf

131. Rousseau A, Leger F, Le Meur Y, Saint-Marcoux F, Paintaud G, Buchler M, and Marquet P. Population Pharmacokinetic Modeling of Oral Cyclosporin Using NONMEM: Comparison of Absorption Pharmacokinetic Models and Design of a Bayesian Estimator. Therapeutic Drug Monitoring. 2004 Feb; 26:23–30. DOI: 10.1097/00007691-200402000-00006. Available from: https://www.ncbi.nlm.nih.gov/pubmed/14749545

132. El-Zailik A, Cheung LK, Wang Y, Sherman V, and Chow DSL. Longitudinal Impacts of Gastric Bypass Surgery on Pharmacodynamics and Pharmacokinetics of Statins. Obesity Surgery. 2019 Apr; 29:2571–83. DOI: 10.1007/s11695-019-03885-6. Available from: https://www.ncbi.nlm.nih.gov/pubmed/31004269

133. Romeijn MM, Kolen AM, Holthuijsen DDB, Janssen L, Schep G, Leclercq WKG, and Dielen FMH van. Effectiveness of a Low-Calorie Diet for Liver Volume Reduction Prior to Bariatric Surgery: a Systematic Review. Obesity Surgery. 2020 Nov; 31(1):350–6. DOI: 10.1007/s11695-020-05070-6. ppublish

134. Tirona RG, Kassam Z, Strapp R, Ramu M, Zhu C, Liu M, Schwarz UI, Kim RB, Al-Judaibi B, and Beaton MD. Apixaban and Rosuvastatin Pharmacokinetics in Nonalcoholic Fatty Liver Disease. Drug Metabolism and Disposition. 2018 Feb; 46(5):485–92. DOI: 10.1124/dmd.117.079624. ppublish

135. Kvitne KE, Robertsen I, Skovlund E, Christensen H, Krogstad V, Wegler C, Angeles PC, Wollmann BM, Hole K, Johnson LK, Sandbu R, Artursson P, Karlsson C, Andersson S, Andersson TB, Hjelmesæth J, Jansson-Löfmark R, and Åsberg A. Short- and long-term effects of body weight loss following calorie restriction and gastric bypass on CYP3A-activity – a non-randomized three-armed controlled trial. Clinical and Translational Science. 2021

Aug; 15:221–33. DOI: 10.1111/cts.13142. Available from: https://ascpt.onlinelibrary.wiley.com/doi/abs/10.1111/cts.13142

136. Malm J and Eklund A. Idiopathic normal pressure hydrocephalus. Practical Neurology. 2006 Feb; 6:14–27. DOI: 10.1136/jnnp.2006.088351. Available from: https://pn.bmj.com/content/practneurol/6/1/14.full.pdf

137. Crook JE, Gunter JL, Ball CT, Jones DT, Graff-Radford J, Knopman DS, Boeve BF, Petersen RC, Jack CR, and Graff-Radford NR. Linear vs volume measures of ventricle size: Relation to present and future gait and cognition. Neurology. 2020 Feb; 94:e549–e556. DOI: 10.1212/wnl.0000000000008673. Available from: https://www.ncbi.nlm.nih.gov/pubmed/31748251

138. Cheng KT. Gadobutrol. *Molecular Imaging and Contrast Agent Database (MICAD)*. Bethesda (MD): National Center for Biotechnology Information (US), 2004. DOI: 10.21203/rs.3.rs-378237/v1. Available from: https://www.ncbi.nlm.nih.gov/pubmed/20641787

139. Valnes LM, Mitusch SK, Ringstad G, Eide PK, Funke SW, and Mardal KA. Apparent diffusion coefficient estimates based on 24 hours tracer movement support glymphatic transport in human cerebral cortex. Scientific Reports. 2020 Jun; 10:9176. DOI: 10.1038/s41598-020-66042-5. Available from: https://www.ncbi.nlm.nih.gov/pubmed/32514105

140. Vinje V, Zapf B, Ringstad G, Eide PK, Rognes ME, and Mardal KA. Human brain solute transport quantified by glymphatic MRI-informed biophysics during sleep and sleep deprivation. Fluids and Barriers of the CNS. 2023 Aug; 20:62. DOI: 10.1186/s12987-023-00459-8. Available from: https://www.ncbi.nlm.nih.gov/pubmed/37596635

141. Verma A, Hesterman JY, Chazen JL, Holt R, Connolly P, Horky L, Vallabhajosula S, and Mozley PD. Intrathecal 99m Tc-DTPA imaging of molecular passage from lumbar cerebrospinal fluid to brain and periphery in humans. Alzheimers and Dementia: Diagnosis, Assessment and Disease Monitoring. 2020 Jan; 12:e12030. DOI: 10.1002/dad2.12030. Available from: https://www.ncbi.nlm.nih.gov/pubmed/32355870

142. Nordin G, Mårtensson A, Swolin B, Sandberg S, Christensen NJ, Thorsteinsson V, Franzson L, Kairisto V, and Savolainen ER. A multicentre study of reference intervals for haemoglobin, basic blood cell counts and erythrocyte indices in the adult population of the Nordic countries. Scandinavian Journal of Clinical and Laboratory Investigation. 2004 Jun; 64:385–98. DOI: 10.1080/00365510410002797. Available from: https://www.ncbi.nlm.nih.gov/pubmed/15223702

143. Staks T, Schuhmann-Giampieri G, Frenzel T, Weinmann HJ, Lange L, and Platzek J. Pharmacokinetics, Dose Proportionality, and Tolerability of Gadobutrol after Single Intravenous Injection in Healthy Volunteers. Investigative Radiology. 1994 Jul; 29:709–15. DOI: 10.1097/00004424-199407000-00008. Available from: https://www.ncbi.nlm.nih.gov/pubmed/7960618

144. Davies J, Siebenhandl-Wolff P, Tranquart F, Jones P, and Evans P. Gadolinium: pharmacokinetics and toxicity in humans and laboratory animals following contrast agent administration. Archives of Toxicology. 2022 Jan; 96:403–29. DOI: 10.1007/s00204-021-03189-8. Available from: https://www.ncbi.nlm.nih.gov/pubmed/34997254

145. Hovd M. Measured GFR from iohexol popPK. Web Page. 2023. Available from: https://www.mgfr.no

146. Clarke M, Gaynon P, Hann I, Harrison G, Masera G, Peto R, and Richards S. CNS-Directed Therapy for Childhood Acute Lymphoblastic Leukemia: Childhood ALL Collaborative Group Overview of 43 Randomized Trials. Journal of Clinical Oncology. 2003 May; 21:1798–809. DOI: 10.1200/jco.2003.08.047. Available from: https://www.ncbi.nlm.nih.gov/pubmed/12721257

147. Murata Ky, Maeba A, Yamanegi M, Nakanishi I, and Ito H. Methotrexate myelopathy after intrathecal chemotherapy: a case report. Journal of Medical Case Reports. 2015 Jun; 9:135. DOI: 10.1186/s13256-015-0597-5. Available from: https://www.ncbi.nlm.nih.gov/pubmed/26055509

148. Dhariwal N, Roy Moulik N, Smriti V, Dhamne C, Chichra A, Srinivasan S, Narula G, and Banavali S. Clinico-radiological profile, management and follow-up of methotrexate induced neurotoxicity in children with acute lymphoblastic leukemia. Leukemia and Lymphoma. 2023 Aug; 64:1971–80. DOI: 10.1080/10428194.2023.2245093. Available from: https://www.ncbi.nlm.nih.gov/pubmed/37565568

149. Niemann A, Mühlisch J, Frühwald MC, Ger J, Hempel G, and Boos J. Therapeutic Drug Monitoring of Methotrexate in Cerebrospinal Fluid After Systemic High-Dose Infusion in Children: Can the Burden of Intrathecal Methotrexate be Reduced? Therapeutic Drug Monitoring. 2010 Aug; 32:467–75. DOI: 10.1097/ftd.0b013e3181e5c6b3. Available from: https://www.ncbi.nlm.nih.gov/pubmed/20571463

150. Hellinger E. Neue Begründung der Theorie quadratischer Formen von unendlichvielen Veränderlichen. Journal für die reine und angewandte Mathematik. 1909 Jul; 1909:210–71. DOI: 10.1515/crll.1909.136.210

151. Bhattacharyya A. On a Measure of Divergence between Two Multinomial Populations. Sankhyā: The Indian Journal of Statistics (1933-1960) 1946; 7:401–6. Available from: http://www.jstor.org/stable/25047882 [Accessed on: 2024 Jan 17]

152. Meer AF van der, Touw DJ, Marcus MAE, Neef C, and Proost JH. Influence of Erroneous Patient Records on Population Pharmacokinetic Modeling and Individual Bayesian Estimation. Therapeutic Drug Monitoring. 2012 Oct; 34:526–34. DOI: 10.1097/ftd.0b013e3182616937. Available from: https://www.ncbi.nlm.nih.gov/pubmed/22846895

153. Sarem S, Nekka F, Ahmed IS, Litalien C, and Li J. Impact of sampling time deviations on the prediction of the area under the curve using regression limited sampling strategies. Biopharmaceutics and Drug Disposition. 2015 Jun; 36:417–28. DOI: 10.1002/bdd.1951. Available from: https://www.ncbi.nlm.nih.gov/pubmed/25845479

154. Alihodzic D, Broeker A, Baehr M, Kluge S, Langebrake C, and Wicha SG. Impact of Inaccurate Documentation of Sampling and Infusion Time in Model-Informed Precision Dosing. Frontiers in Pharmacology. 2020 Mar; 11:172. DOI: 10.3389/fphar.2020.00172. Available from: https://www.ncbi.nlm.nih.gov/pubmed/32194411

155. Dadkhah A, Alihodzic D, Broeker A, Kröger N, Langebrake C, and Wicha SG. Evaluation of the Robustness of Therapeutic Drug Monitoring Coupled with Bayesian Forecasting of Busulfan with Regard to Inaccurate Documentation. Pharmaceutical Research. 2021 Oct; 38:1721–9. DOI: 10.1007/s11095-021-03115-8. Available from: https://www.ncbi.nlm.nih.gov/pubmed/34664209

156. Bayard DS and Neely M. Experiment design for nonparametric models based on minimizing Bayes Risk: application to voriconazole. Journal of Pharmacokinetics and Pharmacodynamics. 2016 Dec; 44:95–111. DOI: 10.1007/s10928-016-9498-5. Available from: https://www.ncbi.nlm.nih.gov/pubmed/27909942

157. Chen R, Schumitzky A, Kryshchenko A, Otalvaro JD, Yamada WM, and Neely M. NPSA: Nonparametric Simulated Annealing for Global Optimization. 2023. DOI: 10.48550/arxiv.2301.12656. Available from: https://arxiv.org/pdf/2301.12656.pdf

158. Otalvaro JD, Yamada WM, Hernandez AM, Zuluaga AF, Chen R, and Neely MN. A proof of concept reinforcement learning based tool for non parametric population pharmacokinetics workflow optimization. Journal of Pharmacokinetics and Pharmacodynamics. 2022 Dec; 50:33–43. DOI: 10.1007/s10928-022-09829-5. Available from: https://www.ncbi.nlm.nih.gov/pubmed/36478350

159. Laboratory of Applied Pharmacokinetics and Bioinformatics. PMcore. Web Page. 2023. Available from: https://github.com/LAPKB/PMcore

References

Paper I

ORIGINAL RESEARCH ARTICLE

Neither Gastric Bypass Surgery Nor Diet-Induced Weight-Loss Affect OATP1B1 Activity as Measured by Rosuvastatin Oral Clearance

Markus Hovd[1] · Ida Robertsen[1] · Line Kristin Johnson[2] · Veronica Krogstad[1] · Christine Wegler[3,4] ·
Kine Eide Kvitne[1] · Marianne Kristiansen Kringen[5,6] · Eva Skovlund[7] · Cecilia Karlsson[8,9] · Shalini Andersson[10] ·
Per Artursson[11] · Rune Sandbu[2,12] · Jøran Hjelmesæth[2,13] · Anders Åsberg[1,14] · Rasmus Jansson-Löfmark[4] ·
Hege Christensen[1]

Abstract

Introduction Rosuvastatin pharmacokinetics is mainly dependent on the activity of hepatic uptake transporter OATP1B1. In this study, we aimed to investigate and disentangle the effect of Roux-en-Y gastric bypass (RYGB) and weight loss on oral clearance (CL/F) of rosuvastatin as a measure of OATP1B1-activity.

Methods Patients with severe obesity preparing for RYGB ($n = 40$) or diet-induced weight loss ($n = 40$) were included and followed for 2 years, with four 24-hour pharmacokinetic investigations. Both groups underwent a 3-week low-energy diet (LED; < 1200 kcal/day), followed by RYGB or a 6-week very-low-energy diet (VLED; < 800 kcal/day).

Results A total of 80 patients were included in the RYGB group (40 patients) and diet-group (40 patients). The weight loss was similar between the groups following LED and RYGB. The LED induced a similar (mean [95% CI]) decrease in CL/F in both intervention groups (RYGB: 16% [0, 31], diet: 23% [8, 38]), but neither induced VLED resulted in any further changes in CL/F. At Year 2, CL/F had increased by 21% from baseline in the RYGB group, while it was unaltered in the diet group. Patients expressing the reduced function *SLCO1B1* variants (c.521TC/CC) showed similar changes in CL/F over time compared with patients expressing the wild-type variant.

Conclusions Neither body weight, weight loss nor RYGB per se seem to affect OATP1B1 activity to a clinically relevant degree. Overall, the observed changes in rosuvastatin pharmacokinetics were minor, and unlikely to be of clinical relevance.

Key Points

Both surgery and diet intervention led to a matched weight loss between the study groups.

Roux-en-Y gastric bypass surgery does not affect OATP1B1 activity in patients with severe obesity.

No dose adjustments of rosuvastatin appear to be necessary following weight loss induced by bariatric surgery and/or low-calorie diet.

✉ Markus Hovd
m.h.hovd@farmasi.uio.no

Extended author information available on the last page of the article

1 Introduction

Obesity represents a global epidemic [1], and is associated with an increased risk of comorbidities including type 2 diabetes, cardiovascular disease and cancer that often requires pharmacological treatment [2, 3]. Severe obesity is classified as a body mass index (BMI) between 35.0 and 39.9 kg/m² in combination with comorbidity, or ≥ 40 kg/m², for which weight loss is the primary treatment [4]. Bariatric surgery has shown superior effects with respect to achieving long-lasting weight loss and improvement of comorbidities compared to non-surgical interventions in patients with severe obesity [5, 6]. The Roux-en-Y gastric bypass (RYGB) procedure reduces the proximal stomach, and the duodenum and proximal intestine are bypassed [7, 8]. Due to this gastrointestinal rearrangement, drug absorption and disposition may be altered. Altered gastric pH, reduced transit-time, and decreased surface area for passive and active absorption, as well as the bypassing of intestinal segments rich in

drug-metabolising enzymes and transporters, are among the suggested mechanisms leading to variable drug disposition following RYGB [9].

The 3-hydroxy-3-methylglutaryl-coenzyme A (HMG-CoA) reductase inhibitor, rosuvastatin, is a commonly used lipid-lowering agent. Rosuvastatin is more hydrophilic compared with most other statins, and it displays a low degree of passive diffusion into tissues [10]. The hepatic uptake transporters organic-anion transporting polypeptides (OATP) 1B1 (*SLCO1B1*), OATP1B3 (*SLCO1B3*), OATP2B1 (*SLCO2B1*), as well as the sodium taurocholate co-transporting polypeptide (NTCP; *SLC10A1*) transport rosuvastatin into the hepatocytes. Organic-anion transporting polypeptides 1B1 contributes to 49–86% of rosuvastatin hepatic uptake, and rosuvastatin is thus considered an established and preferred probe drug to study OATP1B1 activity [11–13]. Rosuvastatin is sparsely metabolised, and the majority of the absorbed dose is excreted unchanged in faeces (~ 76%). Hepatic elimination accounts for approximately 70% of total clearance of rosuvastatin, with biliary excretion, mediated by canalicular transporters such as breast cancer resistance protein (BCRP; *ABCG2*) and permeability-glycoprotein (P-gp; *ABCB1*), as the main clearance mechanism [14, 15]. Genetic polymorphisms of the key hepatic uptake transporter OATP1B1 have been shown to influence rosuvastatin disposition. The single-nucleotide polymorphism (SNP) c.521T>C in *SLCO1B1* is associated with decreased membrane expression of OATP1B1 in vivo [16]. Consequently, systemic exposure of rosuvastatin is reported to be 19–68% higher in patients with c.521TC or c.521CC [17].

In patients with a wide range of body weight, using midazolam as a probe drug, both the activity and protein expression of the quantitatively most important drug metabolising enzyme, cytochrome P450 (CYP) 3A, have been shown to be inversely associated with body weight. This was hypothesised to be due to low-grade inflammation and/or non-alcoholic fatty liver disease (NAFLD) [18–20]. Inflammatory cytokines such as interleukin (IL) 6 and tumour necrosis factor alpha (TNF-α), as well as NAFLD have been associated with lower expression and activity of several CYP enzymes [18, 21]. However, there are limited data regarding the effect of weight loss, inflammation, and NAFLD on drug transporters. The primary aim of this work was to study the short- (6 weeks) and long-term (2 years) effects of weight loss induced by strict diet or RYGB on OATP1B1 activity by investigating the pharmacokinetics of rosuvastatin, and to secondary compare OATP1B1 activity in a control group of normal-to-overweight individuals with patients with severe obesity.

2 Methods

2.1 Study Design and Patients

The COCKTAIL study, a non-randomised, single-centre, 3-armed study, was carried out at the Morbid Obesity Centre, Vestfold Hospital Trust, Norway [22]. Patients with severe obesity (BMI ≥ 35 kg/m^2 in combination with comorbidity or BMI ≥ 40 kg/m^2) scheduled for elective weight-reducing intervention by either RYGB or strict diet were eligible for inclusion. The inclusion and exclusion criteria are fully described in the protocol paper [22]. Additionally, normal-to-overweight (BMI 18.5–29.9 kg/m^2) individuals scheduled for cholecystectomy were included as a cross-sectional control group. The study was approved by the Regional Committee for Medical and Health Research Ethics (2013/2379/REK) and performed in accordance with Good Clinical Practice and the Declaration of Helsinki (NCT02386917). Written informed consent was obtained prior to study participation.

2.2 Study Visits and Procedures

The patient flow in the study has been described previously [20], and is further detailed in Figure S1. Both the RYGB group and the diet group were prescribed an initial 3-week low-energy diet (LED; < 1200 kcal/day), followed by additional 6 weeks of strict caloric restriction (< 800 kcal/day) induced by surgery or a very-low energy diet (VLED), respectively, in order to obtain a similar weight loss between the two groups [22]. All patients were prospectively followed for 2 years. During the study period, four 24-h pharmacokinetic investigations were performed following single oral administration of 20 mg rosuvastatin. Blood samples were obtained via a peripheral venous catheter before and 0.25, 0.5, 1, 1.5, 2, 3, 4, 4.25, 4.5, 5, 5.5, 6, 8, 10, 12, 23, and 24 h post-dose. The investigations were performed at baseline (Week 0); after the 3-week LED (Week 3); after additional 6-week strict calorie restriction (Week 9), and after 2 years (Year 2). For the RYGB group, the investigation at Week 3 was performed the day before surgery. The cross-sectional control group of normal-to-overweight individuals underwent a single 24-h pharmacokinetic study the day before cholecystectomy (Week 0). Hepatic and jejunal biopsies were obtained at the day of surgery in the RYGB group, and hepatic biopsies were obtained in the normal-to-overweight control group at the day of surgery as previously described [23].

2.3 Outcomes

The primary outcomes were short- (Week 3 to Week 9) and long-term (Week 3 to Year 2) changes in oral clearance of rosuvastatin, as a measure of OATP1B1 activity. Secondary

outcomes included changes in rosuvastatin pharmacokinetics over time following RYGB or strict diet, assessed by oral clearance, maximum concentration (C_{max}) and time to maximum concentration (T_{max}), as well as hepatic concentration of OATP1B1.

2.4 Analytical Assay

Plasma concentrations of rosuvastatin were determined by Covance Laboratories (Madison, Wisconsin, USA), as previously described [24]. In brief, buffered plasma samples were extracted by supported liquid extraction. After evaporation, the residue was reconstituted and analysed with liquid chromatography tandem mass spectrometry (LC-MS/MS). The analyte was separated on a C18-column (Aquasil) with a gradient mobile phase of acetonitrile and 0.1% formic acid, using a LC system from Thermo Electron Corporation. Rosuvastatin was detected by MS/MS using a Sciex API 5500 with positive electrospray ionisation, monitoring the m/z 482.2–258.2 transition. The standard curve ranged from 0.04 to 40 ng/mL, using a human plasma sample volume of 0.1 mL. The assay variation coefficients of the rosuvastatin analysis were 7.1%, 4.4% and 4.5% at 0.12 ng/mL, 2 ng/mL, and 20 ng/mL ($n = 130$), respectively.

2.5 Clinical Chemistry and Genotyping

Clinical chemistry analyses were performed at the Department of Laboratory Medicine, Vestfold Hospital Trust, Tønsberg, Norway. Plasma concentrations of C-reactive protein (CRP) and high-sensitivity CRP (hsCRP) were measured using immunoturbidimetry (Advia Chemistry XPT systems, Siemens) at Fürst Medical Laboratory, Oslo, Norway. Genotyping of *SLCO1B1* and *ABCG2* variant alleles were performed using Taqman-based real-time polymerase chain reaction assays at the Center for Psychopharmacology, Diakonhjemmet Hospital, Oslo, Norway. The following variant alleles were assessed for *SLCO1B1*: c.521T>C (rs4149056); *ABCG2*: V12M variant (rs2231137) and reduced-function Q141K variant (rs2231142). Homozygote carriers of the V12M C/C and Q141K G/G were considered as the wild-type haplotype. A TaqMan assay for rs2231137 genotyping was not readily available, and as such an assay for rs4148150 was used, which is in complete disequilibrium ($R^2 = 1$ in Europeans) with rs2231137 [25].

2.6 Quantification of Hepatic and Intestinal Protein Concentration

Proteins were extracted from small intestinal and liver biopsies in an SDS-containing (2% w/v) lysis buffer and quantified as previously described [26, 27]. In short, samples were processed with the multi-enzyme digestion filter-aided sample preparation protocol, using LysC and trypsin [28]. Proteomics analysis was performed with Q Exactive HF or Q Exactive HF-X MS in data-dependent mode. Mass spectrometry (MS) data were processed with MaxQuant (version 1.6.10.43) [29] where proteins were identified by searching MS and MS/MS data of peptides against the human UniProtKB (UP000005640). Spectral raw intensities were normalised with variance stabilisation [30] and were subsequently used to calculate the protein concentrations using the Total Protein Approach [31]. Batch effects were removed by geometric mean centring of proteins from samples analysed at different time points.

2.7 Population Pharmacokinetic Modelling

A population pharmacokinetic model was developed to determine individual rosuvastatin pharmacokinetics at the different study visits. The purpose of the model was to provide accurate estimates of AUC, oral clearance, maximum concentration (C_{max}) and time to maximum concentration (T_{max}) in order to allow for a rational assessment of change over time and between groups. In short, a non-parametric adaptive grid approach implemented in a modified version of Pmetrics 1.9.4 [32] for R 3.6.0 was used. In total, 3630 rosuvastatin concentrations corresponding to 197 18-point and 111 9-point 24-h pharmacokinetic profiles from 98 patients were included. Additional model information and metrics are available in the Supplementary file (Figs S2, S3).

2.8 Pharmacokinetic Calculations

Posterior individual parameter values, as well as posterior individually predicted concentrations obtained from the final population pharmacokinetic model run with the complete dataset were used for all pharmacokinetic calculations. Predictions were made in 12-min intervals, and at each sample point. Area under the concentration-time curve from zero to infinity ($AUC_{0-\infty}$) was calculated with the trapezoidal approximation from individual posterior-predicted concentrations using the 'makeAUC'-function in the Pmetrics package for R. C_{max} and T_{max} were obtained directly from the individual predictions, while oral clearance was calculated by dividing the dose by the $AUC_{0-\infty}$.

2.9 Statistical Analyses and Calculations

Linear mixed effects models were used to evaluate changes over time with the parameter of choice as the dependent variable, while visit, intervention group, and their interaction were treated as fixed effects. Variant of OATP1B1 was added as a fixed effect when evaluating differences in change over time between genotypes. The unique patient identifier was used as a random effect. Model residuals were

evaluated for normality, and if appropriate, the dependent variable was transformed using the natural logarithm. Models with a logarithmically transformed dependent variable were adjusted for the introduced bias. Estimated marginal means and contrasts were used for factor combinations (of visit and intervention group) for all parameters of interest. The cross-sectional analysis at baseline was performed using Welch's two-sample *t* test comparing the control group with patients with severe obesity (RYGB group and diet group combined). Baseline rosuvastatin pharmacokinetics were used to assess differences between genotypes. To explore relationships between variables, Pearson's product-moment correlation was applied. Variables with non-normal distributions (assessed visually) were logarithmically transformed. Predictions of NAFLD and liver fat were performed using metabolic and genetic factors, with NAFLD Liver Fat Score values greater than − 0.640 as a diagnostic of NAFLD [33]. Data are presented as mean ± standard deviation or mean [95% confidence interval (CI)] unless otherwise stated. With the predetermined $\alpha = 0.05$, 95% CIs not including zero and *p* values < 0.05 were considered statistically significant. Confidence intervals from linear mixed effects models were adjusted using Tukey method. All statistical analyses were performed using R 4.0.2 [34].

3 Results

3.1 Patient Characteristics

A total of 108 patients (44, 44 and 20 in the RYGB, diet, and control groups, respectively) were included in the study. In the present analyses, 98 patients (40, 40 and 18 in the RYGB,

diet, and control group, respectively) supplied at least one 24-h pharmacokinetic profile during the study period.

Mean total body weight at baseline was 132 ± 24 kg, 124 ± 23 kg, and 71 ± 11 kg in the RYGB, diet, and control groups, respectively (Table 1). There were no differences between the groups with respect to age, sex, or ethnicity. Routine clinical chemistry was similar in the three groups, except for higher value of ALT in the intervention groups compared with the control group (Table 1). At baseline, 71 of 98 patients had a NAFLD-score above − 0.640, indicative of NAFLD, in the RYGB (90%), diet (82%) and control groups (11%).

3.2 Changes in Body Weight

The initial 3-week LED resulted in a mean weight loss of 5 ± 2% and 5 ± 2% in the RYGB and diet group, respectively. Total weight loss after the additional 6 weeks of VLED induced by RYGB or strict diet was 13 ± 3% and 11 ± 4%, respectively (Fig. 1). At Year 2, the RYGB group demonstrated a total weight loss of 29 ± 9% from baseline. In contrast, several patients in the diet group had regained body weight at Year 2, resulting in a mean total weight loss from baseline of 3 ± 6% (Fig. 1). The hsCRP and predicted liver fat were similar between the RYGB and diet groups at Weeks 0, 3, and 9, but lower in the RYGB group at Year 2 (Fig. 1).

3.3 Baseline Rosuvastatin Pharmacokinetics, Pharmacogenetics, and Proteomics

Cross-sectional comparisons of rosuvastatin pharmacokinetics in patients with severe obesity compared with the control group revealed a 0.9 [95% CI 0.4, 1.4] hour shorter T_{max} in the normal-to-overweight individuals, with no differences

Table 1 Demographic overview of patients at baseline

	RYGB (*n* = 40)	Diet (*n* = 40)	Controls (*n* = 18)
Male/female (*n*)	13/27	14/26	3/15
Age (years)	46 ± 9	49 ± 10	42 ± 15
Weight (kg)	132 ± 24	124 ± 23	71 ± 11
BMI (kg/m^2)	45 ± 6	42 ± 5	25 ± 3
hsCRP (mg/L)	8.2 ± 6.2	7.1 ± 6.6	2.5 ± 3.8
ALT (IU/L)	34 ± 17	32 ± 19	22 ± 15
AST (IU/L)	28 ± 10	28 ± 15	25 ± 11
Creatinine (μmol/L)	58 ± 11	59 ± 14	60 ± 12
Ethnicity (Caucasian/other)	40 / 0	39/1	17/1
SLCO1B1 c.521			
T/T	T/C	C/C	27	12	1	25	14	1	13	4	0[a]

Values are presented as mean (± standard deviation) or count

ALT alanine aminotransferase, *AST* aspartate aminotransferase, *BMI* body mass index, *hsCRP* high-sensitive C-reactive protein, *RYGB* Roux-en-Y gastric bypass

[a]For one individual in the control group, genotype could not be determined
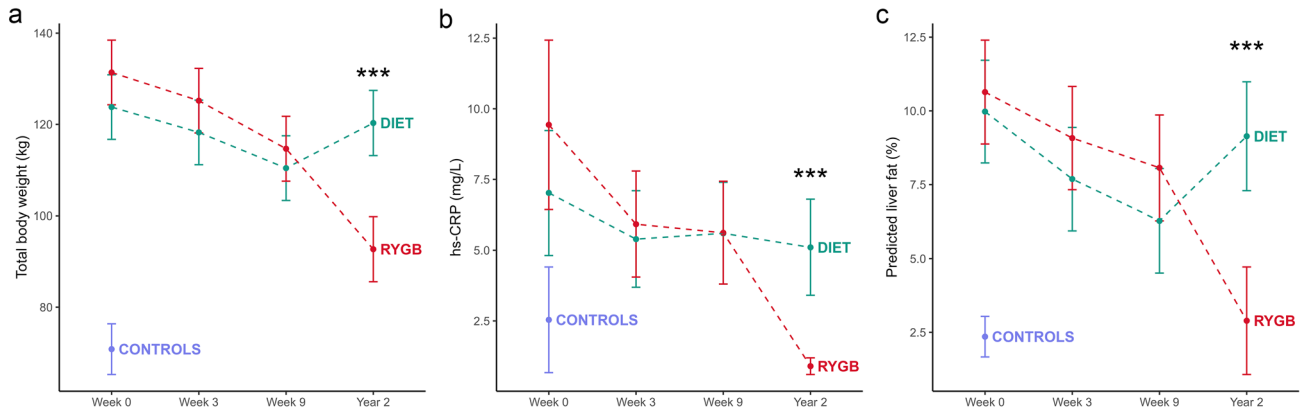
Fig. 1 Groupwise longitudinal overview of change in **a** total body weight, **b** high-sensitive C-reactive protein (hsCRP) and **c** predicted liver fat percentage. For the Roux-en-Y gastric bypass (RYGB) and diet groups, linear mixed model predicted marginal mean and 95% confidence intervals are presented. For the normal-to-overweight control group, observed mean and 95% confidence interval is presented. Comparisons are made between the RYGB and diet groups at each visit, and significant differences are denoted with asterisks. Non-significant differences are not shown *$p < 0.05$; **$p < 0.01$; ***$p < 0.001$

in C_{max} or oral clearance (Fig. 2). At baseline, total body weight was not associated with oral clearance ($r = 0.17$ [95% CI -0.03, 0.36]). No difference in rosuvastatin oral clearance was observed in patients with NAFLD ($n = 69$) compared with those without ($n = 27$), and hsCRP was not associated with oral clearance of rosuvastatin ($r = -0.13$ [95% CI -0.32, 0.07]).

The frequency distribution of *SLCO1B1* genetic variants is presented in Table 1, and there were no differences in frequency distribution between the sexes ($p = 0.0867$). Frequency distribution for the *ABCG2* variants are presented in Table S1. Allele frequencies for all sequence variants investigated did not deviate from the Hardy–Weinberg equilibrium. At baseline, patients with *SLCO1B1* variant c.521TC ($n = 30$) or c.521CC ($n = 2$) demonstrated

30% ($p < 0.001$) lower oral clearance compared to those with c.521TT. Absolute differences in rosuvastatin oral clearance and systemic exposure within the genetic variants of *SLCO1B1* at baseline are presented in Supplementary Tables S2 and S3, respectively.

In the patients undergoing RYGB, hepatic concentration of OATP1B1 was positively associated with oral clearance the day before surgery ($r = 0.36$ [95% CI 0.04, 0.61]), but this was not the case for the control group ($r = -0.09$ [95% CI -0.54, 0.39]) (Fig. S5). Furthermore, there were no differences in mean hepatic concentration of OATP1B1 between the RYGB (2.7 ± 0.9 fmol/μg) and control groups (2.6 ± 0.9 fmol/μg; $p = 0.630$), nor were there any differences between individuals in the combined RYGB and control groups with *SLCO1B1* variant c.521TT (2.8 ± 0.9 fmol/μg) or c.521TC/CC (2.5 ± 0.7 fmol/μg).
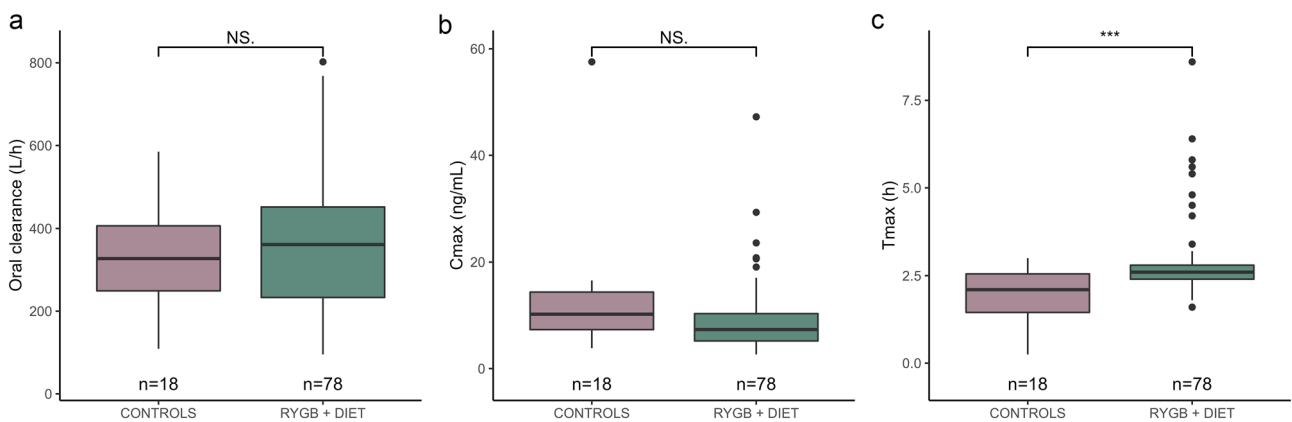
Fig. 2 Comparisons of rosuvastatin **a** oral clearance, **b** maximum concentration (C_{max}) and **c** time to maximum concentration (T_{max}) between patients with severe obesity and a normal- to overweight control group at baseline *$p < 0.05$; **$p < 0.01$; ***$p < 0.001$

3.4 Short- and Long-Term Changes in Rosuvastatin Pharmacokinetics Following RYGB and Strict Diet

A total of 57 patients (RYGB = 29, diet = 28) participated in all four pharmacokinetic investigations. Mean predicted pharmacokinetic profiles of rosuvastatin are shown in supplementary Figure S6, and an overview of pharmacokinetic parameters for all groups across time is provided in Table 2. There were no differences in pharmacokinetic parameters of rosuvastatin between the two intervention groups at baseline (Table 3).

Following the initial 3-week LED, oral clearance decreased by 16% [95% CI 0, 31) and 23% [95% CI 8, 38) in the RYGB and diet groups, respectively (Table 3), and the change was not different between the groups (Fig. 3). Furthermore, no changes in C_{max} or T_{max} were observed (Table 3). In the RYGB and diet groups combined, the change in oral clearance was positively associated with the weight loss ($r = 0.25$ [95% CI 0.03, 0.45]) in the same period, but not associated with change in liver fat ($r = 0.05$ [95% CI − 0.18, 0.27]).

In the RYGB group, a more rapid rosuvastatin absorption, reflected by a 0.9 [95% CI 0.4, 1.7] hour reduction in T_{max} was observed at Week 9, compared with baseline (Table 3). There were no additional changes in oral clearance or C_{max} in either the RYGB or diet groups from Week 3 to Week 9. Still, the within group change in oral clearance during this time period was different between the two groups (Fig. 3).

At Year 2, the RYGB group demonstrated a total increase in oral clearance of 21% [95% CI 1, 41] and 57% [95% CI 31, 83] compared to baseline and Week 9, respectively. The change in oral clearance from Week 9 to Year 2 was 8-fold greater in the RYGB- compared with the diet group (Fig. 3). At Year 2, oral clearance of rosuvastatin was 22% (95% CI 0, 43) higher in the RYGB group than in the diet group (Table 3). Long-term change in oral clearance from baseline to Year 2 was not associated with change in hsCRP (RYGB: $r = 0.13$ [95% CI − 0.24, 0.46]; diet: $r = − 0.13$ [95% CI

− 0.46, 0.25]) or estimated liver fat (RYGB: $r = 0.16$ [95% CI − 0.21, 0.48]; diet: $r = 0.28$ [95% CI − 0.09, 0.57]) in either group. The absorption was still faster at Year 2 in the RYGB group; T_{max} was reduced by 1.1 [95% CI 0.4, 1.9] hour(s) compared with baseline (Table 3), and was 0.8 [95% CI 0.2, 1.4] hour(s) shorter in the RYGB group compared with the diet group. At Year 2, C_{max} in the RYGB group was 27% [95% CI 3, 51] lower compared with Week 9, but not different from C_{max} at baseline or when compared with the diet group at Year 2. The diet group showed no difference from baseline in rosuvastatin pharmacokinetics at Year 2.

Neither short- nor long-term change in oral clearance was different in patients with the reduced-function variant (c.521TC or c.521CC) of *SLCO1B1* from those with the homozygote wild-type variant (c.521TT) in either group (Fig. 4). While a statistically significant difference in change in oral clearance between individuals with the c.521TT and c.521TT/CC variants were found in the diet group only during LED, no differences were found in the combined RYGB and diet groups in the same time period.

4 Discussion

To the best of our knowledge, this is the first longitudinal, prospective pharmacokinetic study in patients with severe obesity, evaluating the effect of RYGB and strict diet on the activity of the hepatic uptake transporter OATP1B1, using rosuvastatin as a probe drug. The main finding was that neither body weight nor weight loss, induced by either RYGB or strict diet, seemed to substantially influence the activity of the hepatic uptake transporter OATP1B1. There were no systematic differences in short- or long-term change in oral clearance between patients with the reduced function variant of *SLCO1B1* or wildtype, providing the main evidence for unchanged OATP1B1 activity following RYGB and weight loss observed in the present study. Also, no statistically significant differences in rosuvastatin pharmacokinetics were shown between patients with severe obesity and the

Table 2 Summary of observed rosuvastatin pharmacokinetic parameters over time across groups

	RYGB				Diet				Controls
	Week 0 (n = 38)	Week 3 (n = 39)	Week 9 (n = 35)	Year 2 (n = 32)	Week 0 (n = 40)	Week 3 (n = 39)	Week 9 (n = 37)	Year 2 (n = 30)	Week 0 (n = 18)
Oral clearance (L/h)	374 ± 23	336 ± 23	306 ± 20	469 ± 18	360 ± 23	277 ± 22	329 ± 22	362 ± 27	337 ± 11
C_{max} (ng/mL)	9.1 ± 8.3	10.2 ± 8.3	14.1 ± 15.5	9.1 ± 9.1	9.0 ± 5.0	10.7 ± 6.6	9.5 ± 5.4	11.0 ± 8.3	12.9 ± 11.8
T_{max} (h)	3.0 ± 1.4	2.5 ± 0.8	2.3 ± 1.1	2.2 ± 1.5	2.7 ± 0.7	2.7 ± 0.9	2.6 ± 1.0	2.7 ± 0.8	2.0 ± 0.7

Values are presented as mean ± standard deviation, and from the final population pharmacokinetic model

C_{max} maximum concentration, *RYGB* Roux-en-Y gastric bypass, T_{max} time at maximum concentration

Table 3 Differences in rosuvastatin pharmacokinetics within groups over time, and differences between groups at each visit

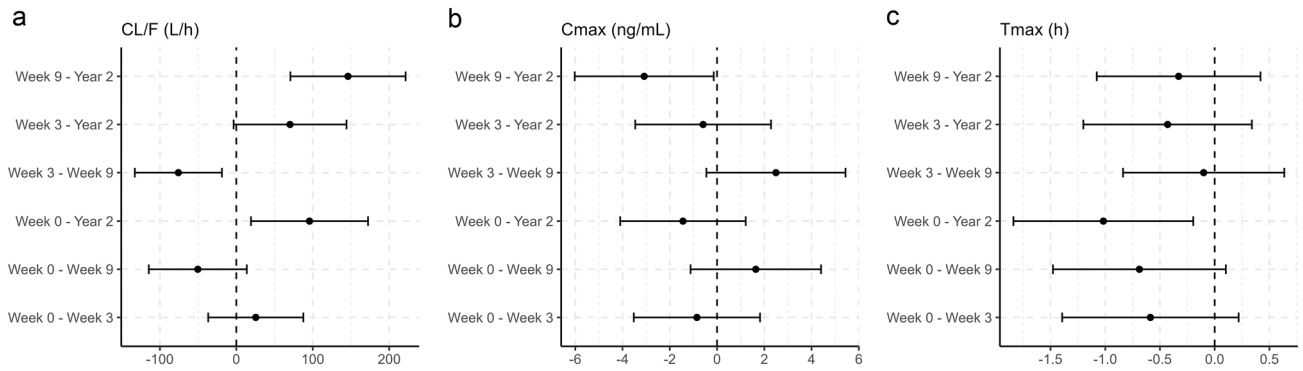|	RYGB					Diet					Difference between groups			
	Week 0–Week 3	Week 0–Week 9	Week 0–Year 2	Week 3–Week 9	Week 9–Year 2	Week 0–Week 3	Week 0–Week 9	Week 0–Year 2	Week 3–Week 9	Week 9–Year 2	Week 0	Week 3	Week 9	Year 2
Oral clearance (L/h)	−60* [−119, 0]	−87* [−147, −27]	80* [3, 157]	−28 [−80, 25]	167* [91, 243]	−85* [−142, −28]	−37 [−96, 23]	−16 [−81, 50]	48 [−5, 102]	21 [−42, 85]	5 [−81, 91]	30 [−39, 100]	−45 [−119, 28]	101* [2, 200]
C_{max} (ng/mL)	1.1 [−1.3, 3.4]	2.3 [−0.3, 5.0]	−0.7 [−3, 1.5]	1.3 [−1.5, 4.0]	−3.0 [−5.8, −0.3]	1.9 [−0.7, 4.5]	0.7 [−1.8, 3.1]	0.7 [−1.9, 3.4]	−1.2 [−4.0, 1.5]	0.0 [−2.7, 2.8]	−0.6 [−3.3, 2.1]	−1.4 [−4.5, 1.7]	1.1 [−2.1, 4.3]	−2.0 [−4.9, 0.9]
T_{max} (h)	−0.6 [−1.4, 0.1]	−0.9* [−1.7, −0.4]	−1.1* [−1.9, −0.4]	−0.3 [−0.9, 0.3]	−0.2 [−0.8, 0.4]	−0.1 [−0.8, 0.7]	−0.3 [−1.0, 0.5]	−0.1 [−0.9, 0.7]	−0.2 [−0.9, 0.5]	0.1 [−0.6, 0.9]	0.2 [−0.4, 0.9]	−0.4 [−1.0, 0.2]	−0.5 [−1.0, 0.1]	−0.8* [−1.4, −0.2]

Values are presented as mean [95% confidence interval] and are obtained from linear mixed model estimated marginal means. Difference between groups is calculated with the RYGB group as reference (RYGB–DIET). Values in bold marked with * are statistically significant to $p < 0.05$

C_{max} maximum observed concentration, RYGB Roux-en-Y gastric bypass, T_{max} time at maximum concentration

normal-to-overweight control group at baseline, suggesting no effect of body weight per se on OATP1B1 activity or rosuvastatin pharmacokinetics. This is supported by similar findings using a semi-mechanistic proteomics-informed model in a subset of the same patients [27].

Given that the changes in rosuvastatin oral clearance were also present in patients with genetically decreased OATP1B1 transport ability, it seems plausible that physiological alterations associated with caloric restriction and/or RYGB induced the observed alterations in oral clearance in the present study. Following the 3-week LED with similar weight loss, oral clearance decreased by approximately 20% in both intervention groups. It is known that caloric restriction may affect both liver size and composition. In a systematic review of LEDs (800–1200 kcal/day) prior to bariatric surgery, liver size was found to be reduced by 12–27%, and approximately 80% of total reduction in liver size was described to occur in the initial two weeks of diet [35]. As rosuvastatin displays a high hepatic extraction ratio (0.63), clearance and bioavailability may be susceptible to changes in both portal and hepatic blood flow [14]. It is possible that hepatic blood flow could be altered following rapid reduction in liver size, as hepatic blood flow has been found to increase following bariatric surgery [36, 37]. A transient increase in portal vein blood flow could thus lead to an increased bioavailability of rosuvastatin, possibly explaining the reduced oral clearance following the initial LED. However, this hypothesis will require further investigation into hepatic haemodynamics following diet-induced weight loss. During the initial LED, change in oral clearance was not associated with change in predicted liver fat content, suggesting that liver composition may be less important with regard to rosuvastatin disposition. Additionally, oral clearance of rosuvastatin was not different in patients with NAFLD-score above the diagnostic cut-off value compared with those with normal scores. This agrees with findings from Tirona and colleagues, who reported no differences in rosuvastatin pharmacokinetics in patients with obesity with magnetic resonance imaging (MRI)-confirmed NAFLD compared to a control group [38]. Furthermore, RYGB or 6 weeks of additional VLED did not induce additional changes in oral clearance despite further reduction in body weight, which indicates that weight loss is not the sole explanation for the observed effects. Nonetheless, a statistically significant between-group difference in the change in oral clearance following RYGB or six weeks of additional VLED was found. However, considering that no significant changes within either group were observed in this period, the observed between-group difference was considered to be less important in the overall interpretation of the results.

At Year 2, no changes in rosuvastatin pharmacokinetics from baseline were observed in the diet group, while the RYGB group demonstrated a net increase in oral clearance

Fig. 3 Between-group differences in within-group change for the Roux-en-Y gastric bypass (RYGB) and diet groups for **a** oral clearance (CL/F), **b** maximum concentration (C_{max}) and **c** time to maximum concentration (T_{max}). Difference between groups are made with the RYGB group as reference (positive values indicate greater change in the RYGB group), and are presented as marginal mean with 95% confidence interval
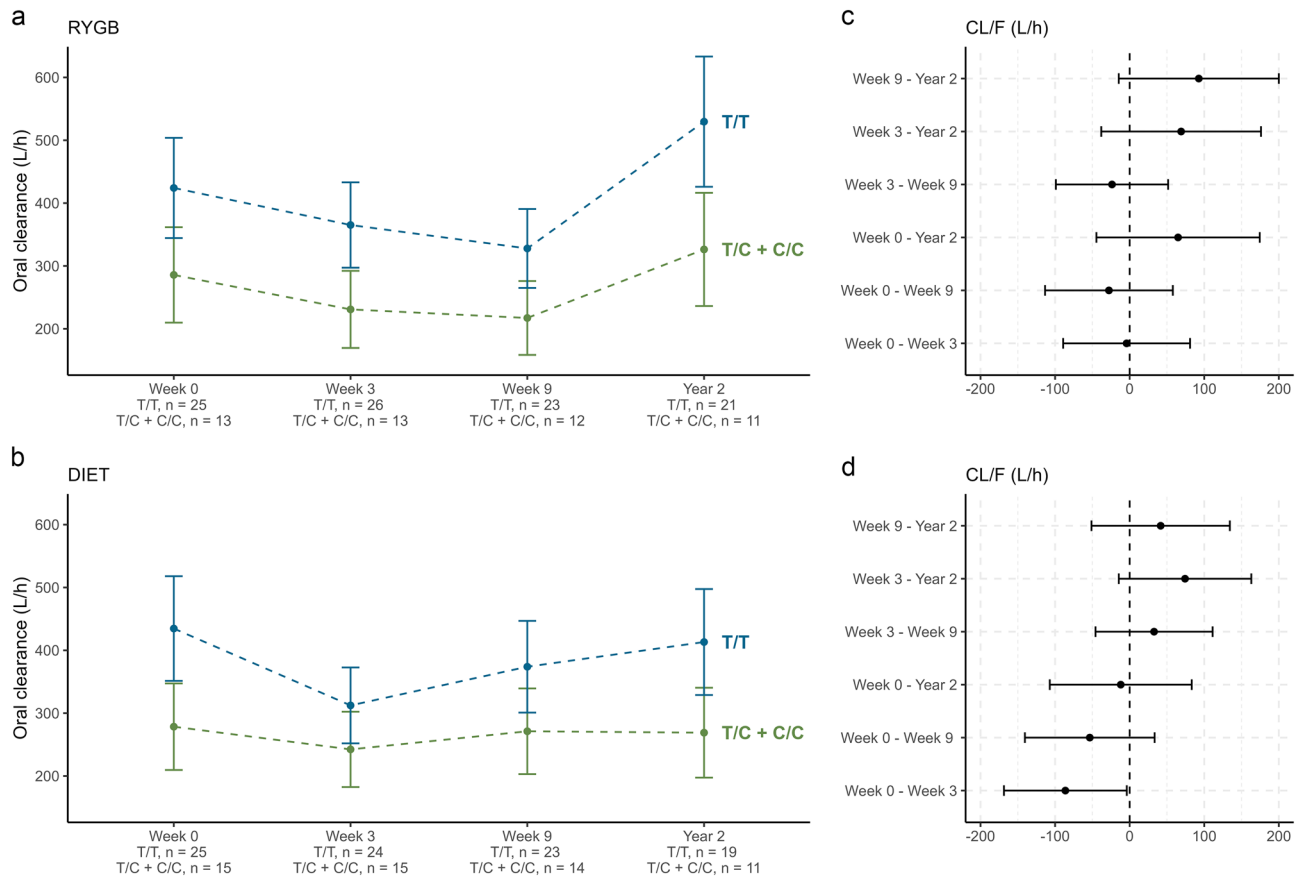
Fig. 4 Longitudinal overview of linear mixed effects model predicted oral clearance for individuals expressing the reduced function variant *SLCO1B1* c.521CC and TC compared with c.521TT in the **a** Roux-en-Y gastric bypass (RYGB) and **b** diet groups, respectively. Data are presented as marginal mean with 95% confidence interval. The between-variant difference in within-variant change for the individuals with *SLCO1B1* c.521TT or TC genotype compared with c.521TT are shown for the **c** RYGB and **d** diet group, presented as marginal mean with 95% confidence interval, with c.521TT as the reference group (positive values indicate greater change in patients with c.521TT)

of approximately 21%. This increase in oral clearance long term seems to be a surgery-specific effect on rosuvastatin absorption, leading to a net reduced bioavailability that may not have been readily apparent or sufficiently developed six weeks post-surgery. Given the anatomical and physiological changes in the gastrointestinal tract following RYGB, and the fact that rosuvastatin is moderately absorbed (~ 50%) [39] and displays a complex, dissolution rate-limited absorption (BCS class II), a reduction in the absorption and thus oral bioavailability after surgery is not unexpected. Surprisingly, this effect was not observed shortly after surgery. Moreover, it cannot be ruled out that other surgery-specific effects, such as alteration in incretins, expression/activity of other drug transporters such as NTCP or gut microbiota, may have contributed to the observed change in oral clearance in the long term. To date, only one study has evaluated the effect of RYGB on rosuvastatin pharmacokinetics. However, with only one dose- and weight-normalised blood sample, the data were not sufficient to draw conclusions regarding the effect of RYGB on the pharmacokinetics of rosuvastatin [40].

At the time of surgery, hepatic expression of OATP1B1 was positively associated with oral clearance in the RYGB group, but no such associations were shown in the control group, despite similar mean hepatic expression of OATP1B1 in the two groups. In contrast to the controls, the RYGB group was subjected to an initial LED, and thus a subsequent weight loss prior to surgery in the present study. This may potentially explain some of these differences, as rosuvastatin oral clearance was already reduced in the RYGB group when biopsies for protein expression measurement were obtained.

A strength of the present study was that oral clearance of rosuvastatin was calculated using a precise measurement of $AUC_{0-\infty}$, obtained from extensive blood-sampling in combination with an internally validated population pharmacokinetic model. Additionally, by including a dietary control group with matched short-term weight loss, we were able to differentiate the effects of surgery and weight loss on rosuvastatin pharmacokinetics. However, it is also important to recognise the limitations of the presented work. Most importantly, without concomitant intravenous administration it is not possible to determine absolute bioavailability of rosuvastatin, which is likely to change following RYGB. As such, true clearance could provide additional mechanistic understanding of the underlying processes. Another weakness was that NAFLD was not confirmed with biopsy or MRI, but predicted based on metabolic factors. It is also important to recognise that rosuvastatin has a reported half-life of 20 h [14], but sampling was only performed up to 24 h. As such, population pharmacokinetic modelling was used for parameter estimation over non-compartmental methods, as the former is not as reliant on rich sampling in the elimination phase. While additional samples may have improved the accuracy of parameter estimation, we could not justify the added patient inconvenience and logistical challenges for this probe drug.

5 Conclusions

In conclusion, neither body weight, weight loss, nor RYGB per se seem to affect OATP1B1 activity. This is primarily substantiated by the fact that individuals with the reduced function variant of *SLCO1B1* showed similar change in oral clearance of rosuvastatin over time. The short-term decrease in oral clearance following LED is reversible, as indicated by the return to baseline values following regained weight in the diet group while the long-term increase in oral clearance observed in the RYGB group appears to be due to a surgery-specific alteration in rosuvastatin disposition leading to an increased oral clearance. Overall, the observed changes in rosuvastatin pharmacokinetics in the present study were small, and dose adjustments of rosuvastatin following RYGB- or diet-induced weight loss appears to be unnecessary.

Declarations

Data availability statement Access to data collected from this study, including anonymised individual participant data, may potentially be made available following publication on e-mail request to the corresponding author. After approval of a proposal, data will be shared with investigators whose proposed use of the data has been approved by the COCKTAIL steering committee, according to the consent given by the participants and Norwegian laws and legislations.

Ethics approval The study was approved by the Regional Committee for Medical and Health Research Ethics (2013/2379/REK).

Consent to participate Written informed consent was obtained from all patients prior to any study-specific procedures.

Consent for publication Not applicable.

Code availability Not applicable.

References

1. Collaboration NCDRF. Trends in adult body-mass index in 200 countries from 1975 to 2014: a pooled analysis of 1698 population-based measurement studies with 19.2 million participants. Lancet. 2016;387(10026):1377–96.
2. Haslam DW, James WP. Obesity. Lancet. 2005;366(9492):1197–209.
3. Abdelaal M, le Roux CW, Docherty NG. Morbidity and mortality associated with obesity. Ann Transl Med. 2017;5(7):161.
4. Garvey WT, Mechanick JI, Brett EM, Garber AJ, Hurley DL, Jastreboff AM, et al. American Association of Clinical Endocrinologists and American College of Endocrinology Comprehensive Clinical Practice Guidelines Formedical Care of Patients with Obesity. Endocr Pract. 2016;22:1–203.
5. Colquitt JL, Pickett K, Loveman E, Frampton GK. Surgery for weight loss in adults. Cochrane Database Syst Rev. 2014;8:003641.
6. Cosentino C, Marchetti C, Monami M, Mannucci E, Cresci B. Efficacy and effects of bariatric surgery in the treatment of obesity: network meta-analysis of randomised controlled trials. Nutr Metab Cardiovasc Dis. 2021;31(10):2815–24.
7. Padwal R, Klarenbach S, Wiebe N, Hazel M, Birch D, Karmali S, et al. Bariatric surgery: a systematic review of the clinical and economic evidence. J Gen Intern Med. 2011;26(10):1183–94.
8. Salte OBK, Svanevik M, Risstad H, Hofso D, Blom-Hogestol IK, Johnson LK, et al. Standard versus distal Roux-en-Y gastric bypass in patients with BMI 50-60 kg/m²: 5-year outcomes of a double-blind, randomized clinical trial. BJS Open. 2021;5(6).
9. Padwal R, Brocks D, Sharma AM. A systematic review of drug absorption following bariatric surgery and its theoretical implications. Obes Rev. 2010;11(1):41–50.
10. Chapman MJ, McTaggart F. Optimizing the pharmacology of statins: characteristics of rosuvastatin. Atheroscler Suppl. 2002;2(4):33–6 (**discussion 6-7**).
11. McFeely SJ, Ritchie TK, Yu J, Nordmark A, Levy RH, Ragueneau-Majlessi I. Identification and evaluation of clinical substrates of organic anion transporting polypeptides 1B1 and 1B3. Clin Transl Sci. 2019;12(4):379–87.
12. Zhang D, Ding Y, Wang X, Xin W, Du W, Chen W, et al. Effects of ABCG2 and SLCO1B1 gene variants on inflammation markers in patients with hypercholesterolemia and diabetes mellitus treated with rosuvastatin. Eur J Clin Pharmacol. 2020;76(7):939–46.
13. Shitara Y, Maeda K, Ikejiri K, Yoshida K, Horie T, Sugiyama Y. Clinical significance of organic anion transporting polypeptides (OATPs) in drug disposition: their roles in hepatic clearance and intestinal absorption. Biopharm Drug Dispos. 2013;34(1):45–78.
14. Martin PD, Warwick MJ, Dane AL, Hill SJ, Giles PB, Phillips PJ, et al. Metabolism, excretion, and pharmacokinetics of rosuvastatin in healthy adult male volunteers. Clin Ther. 2003;25(11):2822–35.
15. Bergman E, Forsell P, Tevell A, Persson EM, Hedeland M, Bondesson U, et al. Biliary secretion of rosuvastatin and bile acids in humans during the absorption phase. Eur J Pharm Sci. 2006;29(3–4):205–14.
16. Niemi M, Pasanen MK, Neuvonen PJ. Organic anion transporting polypeptide 1B1: a genetically polymorphic transporter of major importance for hepatic drug uptake. Pharmacol Rev. 2011;63(1):157–81.
17. Hirota T, Fujita Y, Ieiri I. An updated review of pharmacokinetic drug interactions and pharmacogenetics of statins. Expert Opin Drug Metab Toxicol. 2020;16(9):809–22.
18. Krogstad V, Peric A, Robertsen I, Kringen MK, Vistnes M, Hjelmesaeth J, et al. Correlation of body weight and composition with hepatic activities of cytochrome P450 enzymes. J Pharm Sci. 2021;110(1):432–7.
19. Ulvestad M, Skottheim IB, Jakobsen GS, Bremer S, Molden E, Asberg A, et al. Impact of OATP1B1, MDR1, and CYP3A4 expression in liver and intestine on interpatient pharmacokinetic variability of atorvastatin in obese subjects. Clin Pharmacol Ther. 2013;93(3):275–82.
20. Kvitne KE, Robertsen I, Skovlund E, Christensen H, Krogstad V, Wegler C, et al. Short- and long-term effects of body weight loss following calorie restriction and gastric bypass on CYP3A-activity—a non-randomized three-armed controlled trial. Clin Transl Sci. 2022;15(1):221–33.
21. Jamwal R, Barlock BJ. Nonalcoholic fatty liver disease (NAFLD) and hepatic cytochrome P450 (CYP) enzymes. Pharmaceuticals (Basel). 2020;13(9):222.
22. Hjelmesaeth J, Asberg A, Andersson S, Sandbu R, Robertsen I, Johnson LK, et al. Impact of body weight, low energy diet and gastric bypass on drug bioavailability, cardiovascular risk factors and metabolic biomarkers: protocol for an open, non-randomised, three-armed single centre study (COCKTAIL). BMJ Open. 2018;8(5): e021878.
23. Krogstad V, Peric A, Robertsen I, Kringen MK, Wegler C, Angeles PC, et al. A comparative analysis of cytochrome P450 activities in paired liver and small intestinal samples from patients with obesity. Drug Metab Dispos. 2020;48(1):8–17.
24. Braamskamp M, Langslet G, McCrindle BW, Cassiman D, Francis GA, Gagne C, et al. Efficacy and safety of rosuvastatin therapy in children and adolescents with familial hypercholesterolemia: results from the CHARON study. J Clin Lipidol. 2015;9(6):741–50.
25. Machiela MJ, Chanock SJ. LDlink: a web-based application for exploring population-specific haplotype structure and linking

correlated alleles of possible functional variants. Bioinformatics. 2015;31(21):3555–7.

26. Wegler C, Olander M, Wisniewski JR, Lundquist P, Zettl K, Asberg A, et al. Global variability analysis of mRNA and protein concentrations across and within human tissues. NAR Genom Bioinform. 2020;2(1):lqz010.

27. Wegler C, Prieto Garcia L, Klinting S, Robertsen I, Wisniewski JR, Hjelmesaeth J, et al. Proteomics-informed prediction of rosuvastatin plasma profiles in patients with a wide range of body weight. Clin Pharmacol Ther. 2021;109(3):762–71.

28. Wisniewski JR, Mann M. Consecutive proteolytic digestion in an enzyme reactor increases depth of proteomic and phosphoproteomic analysis. Anal Chem. 2012;84(6):2631–7.

29. Tyanova S, Temu T, Cox J. The MaxQuant computational platform for mass spectrometry-based shotgun proteomics. Nat Protoc. 2016;11(12):2301–19.

30. Huber W, von Heydebreck A, Sultmann H, Poustka A, Vingron M. Variance stabilization applied to microarray data calibration and to the quantification of differential expression. Bioinformatics. 2002;18(suppl_1):S96-104.

31. Wisniewski JR, Rakus D. Multi-enzyme digestion FASP and the 'Total Protein Approach'-based absolute quantification of the *Escherichia coli* proteome. J Proteom. 2014;109:322–31.

32. Neely MN, van Guilder MG, Yamada WM, Schumitzky A, Jelliffe RW. Accurate detection of outliers and subpopulations with Pmetrics, a nonparametric and parametric pharmacometric modeling and simulation package for R. Ther Drug Monit. 2012;34(4):467–76.

33. Kotronen A, Peltonen M, Hakkarainen A, Sevastianova K, Bergholm R, Johansson LM, et al. Prediction of non-alcoholic fatty liver disease and liver fat using metabolic and genetic factors. Gastroenterology. 2009;137(3):865–72.

34. R Core Team. R: A Language and Environment for Statistical Computing. R Foundation for Statistical Computing. 2020.

35. Romeijn MM, Kolen AM, Holthuijsen DDB, Janssen L, Schep G, Leclercq WKG, et al. Effectiveness of a Low-calorie diet for liver volume reduction prior to bariatric surgery: a systematic review. Obes Surg. 2021;31(1):350–6.

36. Immonen H, Hannukainen JC, Kudomi N, Pihlajamaki J, Saunavaara V, Laine J, et al. Increased liver fatty acid uptake is partly reversed and liver fat content normalized after bariatric surgery. Diabetes Care. 2018;41(2):368–71.

37. Honka H, Koffert J, Kauhanen S, Kudomi N, Hurme S, Mari A, et al. Liver blood dynamics after bariatric surgery: the effects of mixed-meal test and incretin infusions. Endocr Connect. 2018;7(7):888–96.

38. Tirona RG, Kassam Z, Strapp R, Ramu M, Zhu C, Liu M, et al. Apixaban and Rosuvas–tatin pharmacokinetics in nonalcoholic fatty liver disease. Drug Metab Dispos. 2018;46(5):485–92.

39. Martin PD, Warwick MJ, Dane AL, Brindley C, Short T. Absolute oral bioavailability of rosuvastatin in healthy white adult male volunteers. Clin Ther. 2003;25(10):2553–63.

40. El-Zailik A, Cheung LK, Wang Y, Sherman V, Chow DS. Longitudinal impacts of gastric bypass surgery on pharmacodynamics and pharmacokinetics of statins. Obes Surg. 2019;29(8):2571–83.

Authors and Affiliations

Markus Hovd[1] [ORCID] · **Ida Robertsen[1]** · **Line Kristin Johnson[2]** · **Veronica Krogstad[1]** · **Christine Wegler[3,4]** · **Kine Eide Kvitne[1]** · **Marianne Kristiansen Kringen[5,6]** · **Eva Skovlund[7]** · **Cecilia Karlsson[8,9]** · **Shalini Andersson[10]** · **Per Artursson[11]** · **Rune Sandbu[2,12]** · **Jøran Hjelmesæth[2,13]** · **Anders Åsberg[1,14]** · **Rasmus Jansson-Löfmark[4]** · **Hege Christensen[1]**

1 Section for Pharmacology and Pharmaceutical Biosciences, Department of Pharmacy, University of Oslo, Blindern, PO 1068, 0316 Oslo, Norway

2 The Morbid Obesity Center, Vestfold Hospital Trust, P.O. Box 2168, 3103 Tønsberg, Norway

3 Department of Pharmacy, Uppsala University, P.O. Box 580, 75123 Uppsala, Sweden

4 DMPK, Research and Early Development, Cardiovascular, Renal and Metabolism, BioPharmaceuticals R&D, AstraZeneca, Pepparedsleden 1, 431 83 Mölndal, Sweden

5 Center for Psychopharmacology, Diakonhjemmet Hospital, Oslo, Norway

6 Department of Health Sciences, OsloMet-Oslo Metropolitan University, Oslo, Norway

7 Department of Public Health and Nursing, Norwegian University of Science and Technology, NTNU, P.O. Box 8905, 7491 Trondheim, Norway

8 Late-stage Development, Cardiovascular, Renal and Metabolism, BioPharmaceuticals R&D, AstraZeneca, Gothenburg, Sweden

9 Department of Molecular and Clinical Medicine, Institute of Medicine, Sahlgrenska Academy, University of Gothenburg, Gothenburg, Sweden

10 Oligonucleotide Discovery, Discovery Sciences, BioPharmaceuticals R&D, AstraZeneca, Gothenburg, Sweden

11 Department of Pharmacy and Science for Life Laboratory, Uppsala University, P.O. Box 580, 75123 Uppsala, Sweden

12 Department of Surgery, Vestfold Hospital Trust, Tønsberg, Norway

13 Department of Endocrinology, Morbid Obesity and Preventive Medicine, Institute of Clinical Medicine, University of Oslo, P.O. Box 1171, 0318 Oslo, Norway

14 Department of Transplantation Medicine, Oslo University Hospital, Nydalen, P.O. Box 4950, 0424 Oslo, Norway

Supplementary Material for Paper I

Neither gastric bypass surgery nor diet-induced weight-loss affect OATP1B1 activity as measured by rosuvastatin oral clearance

Markus Hovd[1], Ida Robertsen[1], Line Kristin Johnson[2], Veronica Krogstad[1], Christine Wegler[3,4], Kine Eide Kvitne[1], Marianne Kristiansen Kringen[5,6], Eva Skovlund[7], Cecilia Karlsson[8,9], Shalini Andersson[10], Per Artursson[11], Rune Sandbu[2,12], Jøran Hjelmesæth[2,13], Anders Åsberg[1,14], Rasmus Jansson-Löfmark[4], Hege Christensen[1]

Corresponding author details: Markus Hovd (m.h.hovd@farmasi.uio.no)

Affiliations:

[1] *Section for Pharmacology and Pharmaceutical Biosciences, Department of Pharmacy, University of Oslo, PO 1068 Blindern, 0316 Oslo, Norway*

[2] *The Morbid Obesity Center, Vestfold Hospital Trust, P.O. Box 2168, 3103 Tønsberg, Norway*

[3] *Department of Pharmacy, Uppsala University, P.O. Box 580, SE-75123, Uppsala, Sweden*

[4] *DMPK, Research and Early Development, Cardiovascular, Renal and Metabolism, BioPharmaceuticals R&D, AstraZeneca, Pepparedsleden 1, 431 83 Mölndal, Sweden*

[5] *Center for Psychopharmacology, Diakonhjemmet Hospital, Oslo, Norway*

[6] *Department of Health Sciences, OsloMet - Oslo Metropolitan University, Oslo, Norway*

[7] *Department of Public Health and Nursing, Norwegian University of Science and Technology, NTNU, P.O. Box 8905, 7491 Trondheim, Norway*

[8] *Late-stage Development, Cardiovascular, Renal and Metabolism, BioPharmaceuticals R&D, AstraZeneca, Gothenburg, Sweden*

[9] *Department of Molecular and Clinical Medicine, Institute of Medicine, Sahlgrenska Academy, University of Gothenburg, Gothenburg, Sweden*

[10] *Oligonucleotide Discovery, Discovery Sciences, BioPharmaceuticals R&D, AstraZeneca, Gothenburg, Sweden.*

[11] *Department of Pharmacy and Science for Life Laboratory, Uppsala University, P.O. Box 580, SE-75123, Uppsala, Sweden*

[12] *Department of Surgery, Vestfold Hospital Trust, Tønsberg, Norway.*

[13] *Department of Endocrinology, Morbid Obesity and Preventive Medicine, Institute of Clinical Medicine, University of Oslo, P.O. Box 1171, 0318 Oslo, Norway*

[14] *Department of Transplantation Medicine, Oslo University Hospital, P.O. Box 4950 Nydalen, 0424 Oslo, Norway*

METHODS

Pharmacokinetic investigations

Patients abstained from food and drugs from 10 pm the evening before the investigations. Blood samples were obtained via a peripheral venous catheter at 0.25, 0.5, 1, 1.5, 2, 3, 4, 4.25, 4.5, 5, 5.5, 6, 8, 10, 12, 23, and 24 hours following rosuvastatin administration. Blood samples were drawn in K2-EDTA vacutainer tubes placed on ice and centrifuged for 10 minutes at 4 ºC (1800 g). Plasma was separated into Cryovials prefilled with 0.2 mL of 0.1 M sodium acetate buffer and frozen at -70ºC within one hour.

Population pharmacokinetic modelling

A population pharmacokinetic model was developed in order to determine rosuvastatin pharmacokinetics in the individual patients. The model was developed using the nonparametric adaptive grid approach, NPAG, [1] implemented in Pmetrics (version 1.9.4) for R (version 3.6.0). A total of 3630 rosuvastatin concentrations corresponding to 197 18-point and 111 9-point 24-hr pharmacokinetic profiles from 98 patients were included. The complete dataset was split into a development- (75%) and validation (25%) set for the purpose of internal validation; 18-point pharmacokinetic profiles were allocated to the development set, with random allocation of 9-point profiles until the development set contained 75% of all pharmacokinetic profiles.

At each pharmacokinetic investigation, a total of 18 blood samples for determination of rosuvastatin concentration were obtained from each individual. Rich pharmacokinetic profiles (all 18 samples) were obtained for analyses in the first 7 and 13 patients in the RYGB- and diet group at week 0, 3 and 9, as well as in the first 6 patients in both groups at year 2. Rich pharmacokinetic profiles were also obtained from the first 6 patients in the normal to overweight control group. Based on these rich profiles, a preliminary population pharmacokinetic model of rosuvastatin was developed. This model was further used to determine a 9-point bioanalysis strategy using the multiple model optimal sampling (*MMopt*) function included in Pmetrics. Based on the best agreement with reference model derived (18-point) rosuvastatin AUC_{0-24} the following nine time points were chosen: 0.5, 1, 1.5, 3, 4.25, 5, 6, 12 and 24 hours post administration. Samples at these nine time points were analyzed for the remaining patients (n = 32, 30 and 12 in the RYGB, diet, and control group, respectively).

The most appropriate pharmacokinetic structural model was assessed by testing 1-, 2-, and 3-compartment models with different absorption pattern (zero and first order and with and without lag time and a Heaviside function) as well as the inclusion of enterohepatic recirculation. The error polynomial was based on the standard deviation of rosuvastatin calibration curves from 0.0400 ng/mL to 40.0 ng/mL with more than 60 replicates each. Both gamma (error = SD*γ) and lambda (error = [SD²

+ $\lambda^2]^{0.5}$) error models were tested, where SD is the standard deviation of the analytical method; SD = 0.0005495041+ 0.0342807720*x + 0.0001165904*x^2 where x is the observed rosuvastatin concentration. Covariates were not included in the model, since a linear mixed model approach including potential covariates was used for the between group and over time analysis. Additionally, the richness of the data assured proper individual predictions without inclusion of covariates. Individual predictions were used to calculate pharmacokinetic parameters for further analysis with linear mixed models. Model selection was primarily based on comparison of the relative root mean squared predictive error (RMSE, %) calculated from the relative predictive error (predicted concentration - observed concentration/observed concentration) (PE, %) of all rosuvastatin concentrations in the development dataset, bias and imprecision, and individual concentration versus time plots. Linear regression slope, R^2-values of the observed versus predicted plots AIC, and BIC also guided model development to a lesser extent.

The models were run on a high-performance computing (HPC) cluster utilizing a modified version of Pmetrics. The standard compute nodes are equipped with 40 CPU cores and 192 GiB memory each, with the full cluster boasting a theoretical performance (Rpeak) of 645 teraflops. The final developed model was validated using the validation dataset (without cycling). Subsequent to this was the validated model cycled until convergence with the complete dataset (combined development and validation datasets) and used to obtain individual parameter predictions to be used in the pharmacokinetic calculations presented below.

RESULTS

Patient flowchart

The patient flow in the study has been described previously [2], and is further detailed in **Figure S1**. Due to technical difficulties, some patients were unable to supply evaluable rosuvastatin pharmacokinetic profiles at all four study visits, whereas one patient in the diet group did not supply any pharmacokinetic profiles.
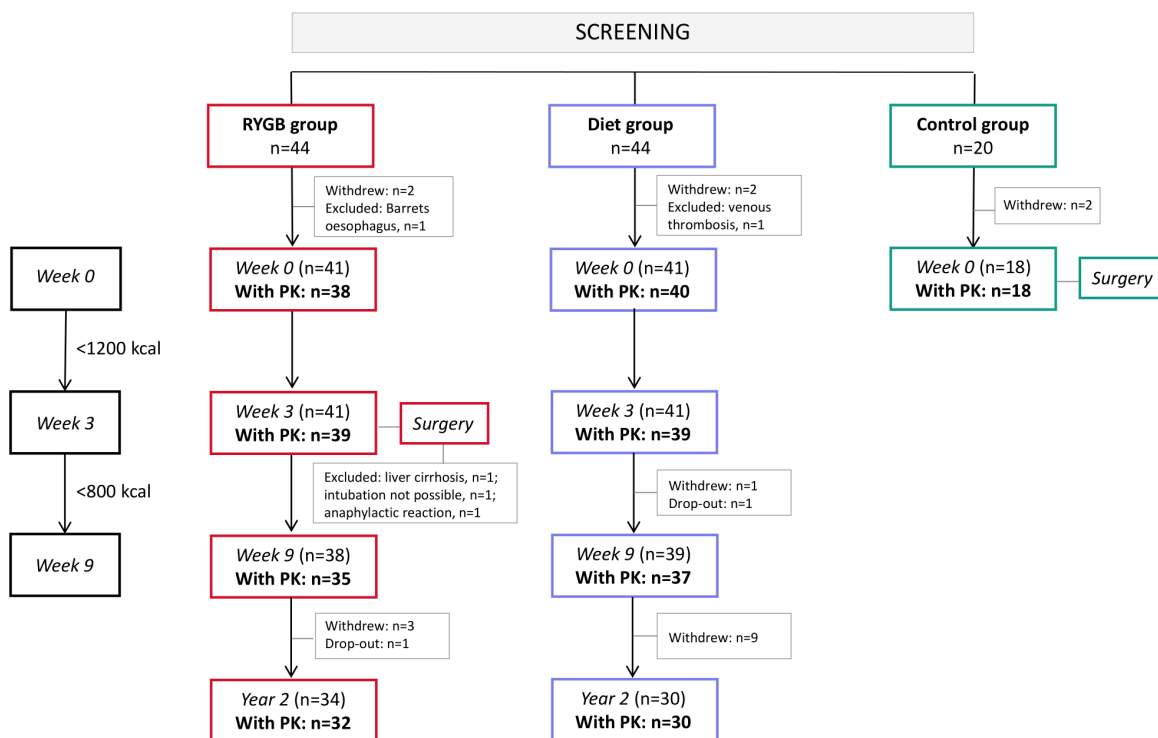
Figure S1: Patient flow in the study, modified from Kvitne et. al [2].

Population pharmacokinetic modelling

In literature, two-compartmental models have previously been used to assess rosuvastatin pharmacokinetics in pediatric patients and patients with renal impairment [3,4], both developed using non-linear mixed-effects modeling. Due to a resampling of the dataset following access to a high-performance computing cluster, AIC values are not included for model comparisons, as this metric is not representative for comparing different datasets. Instead, representative RMSE-values are given indicatively. The one- (RMSE: 36%) and two-compartmental (RMSE: 24%) models tested showed poor predictive performance. Inclusion of enterohepatic recirculation moderately improved model fit (RMSE: 17%). Three-compartment models including enterohepatic recirculation were also tested but did not improve the predictive performance with regard to the PE, RMSE, R^2, bias, and imprecision.

A three-compartment model with two intermediary absorption compartments with individual lag-times and time-dependent transport rates regulated by a modified Heaviside-function (**Figure S2**, **Equation S1**) described the data well. The modified Heaviside function describes how the transport rate from the ith to the jth compartment approximate Ka over time from time Tlag, at a rate adjusted by L (**Equation S1**).

$$K_{i,j} = Ka * \left[\frac{1}{2} * \left(1 + \tan^{-1}\left(\mathrm{L} * (T - Tlag_i)\right) * \frac{2}{\pi} \right) \right] \qquad \textit{Equation S1}$$
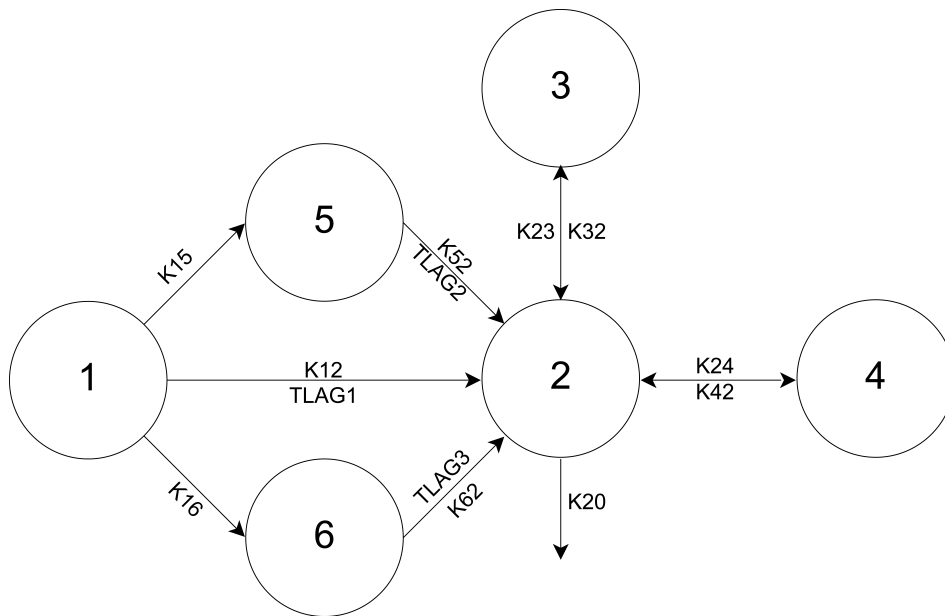
Figure S2: Structural outline of the final pharmacokinetic model. K12, K52 and K62 are described using a modified Heaviside-equation. Absorption from compartment 1 is both direct (K12) and indirect via intermediary compartments 5 and 6. All absorption pathways are associated with individual lag-times for absorption, with time-dependent transport rates adjusted by a modified Heaviside function. Two peripheral compartments (3 and 4) were included. Elimination is of the first-order from the central compartment (2) only. Compartment 2 corresponds to the observed plasma concentrations of rosuvastatin.

The final model described the data well with low predictive error. Predictions mostly fall on or directly around the unity line (**Figure S3 A**), and model residuals appear evenly distributed across the range of concentrations (**Figure S3 B**). While a trend for underpredictions was present for predictions made at the 24-hour sample time (**Figure S3 C**), the residuals at earlier sample times appears evenly distributed.
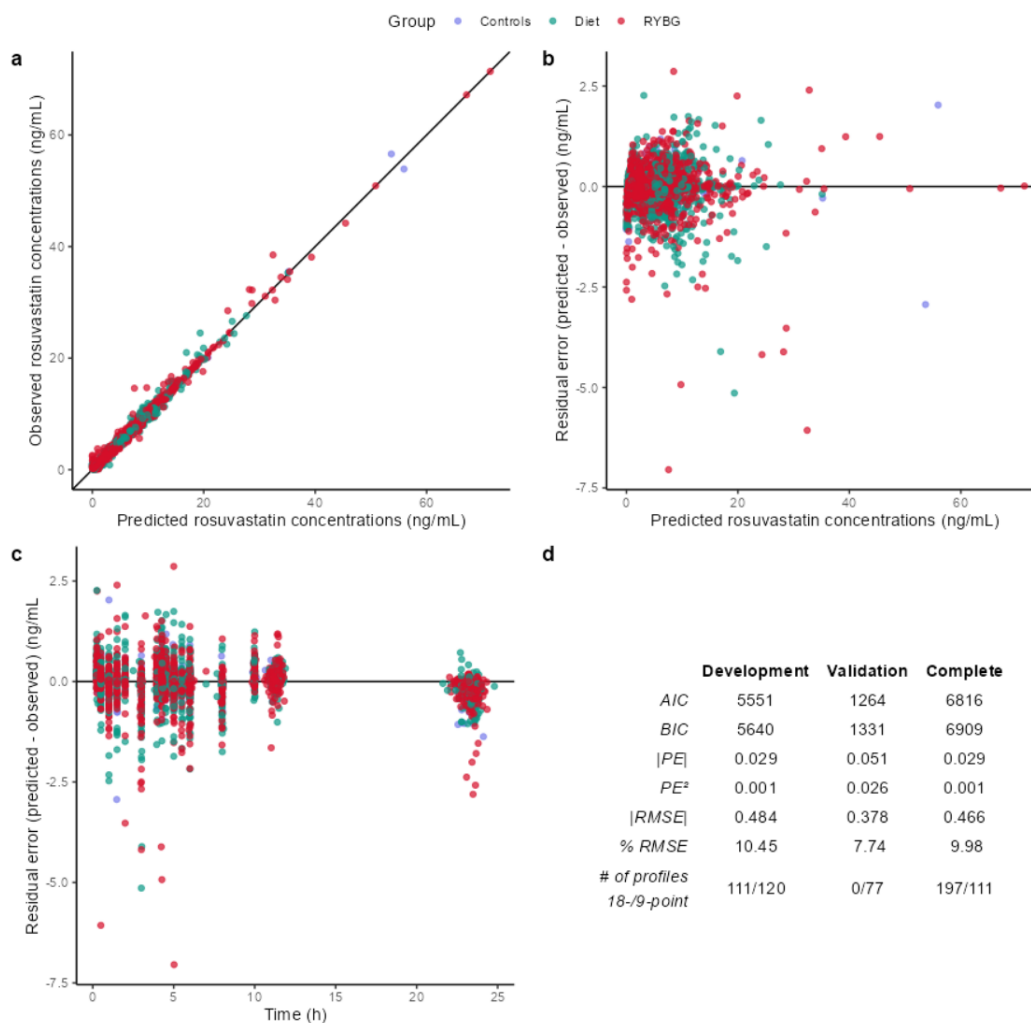
Figure S3: Population pharmacokinetic performance plots and metrics. **a)** Observed rosuvastatin concentrations against posterior individual predicted concentrations. Line represents the identity line. **b)** Residual error against individual observed rosuvastatin concentrations. **c)** Residual error against time. **d)** Tabular presentation of key population model performance metrics for the development (75%), validation (25%) and complete dataset.

The model proved especially efficient at predicting the multiple peaks in the absorption phase of rosuvastatin. Randomly sampled individual concentration-time profiles from each group at each visit are shown in **Figure S3.** Here, the atypical absorption patterns of rosuvastatin are demonstrated, with multiple peaks following absorption.
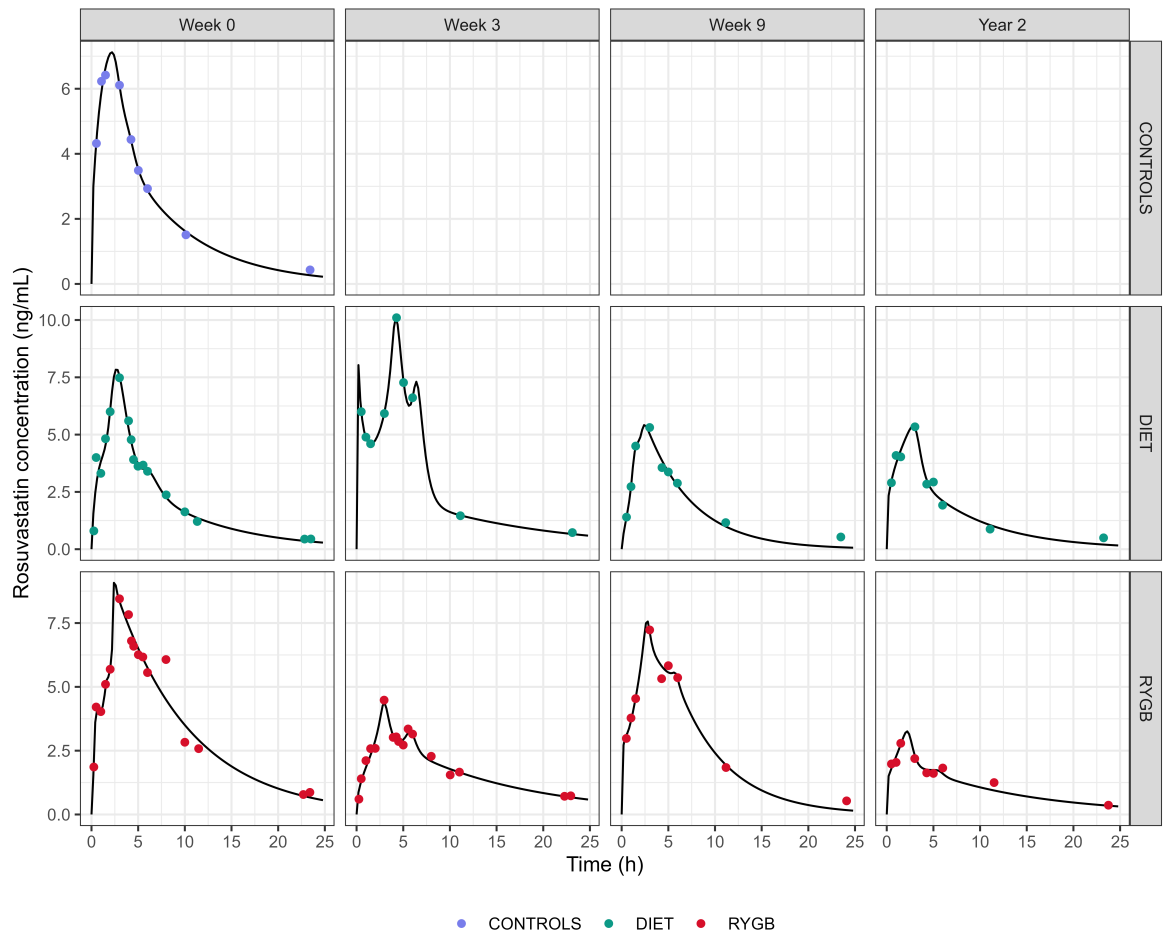
Figure S4: Individual posterior predicted rosuvastatin concentrations (lines) and observed rosuvastatin concentration (points) from one patient in each group at each visit, randomly sampled.

Rosuvastatin proteomics
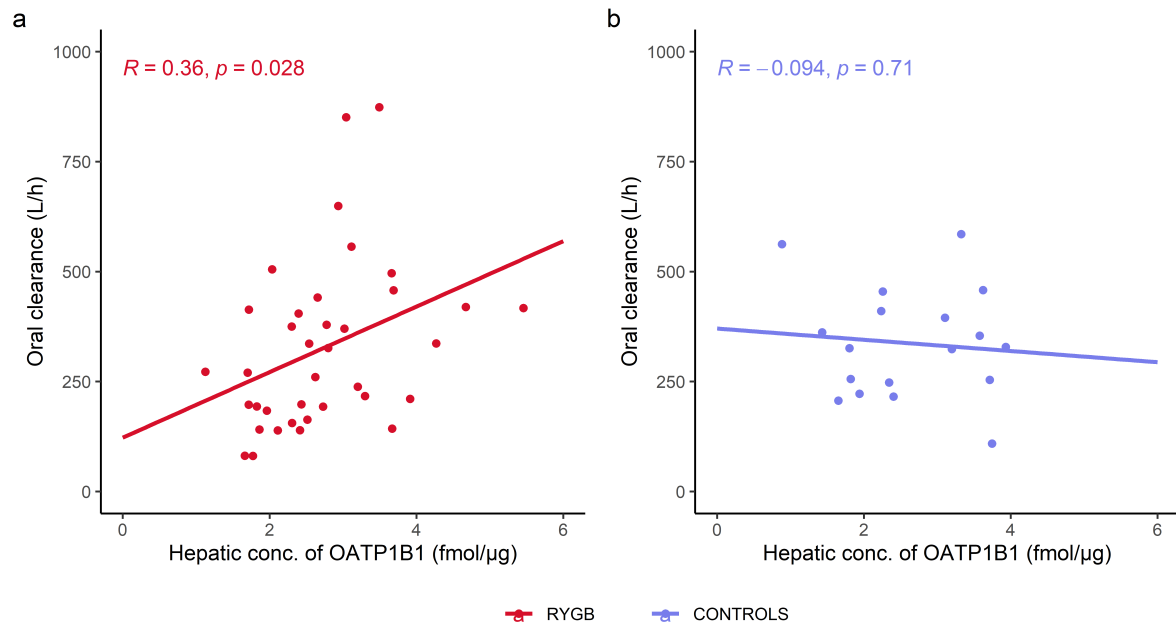
Figure S5: Scatterplot and associations between rosuvastatin oral clearance and hepatic concentration of OATP1B1 in the (a) RYGB (n = 37) and (b) normal to overweight control group (n = 18). Associations are reported using Pearson's product-moment correlation coefficient.
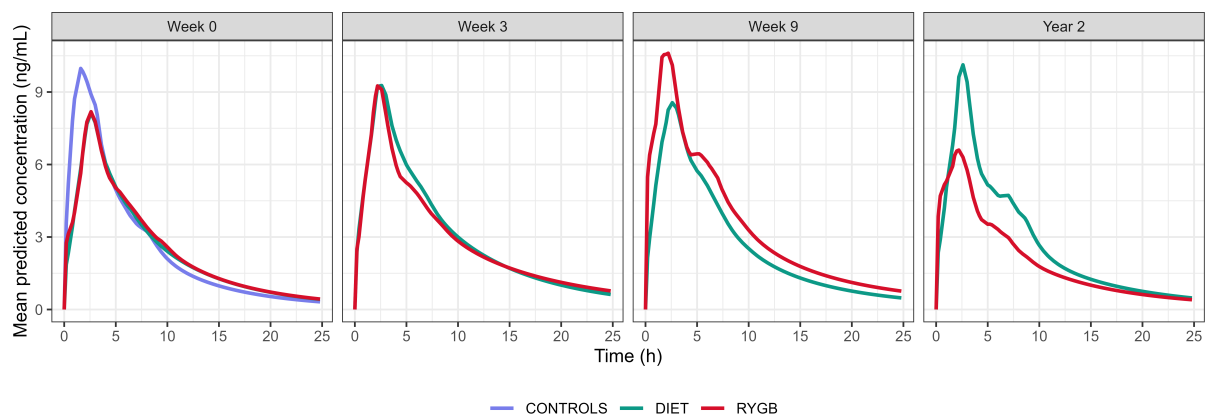
Figure S6: Mean predicted plasma concentration of rosuvastatin at each pharmacokinetic investigation for the normal to overweight control-, RYGB- and diet group. At week 0, the predicted concentration over time is almost completely overlapping in the RYGB- and diet group. Predictions were made in 12-minute intervals.

Rosuvastatin pharmacogenomics

Table S1: Distribution of *ABCG2* variants at baseline.

	RYGB (n = 40)	DIET (n = 40)	CONTROLS (n = 18)
***ABCG2* (BCRP) †**			
Q141K G/G | G/T | T/T	35 | 4 | 1	34 | 6 | 0	15 | 1 | 1
V12M C/C | C/T | T/T	36 | 4 | 0	37 | 3 | 0	17 | 0 | 0

† For one individual in the control group, genotype could not be determined.

Table S2: Differences in oral clearance between pharmacogenetic variants of *SLCO1B1* and *ABCG2* at week 0 (baseline), as determined by Welch's two-sample t-test.

Gene	Variant	*n*	Variant CL/F (L/h)	Wildtype CL/F (L/h)	Absolute difference	% difference	P-value
SLCO1B1	c.521TC/ CC	32	284	403†	-119 [-59, -180]	-30	< .001
ABCG2	V12M C/C Q141K G/T	10	272	377	-105 [-1, -208]	-28	0.047
ABCG2	V12M C/C Q141K T/T	2	172	377	-206 [593, -1005]	-55	0.212
ABCG2	V12M C/T Q141K G/G	7	389	377	12 [139, -116]	3	0.837

CL/F: Oral clearance.

† *SLCO1B1* c.521 TT considered wildtype

Table S3: Differences in systemic exposure between pharmacogenetic variants of *SLCO1B1* and *ABCG2* at week 0 (baseline), as determined by Welch's two-sample t-test.

Gene	Variant	*n*	Variant $AUC_{0-\infty}$	Wildtype $AUC_{0-\infty}$	Absolute difference	% difference	P-value
SLCO1B1	c.521TC+ CC	32	89	56†	32 [49, 16]	57	< .001
ABCG2	V12M C/C Q141K G/T	10	93	63	30 [64, -4]	47	0.079
ABCG2	V12M C/C Q141K T/T	2	145	63	82 [893, -728]	131	0.422
ABCG2	V12M C/T Q141K G/G	7	57	63	-6 [12, -24]	-9	0.483

$AUC_{0-\infty}$: Area under the curve from zero to infinity.

† *SLCO1B1* c.521 T/T considered wildtype

References

1   Neely, M. N., van Guilder, M. G., Yamada, W. M., Schumitzky, A. & Jelliffe, R. W. Accurate detection of outliers and subpopulations with Pmetrics, a nonparametric and parametric pharmacometric modeling and simulation package for R. *Ther. Drug Monit.* **34**, 467-476, doi:10.1097/FTD.0b013e31825c4ba6 (2012).

2   Kvitne, K. E. *et al.* Short- and long-term effects of body weight loss following calorie restriction and gastric bypass on CYP3A-activity - a non-randomized three-armed controlled trial. *Clin. Transl. Sci.* **15**, 221-233, doi:10.1111/cts.13142 (2022).

3   Macpherson, M. *et al.* Population pharmacokinetics of rosuvastatin in pediatric patients with heterozygous familial hypercholesterolemia. *Eur. J. Clin. Pharmacol.* **72**, 19-27, doi:10.1007/s00228-015-1946-4 (2016).

4   Tzeng, T. B. *et al.* Population pharmacokinetics of rosuvastatin: implications of renal impairment, race, and dyslipidaemia. *Curr. Med. Res. Opin.* **24**, 2575-2585, doi:10.1185/03007990802312807 (2008).

Paper II

RESEARCH

Population pharmacokinetic modeling of CSF to blood clearance: prospective tracer study of 161 patients under work-up for CSF disorders

Markus Herberg Hovd[1], Espen Mariussen[2,7], Hilde Uggerud[2], Aslan Lashkarivand[3,4], Hege Christensen[1], Geir Ringstad[5,6] and Per Kristian Eide[3,4*]

Abstract

Background: Quantitative measurements of cerebrospinal fluid to blood clearance has previously not been established for neurological diseases. Possibly, variability in cerebrospinal fluid clearance may affect the underlying disease process and may possibly be a source of under- or over-dosage of intrathecally administered drugs. The aim of this study was to characterize the cerebrospinal fluid to blood clearance of the intrathecally administered magnetic resonance imaging contrast agent gadobutrol (Gadovist, Bayer Pharma AG, GE). For this, we established a population pharmacokinetic model, hypothesizing that cerebrospinal fluid to blood clearance differs between cerebrospinal fluid diseases.

Methods: Gadobutrol served as a surrogate tracer for extra-vascular pathways taken by several brain metabolites and drugs in cerebrospinal fluid. We estimated cerebrospinal fluid to blood clearance in patients with different cerebrospinal fluid disorders, i.e. symptomatic pineal and arachnoid cysts, as well as tentative spontaneous intracranial hypotension due to cerebrospinal fluid leakage, idiopathic intracranial hypertension, or different types of hydrocephalus (idiopathic normal pressure hydrocephalus, communicating- and non-communicating hydrocephalus). Individuals with no verified cerebrospinal fluid disturbance at clinical work-up were denoted references.

Results: Population pharmacokinetic modelling based on 1,140 blood samples from 161 individuals revealed marked inter-individual variability in pharmacokinetic profiles, including differences in absorption half-life (time to 50% of tracer absorbed from cerebrospinal fluid to blood), time to maximum concentration in blood and the maximum concentration in blood as well as the area under the plasma concentration time curve from zero to infinity. In addition, the different disease categories of cerebrospinal fluid diseases demonstrated different profiles.

Conclusions: The present observations of considerable variation in cerebrospinal fluid to blood clearance between individuals in general and across neurological diseases, may suggest that defining cerebrospinal fluid to blood clearance can become a useful diagnostic adjunct for work-up of cerebrospinal fluid disorders. We also suggest that it may become useful for assessing clearance capacity of endogenous brain metabolites from cerebrospinal fluid, as well as measuring individual cerebrospinal fluid to blood clearance of intrathecal drugs.

*Correspondence: p.k.eide@medisin.uio.no

[3] Department of Neurosurgery, Oslo University Hospital—Rikshospitalet, Pb 4950 Nydalen, 0424 Oslo, Norway
Full list of author information is available at the end of the article

Hovd *et al. Fluids and Barriers of the CNS*   (2022) 19:55

Page 2 of 14

Background

While the renal glomerular filtration rate (GFR) is clinically used as marker of clearance of drugs and solutes from blood [1], the cerebrospinal fluid (CSF) to blood clearance has not previously been defined in either healthy individuals nor in individuals with neurological diseases. Possibly, direct measurement of CSF to blood clearance might be useful for understanding diseases of the brain, and consequently lay ground for personalized intrathecal drug administration to the central nervous system (CNS).

Since the dual discoveries of the glymphatic system in 2012 [2] and the meningeal lymphatic system in 2015 [3], there have been renewed interest in how various waste substances are cleared from the brain [4], and not at least the role of meningeal lymphatic vessels [5]. Impaired glymphatic clearance of toxic by-products from brain metabolism to CSF causing deposition of toxic substances in the brain, e.g. deposition of amyloid-β and tau in Alzheimer's disease and α-synuclein in Parkinson's disease, has been proposed as a common pathogenic pathway behind several neurodegenerative disorders [4]. Meningeal lymphatic function seems to be affected in a wide range of diseases, as indicated in animal models of traumatic brain injury [6], malignant brain disease [7–9], stroke [10, 11] and Alzheimer's disease [12], and in patients with Parkinson's disease[13]. Given that impaired molecular clearance from CSF to blood may have a pivotal role in the development of neurological disease; it might be desirable to obtain quantitative data about CSF to blood clearance on an individual basis. For years, levels of brain metabolites from single time points have been measured in CSF, as well as in blood, aiming at identifying the pre-symptomatic phase of dementia disease [14, 15]. On the other hand, direct assessment of clearance dynamics from CSF to blood has not been possible.

Assessment of CSF to blood clearance might as well be useful to tailor dosage of intrathecal drugs. Today, intrathecal drug administration seems promising in order to treat a wide range of diseases within the CNS, such as neuro-inflammatory, neuro-degenerative, neuro-oncologic, and neuro-vascular diseases [16–20]. Many systemically administered drugs, which are supposed to function in CNS, remain to a considerable degree within the systemic circulation due to their inability to cross the blood–brain-barrier (BBB) [21]. Given previous observations of brain wide distribution of CSF tracer administered to the lumbar subarachnoid space in humans [22],

intrathecally administered drugs have potential to better target brain disease directly by their by-passing of the BBB, and assumedly in much lower doses than applied systemically, thereby reducing side effects.

Our group has used intrathecal administration of the magnetic resonance imaging (MRI) contrast agent gadobutrol (serving as a CSF tracer) to explore molecular passage from CSF to the brain [22, 23], meninges [24], calvarial bone [25], extra-cranial lymph nodes [26], as well as to the blood [27]. From this, we suggest that measurements of CSF to blood clearance of gadobutrol may provide an overall estimation of the ability of CSF to remove macromolecules. Since tracer levels in blood are highly correlated with levels of tracer in CSF at MRI [27], resource-demanding imaging may be omitted as part of CSF clearance assessment. Gadobutrol is a hydrophilic substance unable to cross the BBB, which after administration to CSF is excreted along the same pathways as other endogenous substances within CSF, such as the paravascular [4] and meningeal lymphatic pathways [28] suggested from animal studies. In the present work, we investigated the CSF to blood clearance of gadobutrol in patients under clinical work-up of various neurological diseases and CSF disturbances, employing a population pharmacokinetic model based on a large patient material spanning multiple disease categories. The hypothesis was that different CSF diseases present a characteristic profile of CSF to blood clearance.

Methods
Experimental design
A prospective and observational study design was utilized; randomization or a priori sample size calculation was not relevant.

Patients
The study included patients referred to the Department of neurosurgery, Oslo University Hospital—Rikshospitalet, Oslo, Norway, who were examined for tentative CSF disorders, and in whom intrathecal contrast enhanced MRI was considered indicated for clinical reasons. Individuals who were not eligible for inclusion included subjects with a history of hypersensitivity reactions to contrast media agents, severe allergic reactions in general, evidence of renal dysfunction, i.e. glomerular filtration rate (GFR) < 30, age < 18 or > 80 years, or pregnant or breastfeeding women.

Patients were categorized according to tentative diagnosis prior to MRI, and underwent work-up, including

Hovd *et al. Fluids and Barriers of the CNS*   (2022) 19:55

Page 3 of 14

blood sampling, prior to any treatment. The category *reference subjects* (REF) includes individuals in whom we found no apparent evidence of CSF disturbance and no indication for surgery. The group with spontaneous intracranial hypotension (SIH) had an identified CSF leakage that required surgery to close the leakage. The present subjects in the category idiopathic intracranial hypertension (IIH) were shunted and demonstrated clinical improvement thereafter. Patients with pineal cysts (PC) or arachnoid cysts (AC) underwent surgery with cyst removal and demonstrated post-operative clinical improvement. The category idiopathic normal pressure hydrocephalus (iNPH) included patients who based on clinical workup, imaging findings and results of intracranial pressure (ICP) monitoring [29, 30], underwent shunting with a demonstrated clinical improvement thereby qualifying for the diagnosis Definite iNPH according to the Japanese guidelines [31].

Intrathecal administration of gadobutrol
The MRI contrast agent gadobutrol (Gadovist™, Bayer Pharma AG, Berlin, Germany) was administered intrathecally in volumes of 0.10, 0.25 or 0.5 mL (1.0 mmol/mL) at a speed of a few seconds. The intrathecal injection procedure was done at the lumbar level. Correct entrance to the subarachnoid space was verified by CSF backflow from the spinal needle.

The first 80 patients received intrathecal gadobutrol in a dose of 0.50 mmol only, and the latter patients received intrathecal gadobutrol in alternatig doses of 0.10 mmol, 0.25 mmol or 0.5 mmol.

Quantification of gadolinium in blood
Venous blood samples were obtained at empirically determined regular time points up to about 48 h after intrathecal administration of gadobutrol, and were stored at -80 °C. Quantification of gadolinium to estimate concentrations of gadobutrol in blood and plasma was performed as previously described [27]. In short, the whole blood samples were homogenized using an Ultra-Turrax homogenizer (IKA T18). Both plasma and the homogenized whole blood samples were subjected to digestion with ultrapure distilled nitric acid and deionized Milli-Q water in a closed-vessel microwave technique system (UltraCLAVE, Milestone, Italy). The samples were digested according to a 60-min stepwise heating program, with a maximum temperature of 250 °C held for 15 min. Following dilution, samples were analyzed for gadolinium by inductively coupled plasma mass spectrometry (Agilent 7700x, Agilent Technologies), employing indium at 0.1 µg/L as an internal standard. A 5-point standard curve (0.01–10 µg/L) was used. All analytical results were corrected for procedural blank values.

Measured gadolinium concentrations were recalculated to gadobutrol concentrations.

In this work, both plasma and whole-blood gadobutrol were used. Linear regression through the origin was used to determine the plasma to whole blood ratio, and whole blood concentration of gadobutrol was interpolated to plasma concentrations for the purpose of pharmacokinetic modelling.

Gadobutrol population pharmacokinetic modelling
A population pharmacokinetic model was developed in order to determine individual pharmacokinetic parameters of intrathecally administered gadobutrol. A nonparametric adaptive grid approach implemented in Pmetrics (version 1.9.7) for R (version 4.0.0) was used [32]. Based on available literature [33, 34] and previous work [27], both one- and two-compartment structural models were initially considered. The structural models provide the hypothesized framework for which transfer of gadobutrol occurs between compartments. Both the one- and two-compartmental models estimate the transfer of gadobutrol from CSF to blood, and elimination from blood. However, in the two-compartmental model, a peripheral tissue compartment was implemented, allowing gadobutrol to distribute into and from tissue. For the purpose of internal model validation, the dataset was split into a development- (80%) and validation-set (20%). Patients with more than six samples were allocated to the development set, with additional random allocation of profiles until 80% of total profiles. Model selection was primarily based on comparison of the relative root mean squared predictive error (RMSE, %) calculated from the relative predictive error of all gadobutrol concentrations in the development dataset. Additionally, the linear regression slope, R^2-values of the observed versus predicted plots, Akaike's information criteria (AIC) and the Bayesian information criteria (BIC) also guided model development to some extent. Covariates were not included, due to sole interest in individual predictions.

Pharmacokinetic calculations
Posterior individual parameter values, as well as posterior individually predicted concentrations obtained from the final population pharmacokinetic model run with the complete dataset, were used for all pharmacokinetic calculations. Predictions were made in one-minute intervals from time of administration and up to 72 h. The following pharmacokinetic variables were evaluated:

The absorption half-life ($T_{1/2, abs}$) is defined as the time for half the amount of gadobutrol in the CSF to be cleared to blood. This parameter was used as a surrogate marker for CSF to blood clearance of gadobutrol. $T_{1/2, abs}$ was calculated by dividing the

Hovd *et al. Fluids and Barriers of the CNS*   (2022) 19:55

Page 4 of 14

natural logarithm of 2 over the model-estimated coefficient of absorption (K_a) from CSF to blood.

Time to maximum concentration (T_{max}) in plasma and maximum concentration (C_{max}) in plasma were obtained directly from the individual predictions.

Lag-time of absorption to blood (T_{lag}) is the model-estimated time for the tracer to reach the site of clearance in CSF. Longer T_{lag} thus implies that the molecule stays longer within CSF or that it takes longer before the clearance process to blood starts.

Area under the concentration–time curve from zero to infinity ($AUC_{0-\infty}$) was calculated with the trapezoidal approximation from individual posterior predicted concentrations using the 'makeAUC'-function in the Pmetrics package for R. The AUC is a measure of systemic exposure of gadobutrol.

In order to compare parameters across multiple doses, C_{max} and $AUC_{0-\infty}$ were normalized with respect to dose.

Statistical analysis

Comparisons between groups were performed using two-tailed individual samples t-test for continuous variables, and Fishers exact test for categorical variables. Values were visually assessed for normality prior to testing. Differences in parameters and normalized parameters between different doses were assessed using an analysis of variance. For the predefined $\alpha = 0.05$, we considered 95% confidence intervals not including zero and P-values lower than 0.05 to be statistically significant.

Results

Patient material

The study included 161 patients, with a mean ± SD age of 54 ± 19 years (range 19 to 82 years), and with a mean body mass index (BMI) of 28 ± 5 kg/m^2 (range 18 to 41 kg/m^2). Patients were under clinical work-up for possible CSF disorders, with diagnosis categories as indicated in Table 1.

Several groups were statistically significantly different from the reference (REF) cohort, with respect to gender, age, height, body mass index (BMI), and kidney function. A total of 1,140 samples were analyzed for gadobutrol in plasma or whole blood; the mean number of samples was 8 ± 2 in each subject (range 1 to 11 samples).

Gadobutrol blood-to-plasma ratio

In 24 patients, 204 samples were concomitantly analyzed for gadobutrol in both plasma and whole blood. Concentration of gadobutrol in plasma was linearly associated ($\beta = 1.795$, $R^2_{adjusted} = 0.997$; $P < 0.001$) with whole blood concentration of gadobutrol (Fig. 1), and whole blood concentration of gadobutrol was interpolated to plasma concentrations for the purpose of pharmacokinetic modelling, using linear regression through the origin.
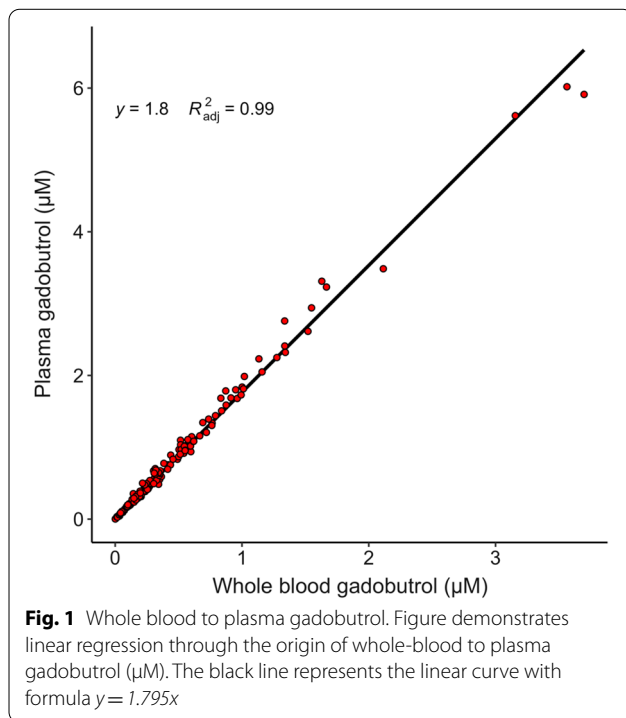
Population pharmacokinetic modeling

Both one- and two-compartment models were initially evaluated. Compared to the one-compartment structural model, a two-compartment model improved the goodness of fit. Furthermore, addition of an absorption lag-time improved the individual predictions, especially in the absorption phase.

Table 1 Demographic overview

	Patient category							
	REF	**PC**	**AC**	**SIH**	**IIH**	**iNPH**	**Comm. HC**	**Non-comm. HC**
Number of subjects	28	13	14	14	15	63	11	3
Ith dose of gadobutrol								
0.10 mmol	0	0	0	0	0	13	0	0
0.25 mmol	3	0	2	4	1	17	3	0
0.50 mmol	25	13	12	10	14	33	8	3
Gender (male/female)	6/22	1/12	8/6[a]	5/9	2/13	37/26[b]	7/4[a]	2/1
Age (years)	39 ± 12	36 ± 13	52 ± 17[a]	50 ± 10[b]	33 ± 11	72 ± 6[c]	49 ± 13[a]	43 ± 29
Height (cm)	172 ± 8	170 ± 5	176 ± 10	172 ± 10	165 ± 7[b]	173 ± 9	178 ± 12	171 ± 7
Weight (kg)	82 ± 15	80 ± 15	82 ± 13	78 ± 23	88 ± 17	81 ± 16	84 ± 20	80 ± 24
BMI (kg/m^2)	28 ± 5	28 ± 4	27 ± 3	26 ± 6	32 ± 5[a]	27 ± 4	26 ± 5	27 ± 6
GFR (ml/min)	103 ± 12	98 ± 12	86 ± 16[b]	95 ± 15	105 ± 13	77 ± 14[c]	92 ± 18	104 ± 15

Data presented as mean ± SD. Differences from the reference group were determined by independent samples t-test for continuous variables and by Fishers exact test for categorical variables ([a]P < 0.05, [b]P < 0.01, [c]P < 0.001). Patient categories: *AC* Arachnoid cyst, *Comm HC* communicating hydrocephalus, *IIH* idiopathic intracranial hypertension, *iNPH* idiopathic normal pressure hydrocephalus, *Non-comm HC* non-communicating hydrocephalus, *PC* pineal cyst, *REF* reference cohort, *SIH* spontaneous intracranial hypotension

Hovd *et al. Fluids and Barriers of the CNS*   (2022) 19:55

Page 5 of 14

Fig. 1 Whole blood to plasma gadobutrol. Figure demonstrates linear regression through the origin of whole-blood to plasma gadobutrol (µM). The black line represents the linear curve with formula *y = 1.795x*

The final population pharmacokinetic model consisted of two compartments with first-order transfer from CSF to blood, and first-order elimination from the central compartment (blood) and absorption lag-time, and the model described the data well (Fig. 2A). The final model ran on the complete dataset achieved a mean prediction error of -0.032, a root mean squared error of 0.283, and a percentage root mean squared error of 18.5%. Akaike's Information Criteria (AIC) and Bayesian Information Criteria (BIC) were 667 and 702, respectively. When assessing residual error for different times, a trend for underprediction was shown during times between 5 and 15 h (Fig. 2B). No systematic trends were found when comparing residual error to the observed concentration of gadobutrol (Fig. 2C). Individual predictions for a random subset of patients are shown in Fig. 2D, demonstrating goodness of fit.

Dose linearity
Mean pharmacokinetic profiles across intrathecally-administered doses of gadobutrol are shown in Fig. 3. No differences in neither absorption half-life, time to maximum concentration, nor dose-normalized maximum concentration were found across the administered doses of gadobutrol. However, a statistically significant difference in dose-normalized $AUC_{0-\infty}$ between the dose levels of 0.1 mmol and 0.5 mmol was found ($\Delta = -5.22$ [95% CI: -9.68, -0.77] µM h). Additionally, mean predictive

error of the population pharmacokinetic model was not different between dose levels.

Inter-individual variability in gadobutrol CSF to blood clearance
Irrespective of diagnosis category, a large degree of inter-individual variability was observed with respect to the pharmacokinetic parameters of intrathecally administered gadobutrol. For the complete dataset, mean absorption half-life was 3.83 ± 2.50 h, with a coefficient of variation (CV) of 65%, which did not vary with dose. Time to maximum concentration (T_{max}) and dose-normalized maximum concentration (C_{max}) were 8.60 ± 4.58 h (CV 53%) and 0.69 ± 0.42 µM (CV 61%) respectively. The large inter-individual variability of pharmacokinetic parameters irrespective of diagnosis is shown in Fig. 4.

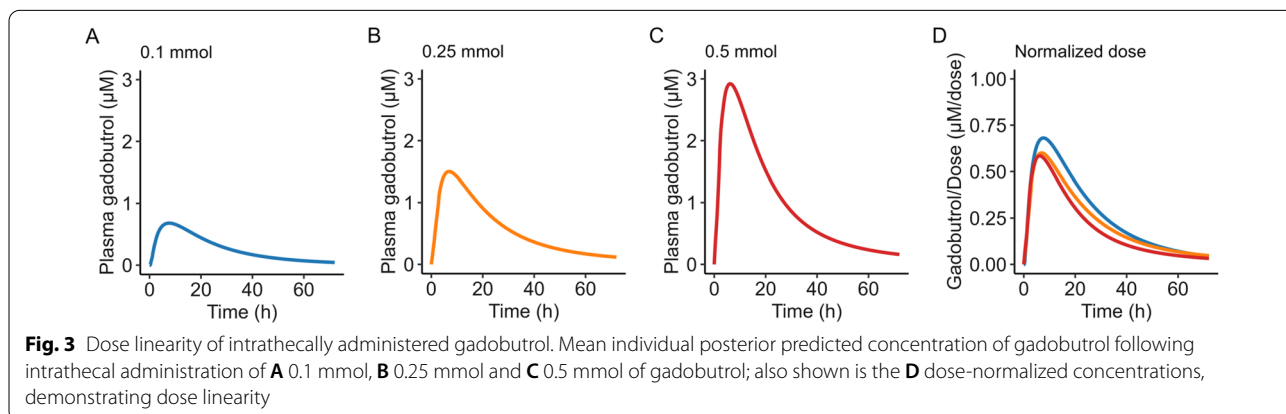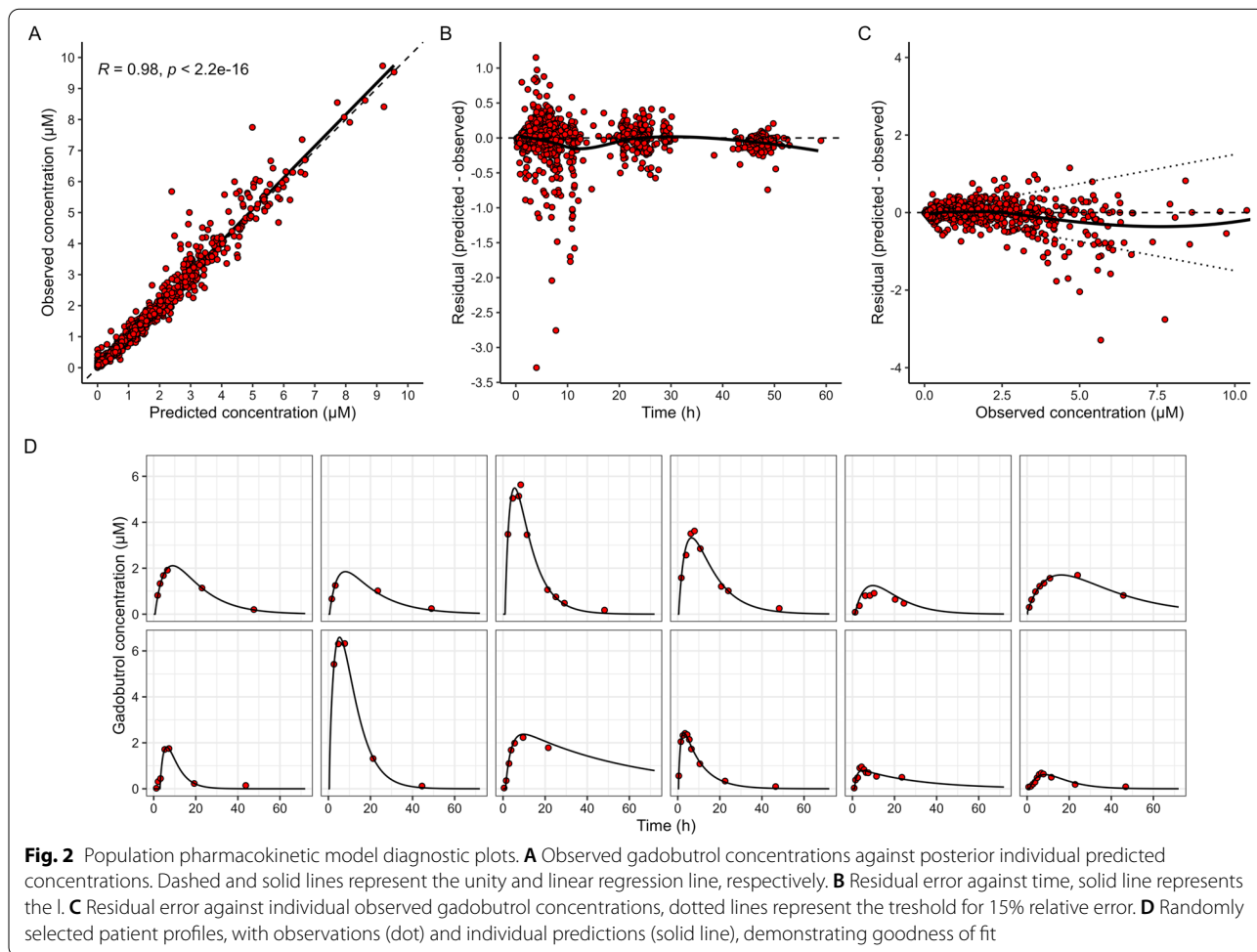### Disease categories show different profiles
A notable degree of variability in pharmacokinetic parameters was observed both within and between disease categories. Individual predicted profiles with group-wise mean predicted profiles are shown in Fig. 5, and pharmacokinetic parameters at group level with comparisons are presented in Table 2. Variability in mean concentration profiles of gadobutrol for the different patient groups is further presented in Fig. 6, illustrating the between group differences.

When compared with the reference cohort, patients with pineal cysts demonstrated a 0.46 [95% CI: 0.03, 0.88] hours longer absorption lag time (Table 2). In this group, several demographic factors were associated with the pharmacokinetic parameters (Fig. 7); T_{max} and dose-normalized AUC_{0-Inf} were positively associated with age, while dose-normalized C_{max} was negatively associated with age, height and weight.

Neither patients with arachnoid cysts nor patients with spontaneous intracranial hypotension demonstrated any difference in pharmacokinetic parameters of intrathecally administered gadobutrol, compared with the reference cohort (Table 2).

In contrast, patients with idiopathic intracranial hypertension showed a 2.25 [95% CI: 0.74, 3.77] hours shorter absorption half-life when compared with the reference group, indicating a greater CSF to blood clearance of gadobutrol. Additionally, a 3.09 [95% CI: -5.74, -0.43] µM h greater dose-normalized $AUC_{0-\infty}$ was found compared with the reference cohort (Table 2).

In iNPH patients, compared with the reference cohort, time to maximum concentration was 2.36 [95% CI: 0.30, 4.41] hours longer, and showed a 5.91 [95% CI: 8.18, 3.63] µM h greater mean $AUC_{0-\infty}$. Additionally, the lag-time was 0.42 [95% CI: 0.09, 0.74] hours longer compared with

Hovd *et al. Fluids and Barriers of the CNS*   (2022) 19:55

Page 6 of 14

Fig. 2 Population pharmacokinetic model diagnostic plots. **A** Observed gadobutrol concentrations against posterior individual predicted concentrations. Dashed and solid lines represent the unity and linear regression line, respectively. **B** Residual error against time, solid line represents the l. **C** Residual error against individual observed gadobutrol concentrations, dotted lines represent the treshold for 15% relative error. **D** Randomly selected patient profiles, with observations (dot) and individual predictions (solid line), demonstrating goodness of fit

Fig. 3 Dose linearity of intrathecally administered gadobutrol. Mean individual posterior predicted concentration of gadobutrol following intrathecal administration of **A** 0.1 mmol, **B** 0.25 mmol and **C** 0.5 mmol of gadobutrol; also shown is the **D** dose-normalized concentrations, demonstrating dose linearity

reference (Table 2); hence, in iNPH the CSF tracer stays longer within the CSF compartment prior to clearance to blood.

Patients with communicating hydrocephalus demonstrated a 0.19 [95% CI: 0.02, 0.37] µM lower dose-normalized maximum concentration of gadobutrol when compared with the reference group, which was the lowest concentration measured in the included disease categories (Table 2). Even though no statistically significant differences between patients with non-communicating hydrocephalus and the reference cohort were found, most likely due to a low number of subjects in the

Hovd *et al. Fluids and Barriers of the CNS*   (2022) 19:55

Page 7 of 14

Fig. 4 Distribution of indivdual pharmacokinetic parameters for entire cohort. Histogram of parameter distribution for the **A** absorption half-life ($T_{1/2, abs}$), **B** time to maximum concentration (T_{max}), **C** maximum concentration (C_{max}), **D** lag-time (T_{lag}), and **E** area under the curve (AUC) from zero to infinity for the entire cohort of patients (n = 161)

aforementioned group, time to maximum concentration was numerically higher (12.33 ± 7.17 h), compared to the reference cohort (7.49 ± 4.09 h), as shown in Table 2.
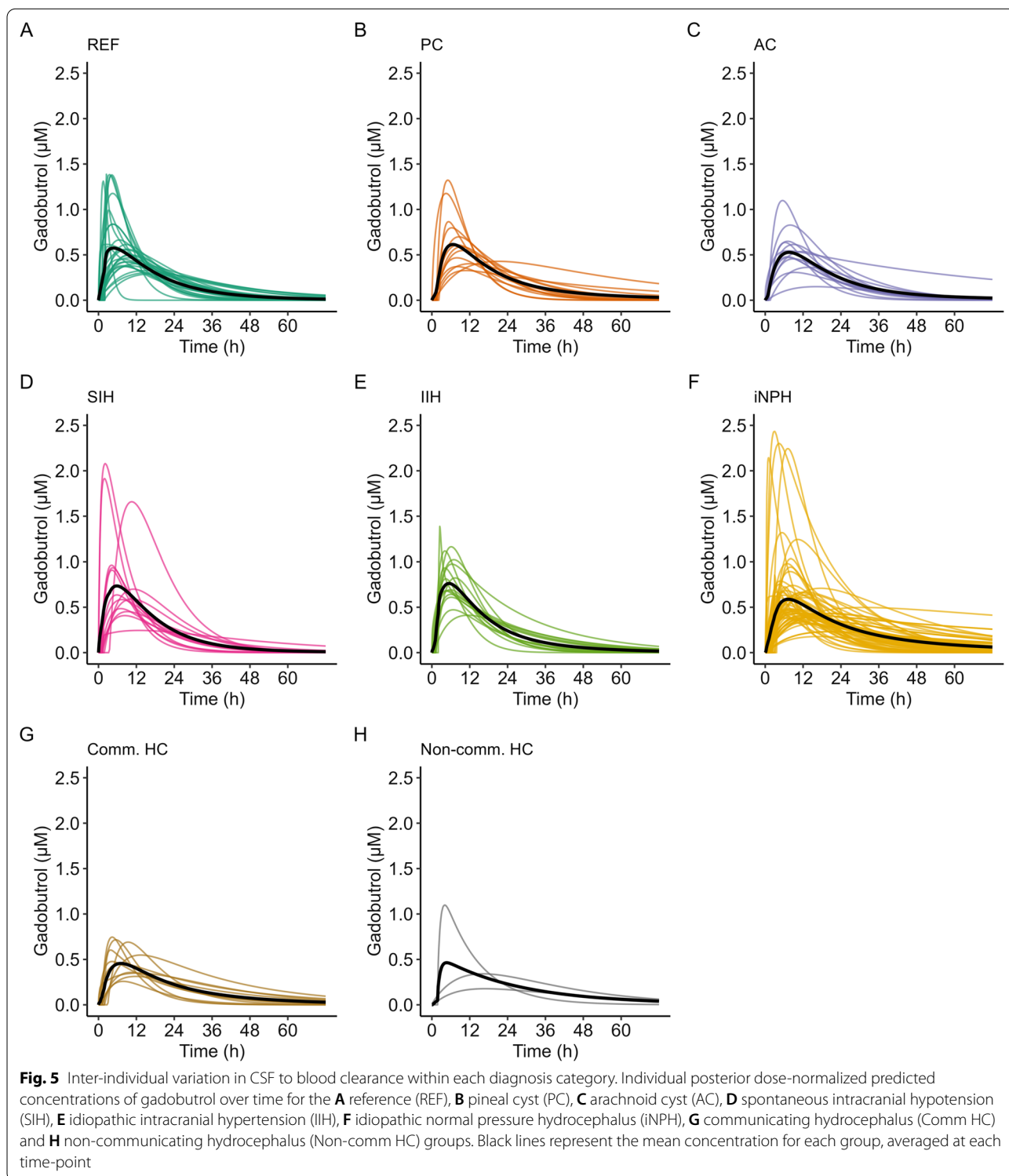
Discussion

In this work, we present a population pharmacokinetic model applied to intrathecally administered gadobutrol that precisely estimates the clearance from CSF to blood in patients with various diseases. The included patients showed a high degree of inter-individual variability in pharmacokinetic parameters both within and between different disease categories of CSF disturbances.

Up to now, the literature on CSF to blood clearance has been scarce. The presently described model is derived from 1,140 blood samples in 161 patients, referring to plasma levels of gadobutrol measured subsequently to intrathecal injections of predefined quantities. Utilizing positron emission tomography (PET), others [35] previously examined clearance of intrathecal ^{99m}Tc-DPTA (technetium-99-diethylene-triamine-pentaacetate) to urine. It also has been demonstrated reduced clearance

of a PET ligand from cerebral ventricles to the nasal turbinate in Alzheimer patients [36]. Furthermore, another recent PET study [37] showed reduced clearance of two PET tracers (^{18}F-THK5351 and ^{11}C-PiB) from ventricular CSF in patients with Alzheimer's disease, providing support to the hypothesis that impaired clearance of amyloid-β from CSF underlies the amyloid cerebral deposition characterizing Alzheimer's disease. However, with regard to PET, a drawback is that radioactive ligands provide a radiation dose to the individual [38], have short half-life (about 6 h for ^{99m}Tc-DPTA), and the diagnostic process is both expensive and time-consuming.

The most significant observation of the present study is the large inter-individual variation in CSF to blood clearance, as well as the differences between CSF disease. Compared to the reference cohort, patients diagnosed with pineal or arachnoid cysts, and to some degree patients with spontaneous intracranial hypotension, did not present any differences in pharmacokinetics of intrathecally administered gadobutrol. On the other hand, a statistically significant longer lag-time was found

101

Hovd *et al. Fluids and Barriers of the CNS*   (2022) 19:55

Page 8 of 14

Fig. 5 Inter-individual variation in CSF to blood clearance within each diagnosis category. Individual posterior dose-normalized predicted concentrations of gadobutrol over time for the **A** reference (REF), **B** pineal cyst (PC), **C** arachnoid cyst (AC), **D** spontaneous intracranial hypotension (SIH), **E** idiopathic intracranial hypertension (IIH), **F** idiopathic normal pressure hydrocephalus (iNPH), **G** communicating hydrocephalus (Comm HC) and **H** non-communicating hydrocephalus (Non-comm HC) groups. Black lines represent the mean concentration for each group, averaged at each time-point

in patients with pineal cysts, but no difference in CSF to blood clearance was found. We conclude that on the group level, these categories may possibly reflect the normal variation.

Patients with idiopathic intracranial hypertension, on the other hand, demonstrated a significantly reduced absorption-half life, possibly indicating faster egress of molecules from CSF to blood due to increased ICP.

**Table 2** Model predicted pharmacokinetic parameters of gadobutrol in blood

	Patient category							
	REF	PC	AC	SIH	IIH	iNPH	Comm. HC	Non-comm. HC
Number of subjects	28	13	14	14	15	63	11	3
$T_{1/2, abs}$ (h)	4.57 ± 3.31 (72%)	4.12 ± 2.14 (52%)	4.86 ± 2.93 (60%)	3.79 ± 2.91 (77%)	2.32 ± 1.61[b] (69%)	4.15 ± 3.07 (74%)	4.62 ± 3.86 (84%)	4.92 ± 3.88 (79%)
T_{max} (h)	7.49 ± 4.09 (55%)	9.00 ± 4.27 (47%)	8.89 ± 2.98 (34%)	7.09 ± 3.44 (49%)	5.8 ± 2.01 (35%)	9.85 ± 5.4 [a] (55%)	8.14 ± 3.44 (42%)	12.33 ± 7.17 (58%)
C_{max} (μM)	0.70 ± 0.38 (54%)	0.66 ± 0.31 (47%)	0.55 ± 0.23 (42%)	0.90 ± 0.58 (64%)	0.83 ± 0.27 (33%)	0.67 ± 0.48 (72%)	0.50 ± 0.17 [a] (34%)	0.54 ± 0.49 (91%)
T_{lag} (h)	0.74 ± 0.67 (91%)	1.20 ± 0.59 [a] (49%)	0.74 ± 0.42 (57%)	1.03 ± 0.89 (86%)	0.88 ± 0.55 (62%)	1.16 ± 0.77 [a] (66%)	1.12 ± 0.87 (78%)	0.96 ± 0.82 (85%)
$AUC_{0-\infty}$ (μM h)	12.58 ± 2.55 (20%)	15.05 ± 3.96 (26%)	13.65 ± 6.13 (45%)	15.36 ± 5.92 (39%)	15.67 ± 4.54[a] (29%)	18.49 ± 8.24[c] (45%)	12.79 ± 4.68 (37%)	13.44 ± 3.6 (27%)

Data presented as mean ± SD (coefficient of variation given in parenthesis). Abbreviations: $T_{1/2, abs}$ = Time to 50% of tracer dose absorbed to blood (absorption half-life), indicative of CSF tracer clearance to blood. T_{max} = Time to maximum concentration. C_{max} = Dose-normalized maximum concentration. T_{lag} = lag-time of absorption. $AUC_{0-\infty}$ = Dose-normalized area under curve from zero to infinity. Significant difference from REF: [a]$P < 0.05$, [b]$P < 0.01$, [c]$P < 0.001$ (independent samples t-test). Patient categories: *AC* arachnoid cyst, *Comm HC* communicating hydrocephalus, *IIH* idiopathic intracranial hypertension, *iNPH*: idiopathic normal pressure hydrocephalus, *Non-comm HC* non-communicating hydrocephalus, *PC* pineal cyst, *REF* reference cohort, *SIH* spontaneous intracranial hypotension

Furthermore, in patients with iNPH, the time to maximum concentration was significantly longer compared to the reference group, and lag-time of absorption was significantly increased. Therefore, in patients with iNPH, the CSF tracer stays longer in the CSF compartment and it requires longer time to reach maximum concentration. The senior authors previously found evidence of reduced CSF turnover in iNPH [23, 39]. In iNPH patients, high grade ventricular reflux of tracer [40] may as well contribute to the increased lag time in these individuals. The CSF to blood clearance of gadobutrol per se was not affected at group level since the absorption half-life or maximum concentration was not different.

We may not from the present data decipher which transport routes gadobutrol follow from the CSF to blood. Emerging evidence points at the role of meningeal lymphatic vessels for molecular egress from CSF to blood, which is supported by findings of reduced clearance of neurotoxic metabolites from CSF when meningeal lymphatic clearance routes are impaired [5]. In humans, the parasagittal dura may be a direct passage route to the meningeal lymphatic structures [24], though molecular efflux from CSF via the cribriform plate seems to be minor [41]. Other possible efflux routes are the cranial and spinal nerve roots [42], and spinal lymphatic pathways [43]. The arachnoid membrane itself has traditionally been considered impermeable to larger molecules [44]. Hence, a CSF tracer study of mice found no signs of tracer propagation beyond the arachnoid layer [45]. Traditionally, it has been thought that CSF egresses via arachnoid granulations to veins, but this view is up to debate [46]. A microscopy study showed endothelial lined gaps and fissures in parasagittal dura of pigs, which might serve as a CSF drainage pathway [47]. In humans, a subset of arachnoid granulations might drain CSF via lymphatic vessels to the venous circulation [48]. Our group showed that the presently used intrathecal tracer gadobutrol enriched in parasagittal dura [24], bone marrow at the skull vertex adjacent or remote to intradiploic dural extensions [25], and in extracranial lymph nodes [49], and demonstrated the feasibility of measuring CSF to blood clearance [27]. The time course of CSF clearance with peak in plasma after 8.60 ± 4.58 h may indicate a major role of the spinal canal given that tracer clearance from CSF peaks to blood occurred far earlier than peak enhancement at the skull vertex [27]. Differences in lag time (T_{lag}) might be related to passage capacity within the thecal sac, but we have previously not found differences between groups for time between lumbar injection and first appearance at the cranio-cervical junction, i.e. spinal transit time [50]. We suggest that the meningeal lymphatic vessels are the main route for egress of molecules from CSF, and that meningeal lymphatic impairment may hamper CSF clearance. In this regard, it is of particular interest that evidence from animal and human studies suggest the meningeal lymphatic function deteriorates with increasing age [45, 51], and that impaired meningeal lymphatic function aggravates pathology seen in animal models of Parkinson's [52] and Alzheimer's [53] diseases. Experimentally, it was shown that impaired meningeal lymphatic function reduced paravascular influx of macromolecules into the brain, and reduced efflux from the interstitial space [54]. In comparison, we previously found in humans that peak CSF tracer enhancement in

Hovd *et al. Fluids and Barriers of the CNS*   (2022) 19:55

Page 10 of 14
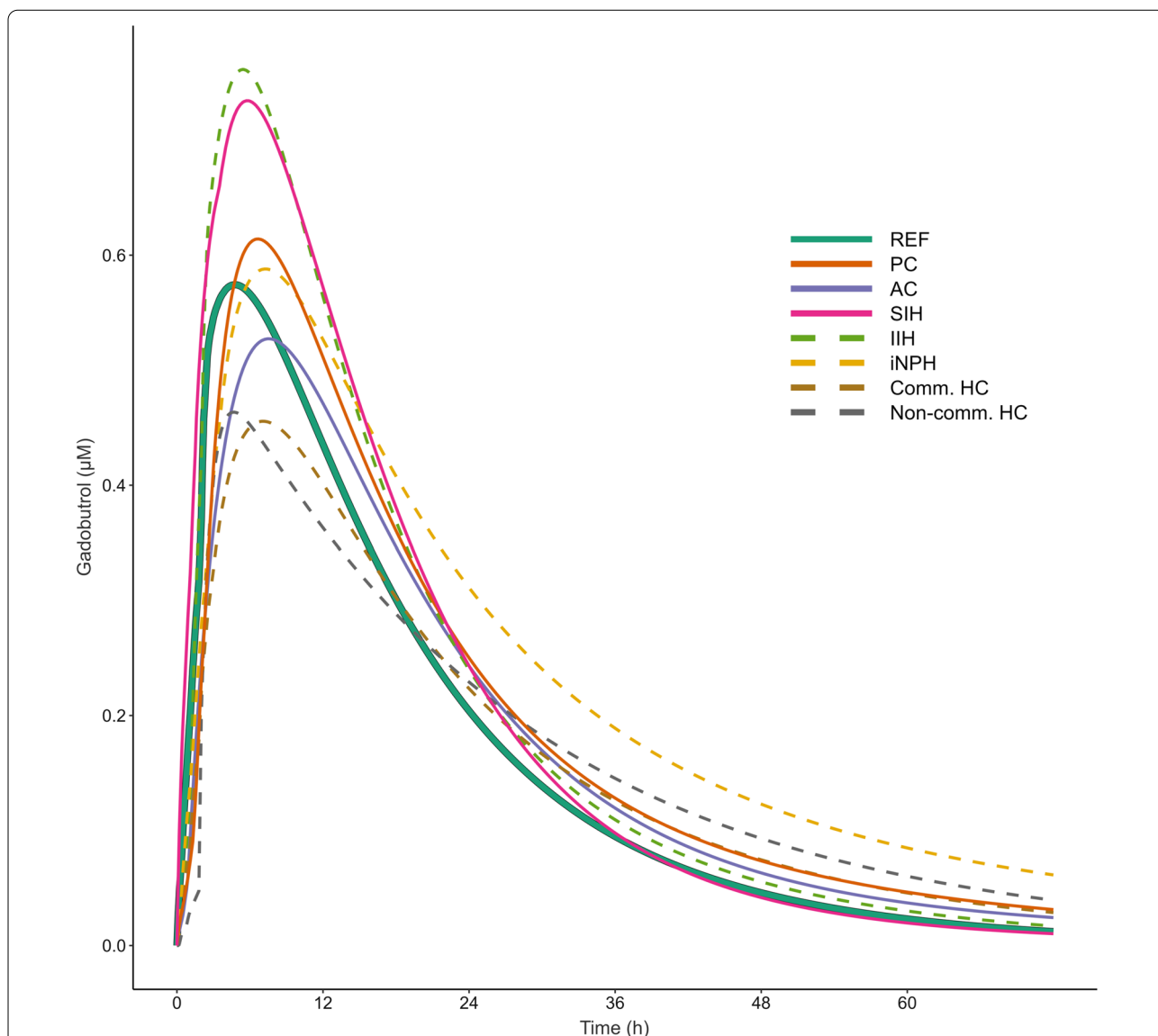
Fig. 6 Mean concentration profiles of gadobutrol for the different patient groups. Individual posterior predicted dose-normalized blood concentrations of intrathecal gadobutrol from the population pharmacokinetic model, averaged at each time-point by group. The reference group is highlighted by a thick solid line. *REF* Reference, *PC* pineal cyst, *AC* arachnoid cyst, *SIH* Spontaneous intracranial hypotension (SIH), *IIH* idiopathic intracranial hypertension, *iNPH* idiopathic normal pressure hydrocephalus, *Comm HC* communicating hydrocephalus, *Non-comm HC* non-communicating hydrocephalus
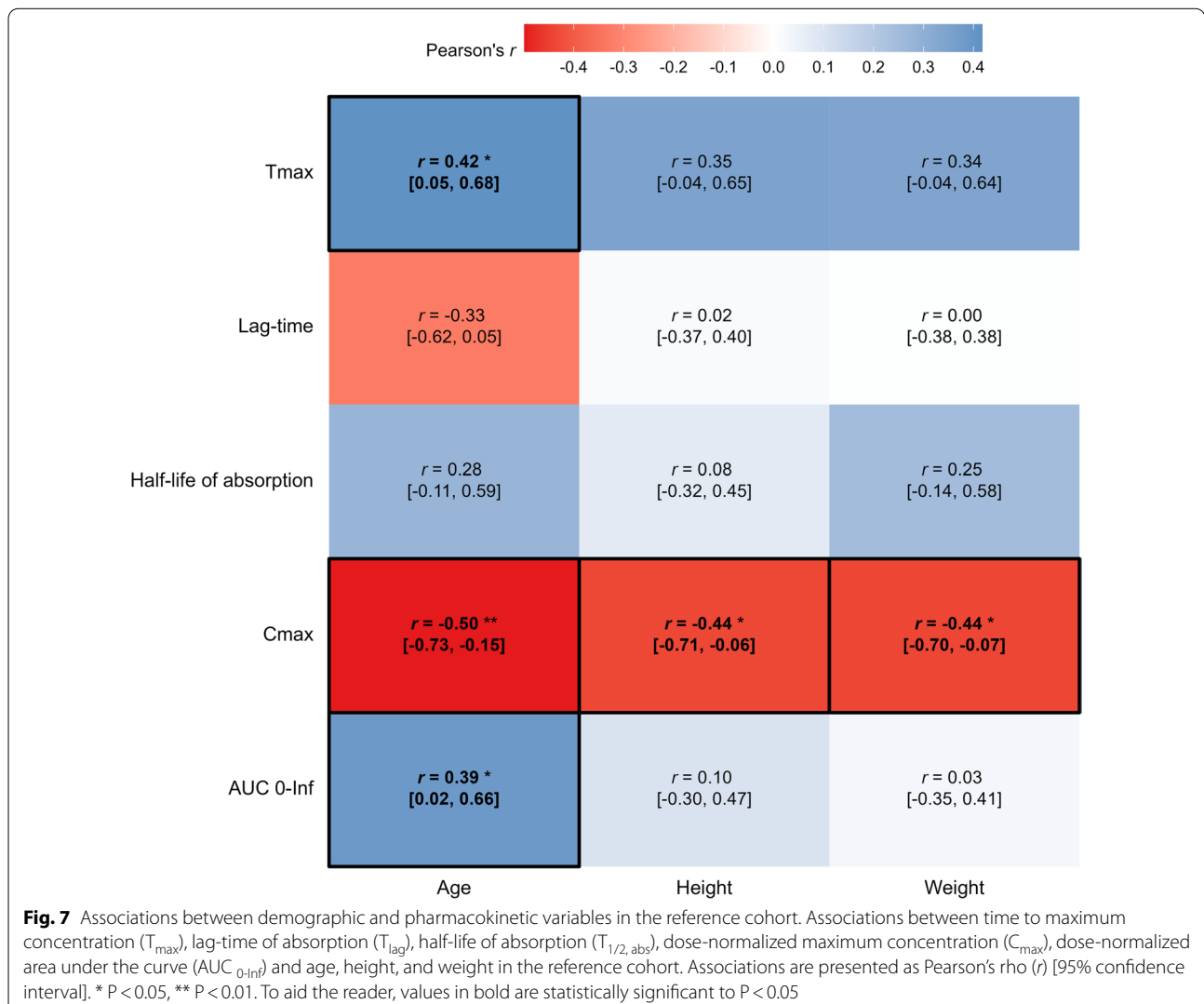
human brain and cervical lymph nodes concurred in time, supporting a role of meningeal lymphatic vessels in molecular drainage from CSF [26].

While plasma levels of gadobutrol primarily reflect clearance from CSF along extra-vascular pathways, a minor leakage of tracer through the BBB may to a limited extent contribute to the clearance as ageing as well as neurodegenerative disease may be accompanied with impaired BBB integrity [55, 56]. Evidence of BBB disruption has also been reported for CSF disease such as IIH [57] and iNPH [58]. After entering to the blood, the plasma half-life of gadobutrol in blood is 1.5 h [59].

The present observations may have several clinical implications; we would like to highlight three areas. First, the present observations suggest that assessing CSF to blood clearance adds to characterization of CSF diseases on the individual level. One example is the identification of CSF leakage in individuals with spontaneous intracranial hypotension; it is well established that it may be very difficult to identify the site of CSF leakage [60].

Fig. 7 Associations between demographic and pharmacokinetic variables in the reference cohort. Associations between time to maximum concentration (T_{max}), lag-time of absorption (T_{lag}), half-life of absorption ($T_{1/2, abs}$), dose-normalized maximum concentration (C_{max}), dose-normalized area under the curve (AUC $_{0-Inf}$) and age, height, and weight in the reference cohort. Associations are presented as Pearson's rho (*r*) [95% confidence interval]. * $P < 0.05$, ** $P < 0.01$. To aid the reader, values in bold are statistically significant to $P < 0.05$

Currently, the visualization of CSF leakage utilizes MRI [60, 61], contrast enhanced computer tomography (CT) myelography [60] as well as intrathecal ^{99m}Tc-DPTA nuclear imaging [62], though the risk of not identifying any leakage site is high. A strategy to measure CSF to blood clearance might be expected to aid in identifying individuals with the most pronounced CSF leakage, even though signs of hyper-accelerated clearance could not be shown at group level for the CSF leakage sub-cohort in this study.

Second, direct measurements of CSF to blood clearance might prove useful in preclinical stages of neurodegenerative and dementia disease. Measurements of circulating substances such as amyloid-β and tau may be used for screening purposes, providing an indicative risk of disease [14]. However, direct measures of CSF to blood clearance may be useful in a subset of individuals at risk. In this regard, it should be noted that about ¼

of amyloid-β is cleared via CSF in rodents [63, 64], and a significant amount of tau is excreted via CSF as the majority does not pass across the BBB. For example, mice without dural lymphatic drainage showed significantly reduced excretion of tau [28], and demonstrated a significant association between blood and CSF levels of tau [28]. We here found that the dementia subtype iNPH was characterized with altered pharmacokinetic variables, including longer time to maximum concentration (T_{max}), longer lag time (T_{lag}) and higher AUC, as compared with reference subjects. However, the difference in AUC may be attributed to the difference in age and renal function compared to the reference cohort.

Third, estimation of CSF to blood clearance may be useful preceding intrathecal drug administration for treatment of neurological disease. Even though it was traditionally thought that a substance within the CSF only passed a few millimeters into the cortical substance

Hovd *et al. Fluids and Barriers of the CNS*   (2022) 19:55

Page 12 of 14

[65], intrathecally injected gadobutrol showed brain-wide distribution in humans [22]. Therefore, intrathecal drugs may directly access the entire extra-vascular part of the CNS in contrast to systemically administered substances that are restricted by the BBB [21]. This, however, may depend on the physiochemical properties of drugs. Examples of intrathecal drugs are antisense oligonucleotides [20, 66], such as Spinraza used for spinal muscular atrophy [17, 67], intrathecal chemotherapy, e.g. methotrexate, used for cancer [68, 69], and adeno-associated viral vector-mediated gene-delivery to CNS in amyotrophic lateral sclerosis, dementia disease and spinocerebellar ataxia [16, 70–73]. However, given the high degree of variation in CSF to blood clearance, there is risk of both over- and under-dosage.

Some limitations should be noted. Gadobutrol is administered off-label as it is not approved for intrathecal use. However, here we used gadobutrol in intrathecal doses of 0.10, 0.25 and 0.50 mmol, which have all been proven safe [50, 74]. Toxic effects have previously not been reported for intrathecal gadobutrol in doses of 1.0 mmol or below [75]. We established dose linearity for the range of 0.10–0.50 mmol, and found no difference in the predictive performance of the population pharmacokinetic model between dose levels. As such, for estimating CSF to blood clearance with population pharmacokinetic modelling, an intrathecal dose of 0.10 mmol appears sufficient. Intrathecal gadobutrol is detected in blood with high sensitivity and accuracy; the present detection threshold was about 1.35 nM, well below the observed concentrations, rendering for use of even lower doses. As gadobutrol shares many of the same molecular properties with radiopaque contrast agents, where many are approved for intrathecal use, utility of on-label contrast agents intrathecally for CSF clearance assessment could be explored in future studies.

In this work, the less tangible absorption half-life was used as a surrogate marker for CSF to blood clearance, instead of actual clearance, due to the lack of accurate determinations of individual CSF volume. However, this does not affect the interpretation or accuracy of the results. With regard to the possible normal CSF to blood clearance in healthy people, it may as well be considered a limitation that we included a range of patients spanning multiple defined CSF disturbances. It was, however, beyond the scope of this work to discuss in detail the underlying diagnoses and the clinical significance of each disease category. Additional work on the subject would benefit from the inclusion of individuals without evident neurological disorders, in order to establish a reference value and level of variability in a healthy population. Furthermore, it remains to be determined whether gadobutrol is a valid marker for clearance of other intrathecally administered drugs and endogenous metabolites of interest in disease such as amyloid-β, tau, and α-synuclein.

Conclusions

In conclusion, this work provides a population pharmacokinetic model of CSF to blood clearance based on 1,140 blood samples from 161 subjects. Our data demonstrates a large degree of inter-individual variability in CSF to blood clearance as well as different clearance profiles across disease categories. CSF clearance function might both be a secondary feature of various neurological diseases, and a primary driver behind disease. As such, extensive clearance may characterize CSF leakage and spontaneous intracranial hypotension, while protracted clearance may be a contributing factor in neurodegenerative diseases. In the therapeutic setting, CSF to blood clearance may prove useful for tailoring dosage of intrathecal drugs, an administration route with prospects of increased utility in the near future.

Hovd *et al. Fluids and Barriers of the CNS*   (2022) 19:55

Page 13 of 14

Declarations

Ethics approval and consent to participate
This present study was approved by The Regional Committee for Medical and Health Research Ethics (REK) of Health Region South-East, Norway (2015/96), the Institutional Review Board of Oslo university hospital (2015/1868), and the National Medicines Agency of Norway (15/04932–7). Participants were included after providing written and oral informed consent.

Consent for publication
Not applicable.

Competing interests
Geir Ringstad received a fee for speaking at the Bayer symposium at the European Congress of Radiology 2020 (Vienna, Austria). Geir Ringstad and Per Kristian Eide also have a patent pending. The other authors disclose no conflict of interests.

Author details
[1]Section for Pharmacology and Pharmaceutical Biosciences, Department of Pharmacy, University of Oslo, Oslo, Norway. [2]Norwegian Institute for Air Research, Kjeller, Norway. [3]Department of Neurosurgery, Oslo University Hospital—Rikshospitalet, Pb 4950 Nydalen, 0424 Oslo, Norway. [4]Institute of Clinical Medicine, Faculty of Medicine, University of Oslo, Oslo, Norway. [5]Division of Radiology and Nuclear Medicine, Department of Radiology, Oslo University Hospital—Rikshospitalet, Oslo, Norway. [6]Department of Geriatrics and Internal Medicine, Sorlandet Hospital, Arendal, Norway. [7]Department of Air Quality and Noise, Norwegian Institute of Public Health, Oslo, Norway.

References
1. Levey AS, Coresh J, Balk E, Kausz AT, Levin A, Steffes MW, Hogg RJ, Perrone RD, Lau J, Eknoyan G. National Kidney Foundation practice guidelines for chronic kidney disease: evaluation, classification, and stratification. Ann Intern Med. 2003;139:137–47.
2. Iliff JJ, Wang M, Liao Y, Plogg BA, Peng W, Gundersen GA, Benveniste H, Vates GE, Deane R, Goldman SA, et al. A paravascular pathway facilitates CSF flow through the brain parenchyma and the clearance of interstitial solutes, including amyloid beta. Sci Transl Med. 2012;4:147ra111.
3. Louveau A, Smirnov I, Keyes TJ, Eccles JD, Rouhani SJ, Peske JD, Derecki NC, Castle D, Mandell JW, Lee KS, et al. Structural and functional features of central nervous system lymphatic vessels. Nature. 2015;523:337–41.
4. Nedergaard M, Goldman SA. Glymphatic failure as a final common pathway to dementia. Science. 2020;370:50–6.
5. Louveau A, Plog BA, Antila S, Alitalo K, Nedergaard M, Kipnis J. Understanding the functions and relationships of the glymphatic system and meningeal lymphatics. J Clin Invest. 2017;127:3210–9.
6. Bolte AC, Dutta AB, Hurt ME, Smirnov I, Kovacs MA, McKee CA, Ennerfelt HE, Shapiro D, Nguyen BH, Frost EL, et al. Meningeal lymphatic dysfunction exacerbates traumatic brain injury pathogenesis. Nat Commun. 2020;11:4524.
7. Song E, Mao T, Dong H, Boisserand LSB, Antila S, Bosenberg M, Alitalo K, Thomas JL, Iwasaki A. VEGF-C-driven lymphatic drainage enables immunosurveillance of brain tumours. Nature. 2020;577:689–94.
8. Hu X, Deng Q, Ma L, Li Q, Chen Y, Liao Y, Zhou F, Zhang C, Shao L, Feng J, et al. Meningeal lymphatic vessels regulate brain tumor drainage and immunity. Cell Res. 2020;30:229–43.
9. Ma Q, Schlegel F, Bachmann SB, Schneider H, Decker Y, Rudin M, Weller M, Proulx ST, Detmar M. Lymphatic outflow of cerebrospinal fluid is reduced in glioma. Sci Rep. 2019;9:14815.
10. Yanev P, Poinsatte K, Hominick D, Khurana N, Zuurbier KR, Berndt M, Plautz EJ, Dellinger MT, Stowe AM. Impaired meningeal lymphatic vessel development worsens stroke outcome. J Cereb Blood Flow Metab. 2020;40:263–75.
11. Chen J, Wang L, Xu H, Xing L, Zhuang Z, Zheng Y, Li X, Wang C, Chen S, Guo Z, et al. Meningeal lymphatics clear erythrocytes that arise from subarachnoid hemorrhage. Nat Commun. 2020;11:3159.
12. Da Mesquita S, Papadopoulos Z, Dykstra T, Brase L, Farias FG, Wall M, Jiang H, Kodira CD, de Lima KA, Herz J, et al. Meningeal lymphatics affect microglia responses and anti-Aβ immunotherapy. Nature. 2021;593:255–60.
13. Ding XB, Wang XX, Xia DH, Liu H, Tian HY, Fu Y, Chen YK, Qin C, Wang JQ, Xiang Z, et al. Impaired meningeal lymphatic drainage in patients with idiopathic Parkinson's disease. Nat Med. 2021;27:411–8.
14. Rissman RA, Trojanowski JQ, Shaw LM, Aisen PS. Longitudinal plasma amyloid beta as a biomarker of Alzheimer's disease. J Neural Transm (Vienna). 2012;119:843–50.
15. Blennow K, Hampel H, Weiner M, Zetterberg H. Cerebrospinal fluid and plasma biomarkers in Alzheimer disease. Nat Rev Neurol. 2010;6:131–44.
16. Chen W, Hu Y, Ju D. Gene therapy for neurodegenerative disorders: advances, insights and prospects. Acta Pharm Sin B. 2020;10:1347–59.
17. Wurster CD, Winter B, Wollinsky K, Ludolph AC, Uzelac Z, Witzel S, Schocke M, Schneider R, Kocak T. Intrathecal administration of nusinersen in adolescent and adult SMA type 2 and 3 patients. J Neurol. 2019;266:183–94.
18. Petrescu GED, Sabo AA, Torsin LI, Calin GA, Dragomir MP. MicroRNA based theranostics for brain cancer: basic principles. J Exp Clin Cancer Res. 2019;38:231.
19. Jadhav S, Avila J, Schöll M, Kovacs GG, Kövari E, Skrabana R, Evans LD, Kontsekova E, Malawska B, de Silva R, et al. A walk through tau therapeutic strategies. Acta Neuropathol Commun. 2019;7:22.
20. Chen Y, Mazur C, Luo Y, Sun L, Zhang M, McCampbell A, Tomassy GS. Intrathecal delivery of antisense oligonucleotides in the rat central nervous system. J Vis Exp. 2019. https://doi.org/10.3791/60274.
21. Pardridge WM. The blood-brain barrier: bottleneck in brain drug development. NeuroRx J Am Soc Exp NeuroTher. 2005;2:3–14.
22. Ringstad G, Valnes LM, Dale AM, Pripp AH, Vatnehol SS, Emblem KE, Mardal KA, Eide PK. Brain-wide glymphatic enhancement and clearance in humans assessed with MRI. JCI Insight. 2018;3:1–16.
23. Ringstad G, Vatnehol SAS, Eide PK. Glymphatic MRI in idiopathic normal pressure hydrocephalus. Brain. 2017;140:2691–705.
24. Ringstad G, Eide PK. Cerebrospinal fluid tracer efflux to parasagittal dura in humans. Nat Commun. 2020;11:1–9.
25. Ringstad G, Eide PK. Molecular trans-dural efflux to skull bone marrow in humans with cerebrospinal fluid disorders. Brain. 2021;145(4):1464–72.
26. Eide PK, Vatnehol SAS, Emblem KE, Ringstad G. Magnetic resonance imaging provides evidence of glymphatic drainage from human brain to cervical lymph nodes. Sci Rep. 2018;8:7194.
27. Eide PK, Mariussen E, Uggerud H, Pripp AH, Lashkarivand A, Hassel B, Christensen H, Hovd MH, Ringstad G. Clinical application of intrathecal gadobutrol for assessment of cerebrospinal fluid tracer clearance to blood. JCI insight. 2021;6:1–13.
28. Patel TK, Habimana-Griffin L, Gao X, Xu B, Achilefu S, Alitalo K, mckee CA, Sheehan PW, Musiek ES, Xiong C, et al. Dural lymphatics regulate clearance of extracellular tau from the CNS. Mol Neurodegener. 2019;14:11.
29. Eide PK, Sorteberg W. Diagnostic intracranial pressure monitoring and surgical management in idiopathic normal pressure hydrocephalus: a 6-year review of 214 patients. Neurosurgery. 2010;66:80–91.
30. Eide PK, Sorteberg W. Outcome of surgery for idiopathic normal pressure hydrocephalus: role of preoperative static and pulsatile intracranial pressure. World Neurosurg. 2016;86:186–93.
31. Mori E, Ishikawa M, Kato T, Kazui H, Miyake H, Miyajima M, Nakajima M, Hashimoto M, Kuriyama N, Tokuda T, et al. Guidelines for management of idiopathic normal pressure hydrocephalus: second edition. Neurol Med Chir (Tokyo). 2012;52:775–809.
32. Neely MN, van Guilder MG, Yamada WM, Schumitzky A, Jelliffe RW. Accurate detection of outliers and subpopulations with Pmetrics, a nonparametric and parametric pharmacometric modeling and simulation package for R. Ther Drug Monit. 2012;34:467–76.
33. Hahn G, Sorge I, Gruhn B, Glutig K, Hirsch W, Bhargava R, Furtner J, Born M, Schröder C, Ahlström H, et al. Pharmacokinetics and safety of gadobutrol-enhanced magnetic resonance imaging in pediatric patients. Invest Radiol. 2009;44:776–83.
34. Kunze C, Mentzel HJ, Krishnamurthy R, Fleck R, Stenzel M, Bhargava R, Burrowes D, Sutter G, Schultze-Mosgau M, Santiuste M, Hahn G. Pharmacokinetics and safety of macrocyclic gadobutrol in children aged younger than

Hovd *et al. Fluids and Barriers of the CNS*   (2022) 19:55

Page 14 of 14

2 years including term newborns in comparison to older populations. Invest Radiol. 2016;51:50–7.

35. Verma A, Hesterman JY, Chazen JL, Holt R, Connolly P, Horky L, Vallabhajosula S, Mozley PD. Intrathecal (99m)Tc-DTPA imaging of molecular passage from lumbar cerebrospinal fluid to brain and periphery in humans. Alzheimers Dement (Amst). 2020;12: e12030.

36. de Leon MJ, Li Y, Okamura N, Tsui WH, Saint-Louis LA, Glodzik L, Osorio RS, Fortea J, Butler T, Pirraglia E, et al. cerebrospinal fluid clearance in Alzheimer disease measured with dynamic PET. J Nucl Med. 2017;58:1471–6.

37. Li Y, Rusinek H, Butler T, Glodzik L, Pirraglia E, Babich J, Mozley PD, Nehmeh S, Pahlajani S, Wang X, et al. Decreased CSF clearance and increased brain amyloid in Alzheimer's disease. Fluids Barriers CNS. 2022;19:21.

38. Hesterman JY, Kost SD, Holt RW, Dobson H, Verma A, Mozley PD. Three-dimensional dosimetry for radiation safety estimates from intrathecal administration. J Nucl Med. 2017;58:1672–8.

39. Eide PK, Ringstad G. Delayed clearance of cerebrospinal fluid tracer from entorhinal cortex in idiopathic normal pressure hydrocephalus: a glymphatic magnetic resonance imaging study. J Cereb Blood Flow Metab. 2019;39:1355–68.

40. Eide PK, Pripp AH, Ringstad G. Magnetic resonance imaging biomarkers of cerebrospinal fluid tracer dynamics in idiopathic normal pressure hydrocephalus. Brain Commun. 2020;2:1–16.

41. Melin E, Eide PK, Ringstad G. In vivo assessment of cerebrospinal fluid efflux to nasal mucosa in humans. Sci Rep. 2020;10:1–10.

42. Pollay M. The function and structure of the cerebrospinal fluid outflow system. Cerebrospinal Fluid Res. 2010;7:9.

43. Jacob L, Boisserand LSB, Geraldo LHM, de Brito NJ, Mathivet T, Antila S, Barka B, Xu Y, Thomas JM, Pestel J, et al. Anatomy and function of the vertebral column lymphatic network in mice. Nat Commun. 2019;10:4594.

44. Weller RO. Microscopic morphology and histology of the human meninges. Morphologie. 2005;89:22–34.

45. Ma Q, Ineichen BV, Detmar M, Proulx ST. Outflow of cerebrospinal fluid is predominantly through lymphatic vessels and is reduced in aged mice. Nat Commun. 2017;8:1434.

46. Brinker T, Stopa E, Morrison J, Klinge P. A new look at cerebrospinal fluid circulation. Fluids Barriers CNS. 2014;11:10.

47. Kutomi O, Takeda S. Identification of lymphatic endothelium in cranial arachnoid granulation-like dural gap. Microscopy (Oxf). 2020;69(6):391–400.

48. Yağmurlu K, Sokolowski J, Soldozy S, Norat P, Çırak M, Tvrdik P, Shaffrey ME, Kalani MYS: A subset of arachnoid granulations in humans drain to the venous circulation via intradural lymphatic vascular channels. J Neurosurg 2021:1–10.

49. Eide PK, Vatnehol SAS, Emblem KE, Ringstad G. Magnetic resonance imaging provides evidence of glymphatic drainage from human brain to cervical lymph nodes. Sci Rep. 2018;8:1–10.

50. Halvorsen M, Edeklev CS, Fraser-Green J, Lovland G, Vatnehol SAS, Gjertsen O, Nedregaard B, Sletteberg R, Ringstad G, Eide PK. Off-label intrathecal use of gadobutrol: safety study and comparison of administration protocols. Neuroradiology. 2021;63:51–61.

51. Zhou Y, Cai J, Zhang W, Gong X, Yan S, Zhang K, Luo Z, Sun J, Jiang Q, Lou M. Impairment of the Glymphatic pathway and putative meningeal lymphatic vessels in the aging human. Ann Neurol. 2020;87:357–69.

52. Zou W, Pu T, Feng W, Lu M, Zheng Y, Du R, Xiao M, Hu G. Blocking meningeal lymphatic drainage aggravates Parkinson's disease-like pathology in mice overexpressing mutated alpha-synuclein. Transl Neurodegeneration. 2019;8:7.

53. Wang L, Zhang Y, Zhao Y, Marshall C, Wu T, Xiao M. Deep cervical lymph node ligation aggravates AD-like pathology of APP/PS1 mice. Brain Pathol. 2019;29:176–92.

54. Da Mesquita S, Louveau A, Vaccari A, Smirnov I, Cornelison RC, Kingsmore KM, Contarino C, Onengut-Gumuscu S, Farber E, Raper D, et al. Functional aspects of meningeal lymphatics in ageing and Alzheimer's disease. Nature. 2018;560:185–91.

55. Montagne A, Barnes SR, Sweeney MD, Halliday MR, Sagare AP, Zhao Z, Toga AW, Jacobs RE, Liu CY, Amezcua L, et al. Blood-brain barrier breakdown in the aging human hippocampus. Neuron. 2015;85:296–302.

56. Montagne A, Nation DA, Sagare AP, Barisano G, Sweeney MD, Chakhoyan A, Pachicano M, Joe E, Nelson AR, D'Orazio LM, et al. APOE4 leads to blood-brain barrier dysfunction predicting cognitive decline. Nature. 2020;581:71–6.

57. Hasan-Olive MM, Hansson HA, Enger R, Nagelhus EA, Eide PK. Blood-brain barrier dysfunction in idiopathic intracranial hypertension. J Neuropathol Exp Neurol. 2019;78:808–18.

58. Eide PK, Hansson HA. Blood-brain barrier leakage of blood proteins in idiopathic normal pressure hydrocephalus. Brain Res. 2020;1727:1–13.

59. Staks T, Schuhmann-Giampieri G, Frenzel T, Weinmann HJ, Lange L, Platzek J. Pharmacokinetics, dose proportionality, and tolerability of gadobutrol after single intravenous injection in healthy volunteers. Invest Radiol. 1994;29:709–15.

60. Farb RI, Nicholson PJ, Peng PW, Massicotte EM, Lay C, Krings T, terBrugge KG. Spontaneous intracranial hypotension: a systematic imaging approach for CSF leak localization and management based on mri and digital subtraction myelography. AJNR Am J Neuroradiol. 2019;40:745–53.

61. Rahman M, Bidari SS, Quisling RG, Friedman WA. Spontaneous intracranial hypotension: dilemmas in diagnosis. Neurosurgery. 2011;69:4–14 (**discussion 14**).

62. Novotny C, Pötzi C, Asenbaum S, Peloschek P, Suess E, Hoffmann M. SPECT/CT fusion imaging in radionuclide cisternography for localization of liquor leakage sites. J Neuroimaging. 2009;19:227–34.

63. Roberts KF, Elbert DL, Kasten TP, Patterson BW, Sigurdson WC, Connors RE, Ovod V, Munsell LY, Mawuenyega KG, Miller-Thomas MM, et al. Amyloid-β efflux from the central nervous system into the plasma. Ann Neurol. 2014;76:837–44.

64. Feng W, Zhang Y, Wang Z, Xu H, Wu T, Marshall C, Gao J, Xiao M. Microglia prevent beta-amyloid plaque formation in the early stage of an Alzheimer's disease mouse model with suppression of glymphatic clearance. Alzheimer's Res Ther. 2020;12:125.

65. Pardridge WM. Drug transport in brain via the cerebrospinal fluid. Fluids Barriers CNS. 2011;8:7.

66. Mazur C, Powers B, Zasadny K, Sullivan JM, Dimant H, Kamme F, Hesterman J, Matson J, Oestergaard M, Seaman M, et al. Brain pharmacology of intrathecal antisense oligonucleotides revealed through multimodal imaging. JCI Insight. 2019. https://doi.org/10.1172/jci.insight.129240.

67. Finkel RS, Chiriboga CA, Vajsar J, Day JW, Montes J, De Vivo DC, Yamashita M, Rigo F, Hung G, Schneider E, et al. Treatment of infantile-onset spinal muscular atrophy with nusinersen: a phase 2, open-label, dose-escalation study. Lancet. 2016;388:3017–26.

68. Byrnes DM, Vargas F, Dermarkarian C, Kahn R, Kwon D, Hurley J, Schatz JH. Complications of intrathecal chemotherapy in adults: single-institution experience in 109 consecutive patients. J Oncol. 2019;2019:4047617.

69. Livshits Z, Rao RB, Smith SW. An approach to chemotherapy-associated toxicity. Emerg Med Clin North Am. 2014;32:167–203.

70. Nguyen AD, Nguyen TA, Zhang J, Devireddy S, Zhou P, Karydas AM, Xu X, Miller BL, Rigo F, Ferguson SM, et al. Murine knockin model for progranulin-deficient frontotemporal dementia with nonsense-mediated mRNA decay. Proc Natl Acad Sci U S A. 2018;115:E2849-e2858.

71. McCampbell A, Cole T, Wegener AJ, Tomassy GS, Setnicka A, Farley BJ, Schoch KM, Hoye ML, Shabsovich M, Sun L, et al. Antisense oligonucleotides extend survival and reverse decrement in muscle response in ALS models. J Clin Invest. 2018;128:3558–67.

72. Niu C, Prakash TP, Kim A, Quach JL, Huryn LA, Yang Y, Lopez E, Jazayeri A, Hung G, Sopher BL, et al. Antisense oligonucleotides targeting mutant Ataxin-7 restore visual function in a mouse model of spinocerebellar ataxia type 7. Sci Transl Med. 2018. https://doi.org/10.1126/scitranslmed.aap8677.

73. Hardcastle N, Boulis NM, Federici T. AAV gene delivery to the spinal cord: serotypes, methods, candidate diseases, and clinical trials. Expert Opin Biol Ther. 2018;18:293–307.

74. Edeklev CS, Halvorsen M, Lovland G, Vatnehol SAS, Gjertsen O, Nedregaard B, Sletteberg R, Ringstad G, Eide PK. Intrathecal use of gadobutrol for glymphatic MR imaging: prospective safety study of 100 patients. AJNR Am J Neuroradiol. 2019;40:1257–64.

75. Patel M, Atyani A, Salameh JP, McInnes M, Chakraborty S. Safety of intrathecal administration of gadolinium-based contrast agents: a systematic review and meta-analysis. Radiology. 2020. https://doi.org/10.1148/radiol.2020191373.

Publisher's Note

Paper III

A Method for Evaluating Robustness of Limited Sampling Strategies—Exemplified by Serum Iohexol Clearance for Determination of Measured Glomerular Filtration Rate

Markus Hovd [1,*], Ida Robertsen [1], Jean-Baptiste Woillard [2] and Anders Åsberg [1,3]

1 Section for Pharmacology and Pharmaceutical Biosciences, Department of Pharmacy, University of Oslo, P.O. Box 1068 Blindern, 0316 Oslo, Norway; ida.robertsen@farmasi.uio.no (I.R.); anders.asberg@farmasi.uio.no (A.Å.)
2 Inserm, Univ. Limoges, CHU Limoges, Pharmacology & Toxicology, U 1248, F-87000 Limoges, France; jean-baptiste.woillard@unilim.fr
3 Department of Transplantation Medicine, Oslo University Hospital, P.O. Box 4950 Nydalen, 0424 Oslo, Norway
* Correspondence: m.h.hovd@farmasi.uio.no

Abstract: In combination with Bayesian estimates based on a population pharmacokinetic model, limited sampling strategies (LSS) may reduce the number of samples required for individual pharmacokinetic parameter estimations. Such strategies reduce the burden when assessing the area under the concentration versus time curves (AUC) in therapeutic drug monitoring. However, it is not uncommon for the actual sample time to deviate from the optimal one. In this work, we evaluate the robustness of parameter estimations to such deviations in an LSS. A previously developed 4-point LSS for estimation of serum iohexol clearance (i.e., dose/AUC) was used to exemplify the effect of sample time deviations. Two parallel strategies were used: (a) shifting the exact sampling time by an empirical amount of time for each of the four individual sample points, and (b) introducing a random error across all sample points. The investigated iohexol LSS appeared robust to deviations from optimal sample times, both across individual and multiple sample points. The proportion of individuals with a relative error greater than 15% (P15) was 5.3% in the reference run with optimally timed sampling, which increased to a maximum of 8.3% following the introduction of random error in sample time across all four time points. We propose to apply the present method for the validation of LSS developed for clinical use.

1. Introduction

The area under the plasma concentration-time curve (AUC) is a clinically useful variable for systemic drug exposure. Within several therapeutic fields, AUC-targeted therapeutic drug monitoring (TDM) is becoming more clinically acknowledged [1]. Accurate estimation of AUC either requires multiple samples within a dose interval when applying the trapezoidal method, or knowledge of the individuals' pharmacokinetic parameters, e.g., clearance. The use of the trapezoidal method in this aspect is time-consuming for both patients and healthcare professionals and not feasible in a clinical setting. However, with Bayesian estimates (BE) based on, for example, a population pharmacokinetic model or the use of a linear regression model, accurate estimates of pharmacokinetic parameters and AUC may be obtained by using a limited number of optimally timed samples [2]. Such limited sampling strategies (LSS) may reduce the number of samples and limit the length of the study visit to make AUC-targeted TDM clinically applicable [3].

In a real-life setting, it is not uncommon for actual sample times to deviate from the optimal LSS sample times. In contrast to multiple linear regression (MLR) models where

111

coefficients are determined for pre-defined or binned sample times, BE approaches are generally considered more flexible with regard to the timing of the samples, as long as the exact sample times are recorded [4].

According to pharmacokinetic theory, clearance of an intravenously administered drug may be determined by dividing the dose by the AUC. The glomerular filtration rate (GFR) is a clinically important marker for renal function and is typically estimated from blood concentrations of endogenous markers (eGFR). However, the most accurate metric of renal function is the measured GFR (mGFR) assessed by determining the AUC of an exogenous substance subject to clearance via filtration in the kidney [5]. The gold standard of these exogenous markers is inulin but it is difficult to obtain injection-quality inulin nowadays and the analytical assay is also somewhat challenging. Due to this, the contrast agent iohexol has become the new gold standard for mGFR as it shows high concordance with inulin-derived mGFR given optimal sampling times in relation to absolute GFR level [6]. Iohexol exhibits a low degree of protein-binding, low toxicity for the needed doses, no tubular secretion or reabsorption, and is generally stable in plasma/serum [7]. As iohexol is fully excreted by the kidneys, mGFR may be determined by measuring the clearance of iohexol. For this, both MLR- and BE-based LSS are available in the literature. Of these, BE-based methods have been shown to be more flexible and accurate than MLR [8].

We have previously demonstrated the feasibility of a BE-based 4-point LSS to accurately determine mGFR over the range of 14 to 149 mL/min using iohexol serum clearance [9]. Our LSS includes four samples within 5 h following intravenous administration of iohexol. Here, we accurately determine the iohexol serum clearance by dividing the administered dose by the AUC. As such, this method is equally viable for evaluating the effect of shifts in sample time on AUC, as well as mGFR. While the effect of a deviation in time from LSS based on MLR has been evaluated previously [10], the effect of deviations in sample time on parameter estimates in the BE-based methods has not been readily studied and is rarely considered during LSS development or their clinical use. In this work, we demonstrate a general method for evaluating the robustness of an LSS, using the iohexol model for AUC-based mGFR determination as an example. The effect of deviations in time, both across individual and multiple time points, on AUC and model estimated parameters are evaluated.

2. Materials and Methods

2.1. Population Pharmacokinetics Model and Limited Sampling Strategy of Iohexol

The population pharmacokinetic model and associated LSS for iohexol serum clearance have previously been described in detail [9]. In short, a non-parametric adaptive grid (NPAG) approach implemented in Pmetrics [11] for R [12] was used. The model consisted of two compartments, parameterized in clearance (CL) from the central compartment, the volume of central (V) and peripheral (Vp) compartments, and inter-compartmental blood flow (Q), allometrically scaled for body weight using power factors of 0.75 for CL and Q and 1 for V and Vp. The model was developed on rich data from 176 patients (1131 samples), and externally validated in a cohort of 43 patients (395 samples). The 4-point sampling strategy optimized for clinical use included samples at 10 min, 30 min, 2 h, and 5 h following intravenous administration of 3235 mg iohexol (Omnipaque 300 mg I/mL, GE Healthcare AS, Oslo, Norway). A public, web-based interface to this model was developed and is freely available at https://www.mgfr.no.

2.2. Semi-Parametric Simulation from Support Points

To evaluate the robustness of the previously developed LSS of iohexol, simulations were performed to obtain pharmacokinetic profiles from a similar parameter distribution (i.e., population) as the original dataset. Our simulation method did not include covariates, and as such, a covariate-free version of the model was used. This model was developed and evaluated using the original development and validation datasets. Model diagnostic plots and performance metrics are available in Figure S1 and Table S1.

Briefly, the NPAG algorithm estimates the joint population parameter distribution, which is used as a Bayesian prior for individual parameter estimation. The algorithm has recently been explained in detail by Yamada et al., 2020 [13]. The population parameter distribution is a discrete distribution provided as a set of support points, each a vector of length D with an associated probability, where D is the number of parameters. The discrete distribution may be transformed to a continuous distribution for the purpose of sampling a wider range of possible parameter combinations. To accomplish this, we assume a Gaussian distribution over each support point, forming a Gaussian mixture distribution. The probability density function for the multivariate Gaussian mixture is defined as

$$p(x \mid \mu, \Sigma) = N(\mu, \Sigma) \tag{1}$$

where μ and Σ are the vector of means and the matrix of variances, respectively. Values of μ are readily obtained from the individual support point vectors. In order to determine Σ, the univariate Gaussian mixture was evaluated for each parameter, the density for which is

$$p(x) = \sum_{i=1}^{K} \pi_i * N(x \mid \mu_i, \sigma_i) \quad \text{satisfying} \quad \sum_{i=1}^{K} \pi_i = 1 \tag{2}$$

where π is the weighting (or probability) for the Kth Gaussian distribution with mean μ and variance σ. For each parameter, a common σ, and thus, the proposed element of Σ, was determined by minimizing the sum of the squared distance between the simulated and observed (individual posterior) parameter distribution. Minimization was performed using the built-in optim-function in R, implementing Brent's method. Sampling from the mixture distribution is achieved by first sampling the mixture components, i.e., the support points, with replacement, weighted by their probability. Then, multivariate normal sampling of parameters was accomplished using the rtmvnorm function implemented in the tmvtnorm (version 1.5) package for R (version 4.1.3) [14]. Rejection sampling was used to respect the boundaries of the population pharmacokinetic model. A successful simulation was evaluated by the overlapping index for empirical distributions [15], for which values equal to or above 85% were considered acceptable, comparable to an error of 15%. In order to generate concentration-time profiles from the simulated parameter vectors, the population pharmacokinetic model was rewritten to be used in the mrgsolve [16] package for R (Supplementary Code S1). Simulated sampling was performed in 1 min intervals from 0 to 24 h following a dose of 3235 mg of iohexol. No systematic or random error was added to the measurements.

GFR was calculated by dividing dose by the AUC from zero to infinity ($AUC_{0-\infty}$). Simulated profiles with GFR < 15 mL/min or GFR > 115 mL/min were excluded, as they were outside the validated range of the LSS and will not be explored in this work. As such, both AUC and GFR are conversely evaluated in this work.

2.3. Deviation from Optimal Sample Times

The robustness of the 4-point sampling strategy for iohexol serum clearance was evaluated at each of the sample points with empirically selected deviations in time; 10 min (± 2, 4, 5, and 6 min), 30 min (± 5, 10, and 15 min), 2 h (± 5, 15, 30, and 60 min), and 5 h (± 5, 15, 30, 60, 120 and +180, 420, and 1140 min), in addition to a reference run with the original sample times. Each shift was run separately, with cycling, and using the support points of the covariate-free model ran on the complete dataset as a Bayesian prior, as specified in the original publication [9].

In order to evaluate the effect of deviation over multiple sample times, a random normally distributed error, centered around each respective sample point, and with a relative standard deviation (RSD) of 5, 10, 15, 20, and 25% was added to all sample points, truncated (using rejection sampling) at each point to prevent overlap; 10 min (5–15 min), 30 min (15–60 min), 2 h (1–3 h), and 5 h (3–8 h). As a measure of robustness to the aforementioned shifts in sample times, both the mean absolute prediction error in mGFR

and the proportion of individuals with relative prediction error greater than 15% (P15) were used. Here, a P15 less than 15% was considered acceptable.

2.4. Optimal Sample Windows

Based on the results of deviation in both individual and multiple sample points, two approaches to empirical sample windows were used. For deviation in individual sample time, assuming otherwise no deviation in the remaining sample points, the time intervals for which the mean error was lower than 2 mL/min may be used. For deviation across all sample times, the level of RSD associated with an acceptable P15 was used to calculate empirical sample windows for all sample points by calculating the 90% confidence interval for the normal distribution centered at each sample point, truncated to avoid overlap between samples.

3. Results

3.1. Simulated Profiles

A total of 400 pharmacokinetic profiles were simulated, of which 58 and 3 were excluded due to a simulated GFR of less than 15 mL/min or greater than 115 mL/min, respectively, yielding a total of 339 profiles used in the analysis. The variances that minimized the distance between observed and simulated parameter densities were 0.61, 2.2, 1.2, and 0.9 units, for CL, Q, V, and Vp, respectively. Simulated parameter densities demonstrated satisfactory overlap with the observed posterior parameter densities from the original population pharmacokinetic model (91, 92, 90, and 86% for CL, Q, V, and Vp, respectively) (Figure 1). Compared to the posterior, none of the simulated parameters had a difference in weighted mean greater than 15% (Table 1). The simulated profiles (n = 339) were further grouped based on the estimated mGFR in relation to the chronic kidney disease (CKD) stages; stage 4:15–29 mL/min (n = 90), stage 3B: 30–44 mL/min (n = 100), stage 3A: 45–59 mL/min (n = 57), stage 2: 60–90 mL/min (n = 73), and stage 1: >90 mL/min (n = 19).
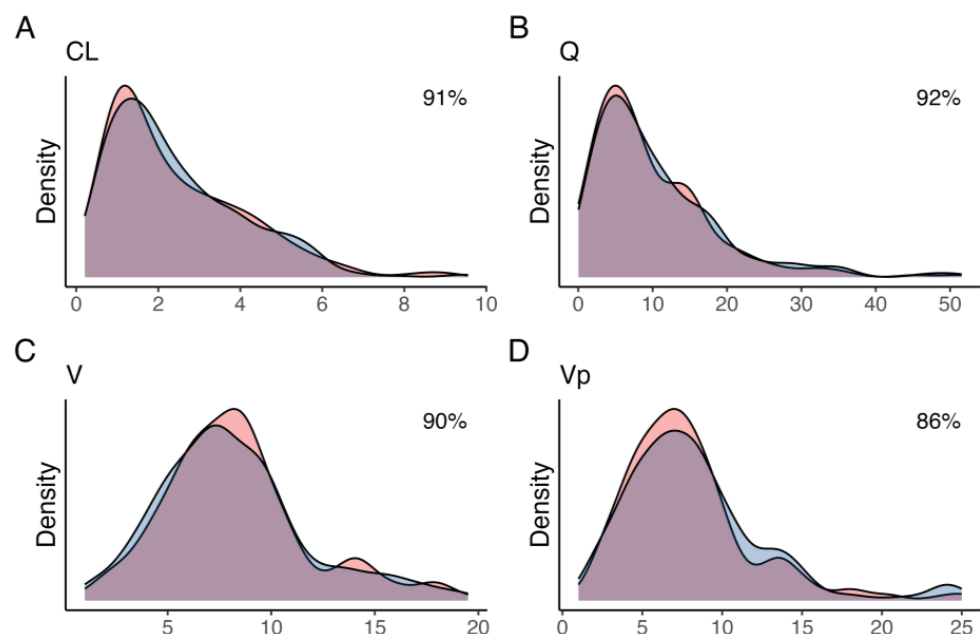
Figure 1. Kernel density estimates for the posterior (blue) and simulated (red) for (**A**) clearance from the central compartment (CL), (**B**) inter-compartmental clearance (Q), (**C**) central volume (V), and (**D**) peripheral volume (Vp). The overlap coefficient for empirical distributions between the posterior and simulated parameter distribution is shown in the top-right corner.

Table 1. Weighted mean and weighted median (95% credibility interval) of the population pharmacokinetic model parameters support points for the original and simulated dataset.

	Weighted Mean		Weighted Median (95% Credibility Interval)	
	Original	Simulated	Original	Simulated
CL (L/h)	2.89	2.84	1.95 (1.54–2.60)	2.42 (2.16–2.72)
V (L)	10.36	9.32	10.11 (9.19–10.91)	8.98 (8.25–9.57)
Vp (L)	9.20	7.98	7.95 (7.23–8.60)	7.46 (7.06–7.81)
Q (L/h)	10.65	11.37	8.03 (6.53–9.23)	8.65 (7.50–9.72)

3.2. LSS Performance on Simulated Profiles

The LSS performance on the simulated profiles was evaluated by sampling at precisely 10 min, 30 min, 2 h, and 5 h. The mean absolute and relative error in GFR were 1.5 ± 2.2 mL/min and $4.1 \pm 5.5\%$, respectively (Table 2). In total, 6.5% of the simulated profiles demonstrated an absolute error greater than 5 mL/min, and 1.2% demonstrated an error greater than 10 mL/min. The proportion of individuals with an error larger than 15% (P15) was 5.3%, seemingly increasing with decreased GFR, as expected (Table 2).

Table 2. Limited sampling strategy performance on determining mGFR for the simulated profiles, presented as the absolute and relative error from the simulated "true" GFR. Data are presented as mean $\pm$ standard deviation.

| Group	Absolute Error (mL/min)	Relative Error (%)	P15 (%)	*n*
All profiles	1.5 ± 2.2	4.1 ± 5.5	5.3	339
CKD Stage 4 (15–29 mL/min)	1.5 ± 1.3	6.3 ± 5.8	7.8	90
CKD Stage 3b (30–44 mL/min)	1.9 ± 2.2	5.4 ± 6.0	8.0	100
CKD Stage 3a (45–59 mL/min)	1.0 ± 1.6	2.2 ± 3.4	1.8	57
CKD Stage 2 (60–90 mL/min)	1.3 ± 3.0	1.9 ± 4.4	2.7	73
CKD Stage 1 (90–115 mL/min)	1.2 ± 2.2	1.2 ± 1.9	0.0	19

3.3. Effect of Shifts in Sample Times on Estimated GFR

A graphical representation of the effect of deviations in individual sample time on estimated GFR is shown in Figure 2. In all cases, the mean absolute error was below 4 mL/min, and the median absolute error was below 2.5 mL/min. For the 10 min sample, delays by up to 6 min increased P15 to a maximum of 9%. Sampling 5 and 6 min prior, effectively at 4 and 5 min post-dose, was not evaluable by the model, and these times were not included. In contrast, delaying the 30 min sample less than 15 min reduced P15 to 4%, while sampling up to 15 min earlier increased P15 to 16%. The 2 h sample exhibits a similar pattern, with reduced P15 for delayed samples, down to 4% at 60 min delayed. The 5 h sample was mostly unaffected by up to 7 h delay in sampling. However, delaying the sample to 24 h post iohexol administration drastically reduced the predictive performance as expected; P15 increased to 18%, and the mean absolute error was 2.9 ± 3.5 mL/min. In order to evaluate these trends for each CKD stage, the median error for each shift is shown in Figure 3.

Applying random, normally distributed noise with an RSD equal to 5 and 10% across all sample times led to a P15 of 7.7% in both cases, and a maximum P15 of 8.3% was achieved in the case of an RSD of both 20% and 25% (Figure 4). For the simulated profiles with CKD stage 1 (GFR 90–115 mL/min), P15 was 0% for all levels of RSD, and a maximum of 4.1% at 5% RSD for profiles with GFR 60–90 mL/min. In contrast, simulated profiles with GFR between 45–55 mL/min, 30–44 mL/min, and 15–15 mL/min incurred a P15 of 7%, 14%, and 10% at 25% RSD, respectively.
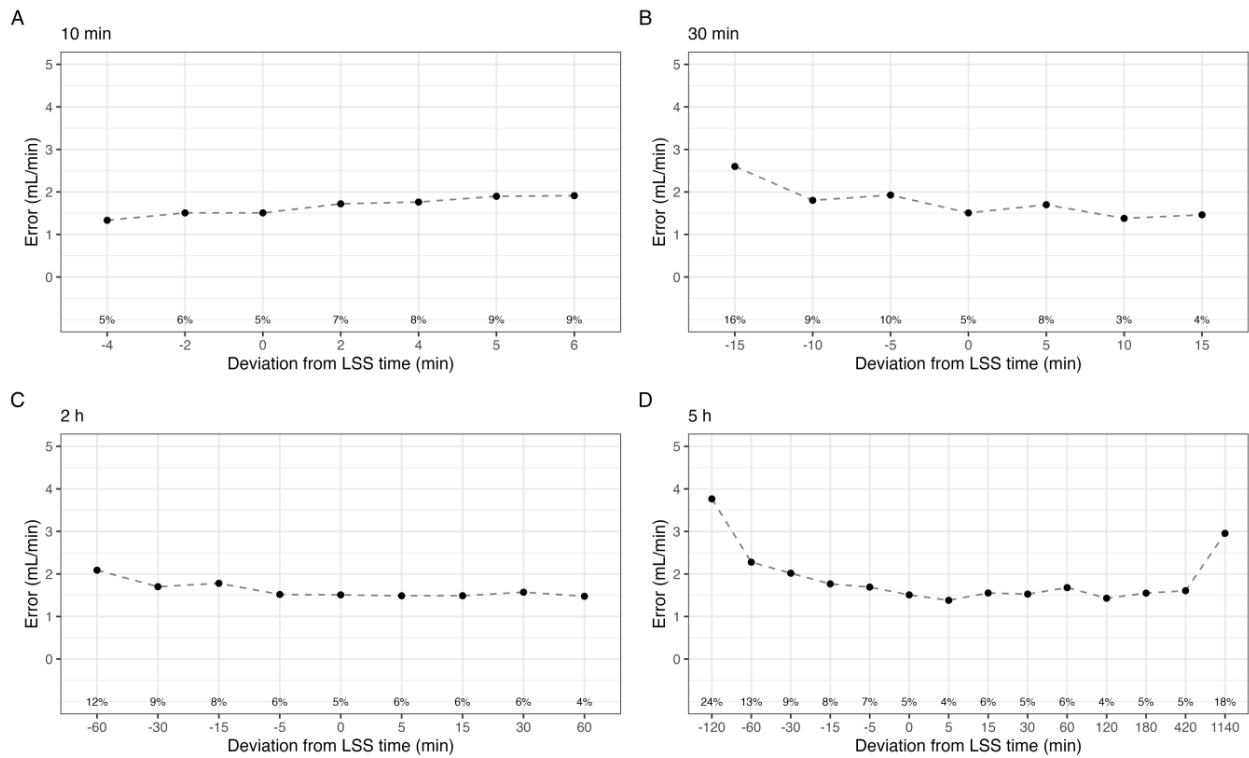
Figure 2. Mean absolute error in estimated GFR by the shift in sample time at point (**A**) 10 min, (**B**) 30 min, (**C**) 2 h, and (**D**) 5 h. Labels indicate the percentage of individuals with a relative error greater than 15% (P15).
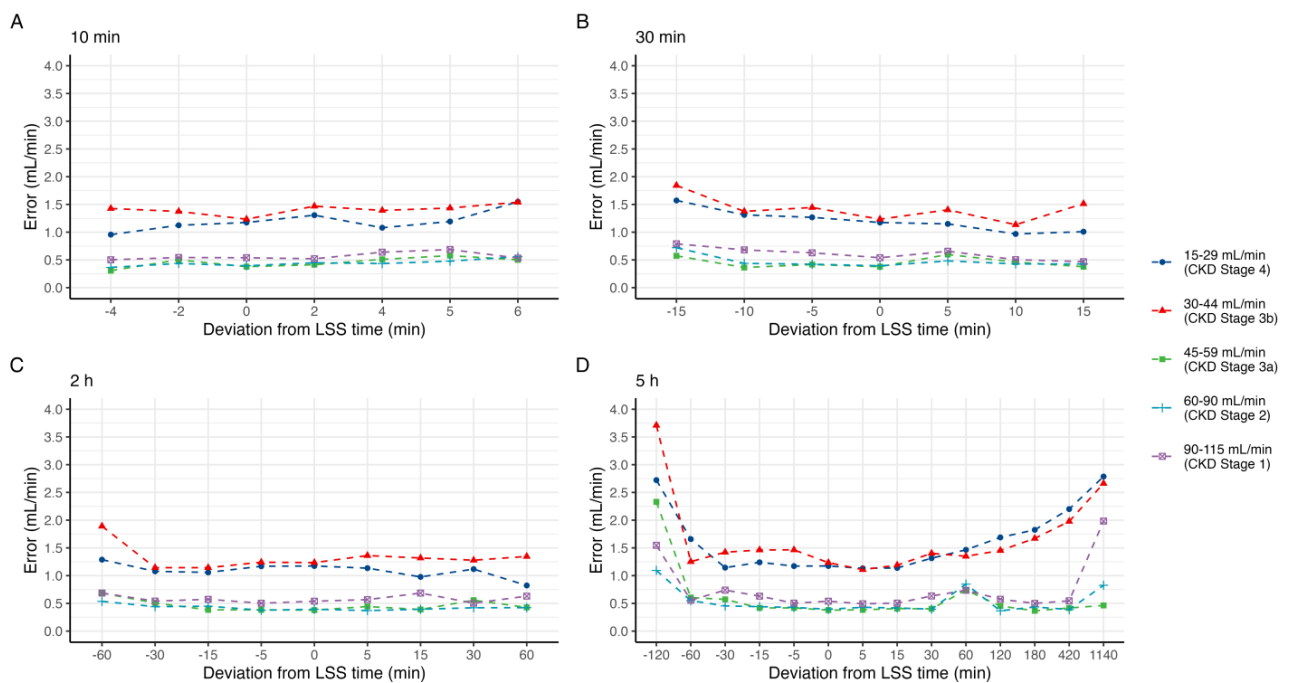
Figure 3. Median absolute error in predicted mGFR by deviation in sample time at point (**A**) 10 min, (**B**) 30 min, (**C**) 2 h, and (**D**) 5 h, grouped by CKD stage.
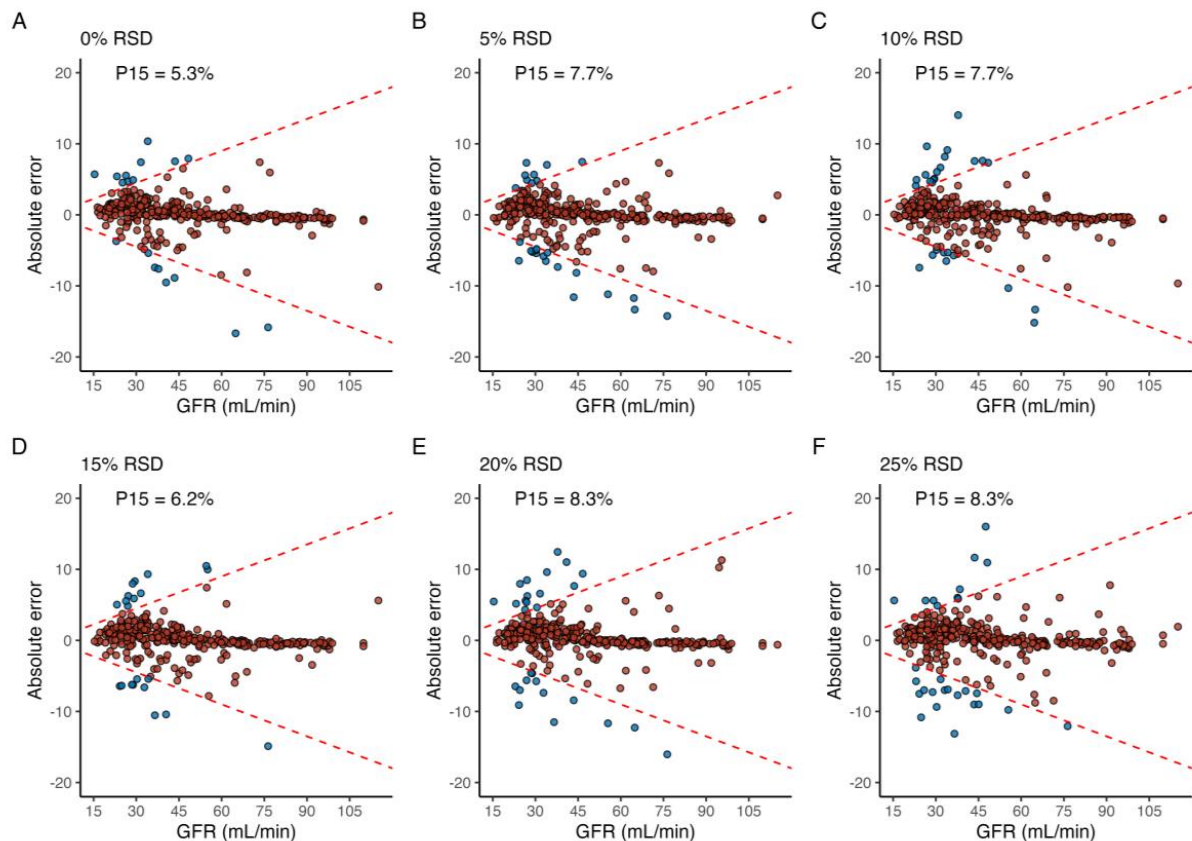
Figure 4. The effect of shifts in time over multiple sample points, where the (**A**) reference run is compared to when shifts in sample time are normally distributed around the optimal sample time with a relative standard deviation (RSD) of (**B**) 5%, (**C**) 10%, (**D**) 15%, (**E**) 20%, and (**F**) 25%. Blue and red fill indicates an individual error greater than or less than 15%, respectively. The label in the upper-left corner denotes the proportion of individuals with a relative prediction error greater than 15% (P15) for each level of RSD.

### 3.4. Optimal Sample Windows

The intervals around the deviation in individual optimal sample times that provide a mean error in predicted GFR less than 2 mL/min, and conversely a low error in AUC, were 6–16 min (10 min), 20–45 min (30 min), 1.5–3 h (2 h), and 4.75–12 h (5 h) (Figure 5A). A careful estimate of the optimal sample window may be obtained by, e.g., the 90% confidence interval for the normal distribution with optimal sample times as the mean, and an RSD of 25%. As such, an estimate of optimal sample windows for the present LSS, without considering the absolute renal function of the patient, are 6–12 min (10 min), 18–42 min (30 min), 1–3 h (2 h), and 2.5–7.4 h (5 h) (Figure 5B), assuming no overlap.

3.5. Effect of Shifts in Sample Times on Model Parameters

Supplementary to the effect of a deviation from optimal sample time on predicted GFR, and conversely, predicted AUC_{0-inf}, changes in estimated model parameters were also evaluated. A graphical representation of the model-estimated parameter densities across all evaluated shifts is shown in Figure 6. When compared with the true parameter densities of the simulated data, the reference run with optimally timed samples achieved a relative error in mean population model parameter estimates in CL, V, Vp, and Q of 1.5%, 0.6%, 6.9%, and 3.8%, respectively. However, the mean individual relative errors in the same estimates in CL, V, Vp, and Q were 7.4%, 7.6%, 22.7%, and 495%.
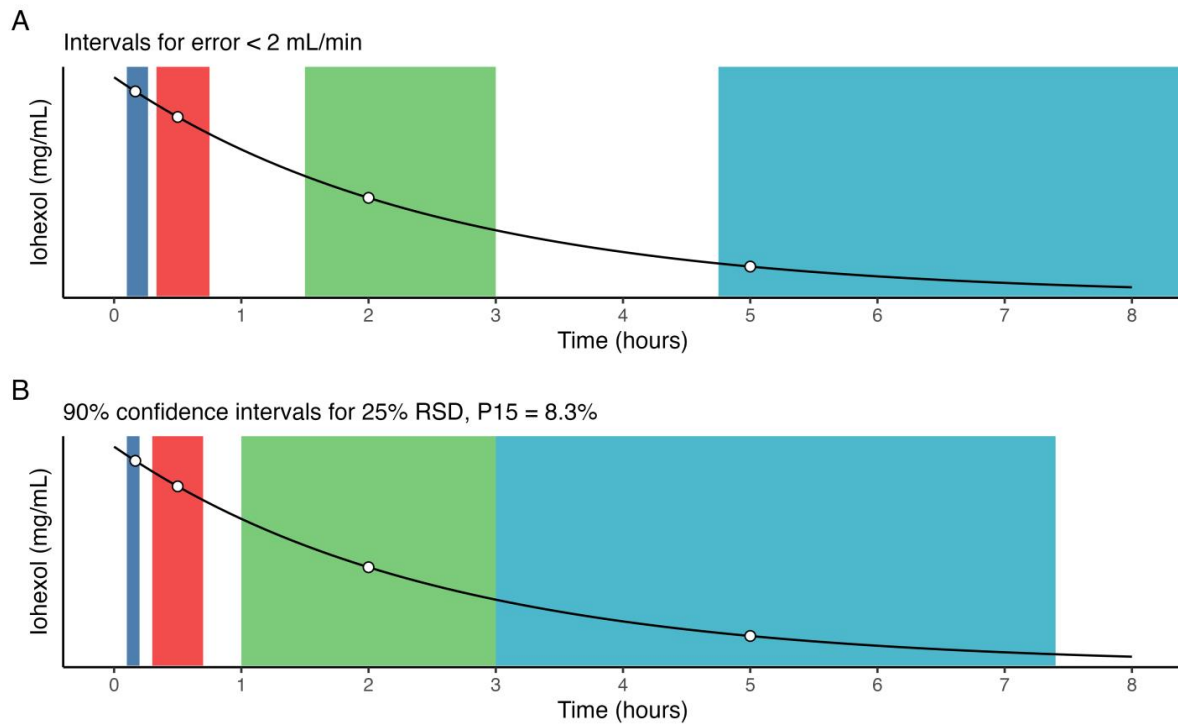
Figure 5. Empirical estimates of optimal sample windows for (**A**) deviations in individual sample times, assuming all other points are sampled optimally, resulting in mean error < 2 mL/min, and (**B**) deviations across all sample times, normally distributed around each sample point with 25% RSD, resulting in a P15 = 8.3%.
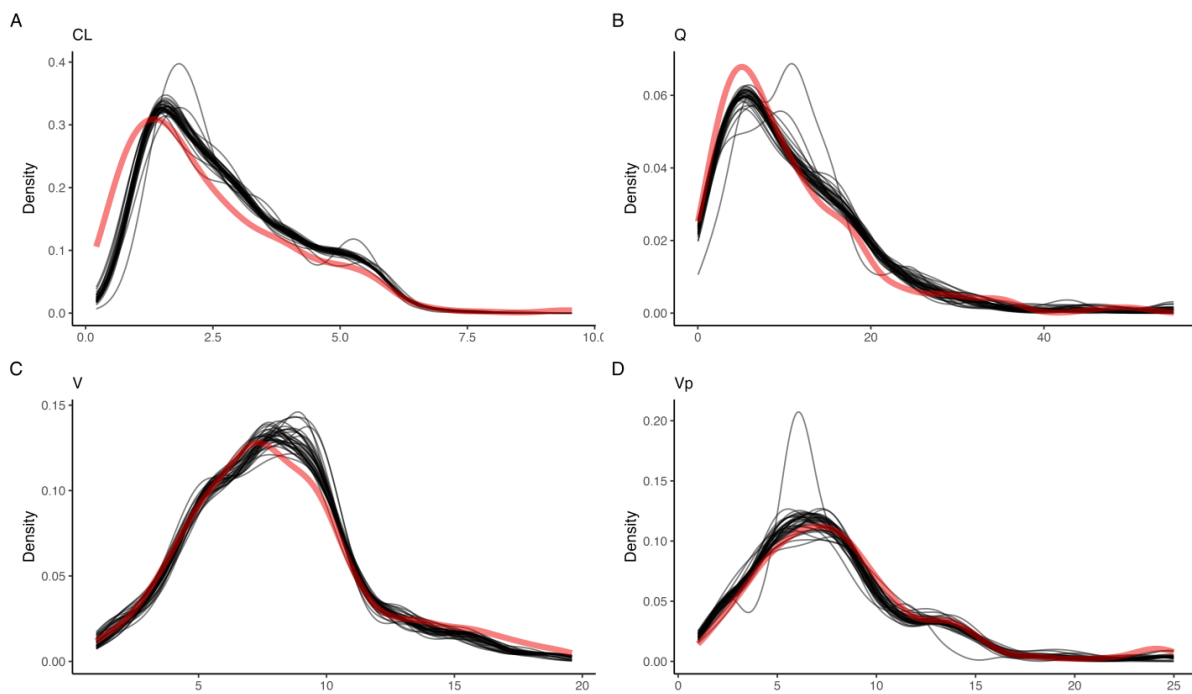
Figure 6. Kernel density estimates for all empirical deviations in time (black), compared to the observed posterior (red) for (**A**) clearance from the central compartment (CL), (**B**) inter-compartmental clearance (Q), (**C**) central volume (V), and (**D**) peripheral volume (Vp).

4. Discussion

In this work, we demonstrate an intuitive approach to evaluating the robustness of LSS, with direct clinical applications. The method was applied to a previously published model for serum iohexol clearance used for the determination of mGFR based on accurate estimates of $AUC_{0\text{-inf}}$. To our knowledge, this is the first work evaluating the robustness of LSS in such a setting. Overall, the 4-point LSS appears robust to shifts in both single and multiple sample times, especially for profiles with medium to good GFR, i.e., above 45 mL/min. An interesting finding is that the robustness is affected by patient absolute clearance or GFR, in this case, and that acceptable sample time deviations should be adapted also based on this information. This is especially useful in scenarios when a rough estimate of the patient clearance is known based on clinical history, but the exact mGFR is desired, e.g., for dose-adjustment of drugs.

In the case of LSS employing MLR, Sarem and colleagues have previously evaluated the effect of deviations in sample time on AUC only [10]. The present work applies this methodology to BE-based LSS and evaluates not only the effect of such deviations on AUC but also the effect on parameter estimates at the individual and population levels. Additionally, BE-based methods have been shown to outperform LSS based on MLR in the case of iohexol clearance for the determination of mGFR [8,9]. The BE-based method was evaluated with a restriction of sampling within standard laboratory opening hours, i.e., the whole procedure was finalized within 5 h, while the MLR-base method allowed sampling up to 24 h after dosing. The BE-based model was not only more accurate but also better adapted to clinical practice [9]. With the development of easily and freely accessible interfaces to these otherwise complicated BE-based models, such as the one we provide at https://www.mgfr.no, the barrier to implementation in a clinical setting is significantly lowered, becoming similar to that of MLR.

When evaluating deviations in sample time for individual sample points, and assuming otherwise optimal sampling, no clinically significant increase in either mean absolute error or P15 was found across shifts in the 10 min sample, and the 30 min sample may be delayed by 15 min, even favorably so. As for the 2 h and 5 h samples, either may be accelerated by up to 30 min without increasing the P15 above 10%. This may potentially save time for both the patient and healthcare personnel during AUC-guided TDM. In this work, delaying individual samples improved the predictive performance of the LSS, likely due to the abundance of simulated profiles with low GFR. Previous history or indication of the patient's AUC and/or mGFR, it is possible to make specific recommendations. For example, parameter estimation in patients with high AUC, and conversely, low mGFR, may benefit more from delayed sampling, and vice versa. A challenge is that individual pharmacokinetic parameters are subject to change over time, but a Bayesian framework compatible with the present method has previously been described by Bayard and Jelliffe [17].

The introduction of random error with an RSD of 25% was associated with a P15 of 8.3%, compared to 5.3% in the reference run. The level of RSD yielding an acceptable P15 could be viewed as a surrogate marker for LSS robustness to shifts across multiple sample times for implementation in the clinic. As demonstrated, this may be tailored to the study population as a whole, or individual sub-groups of patients with, e.g., different stages of CKD. The empirically determined optimal sample windows allow for added granularity with regard to the diligence required for sample collection. However, this does not address the minimum distance required between two given samples, which is likely to affect the accuracy of parameter estimates.

With respect to the model estimated parameters, the effect of empirical deviations in individual sample times on the population level was negligible, as indicated by a low relative error in mean parameter values and the fact that the population parameter densities mostly overlapped the simulated, true density. However, individual parameter estimates varied significantly—especially the peripheral volume and inter-compartmental clearance were often misidentified. This is not surprising, as these parameters are seldom identifiable. This misidentification did not have any effect on the predictive performance of

119

the model, i.e., estimates of individual $AUC_{0-\infty}$, here translated to mGFR. All runs exhibited exceptionally low mean prediction errors and relative root-mean-squared errors. This was observed during early method development and for this reason, iohexol serum clearance, and thus GFR, was calculated by dividing dose by $AUC_{0-\infty}$. This further highlights the need for a more robust evaluation of LSS, especially when model parameters are used directly. Our results demonstrate the clinical application of evaluating the robustness of BE-based LSS. Previously, the effect of a deviation in sample time was unknown but has now been quantified for the present model and population. With this information, one may look up the deviation in sample time for the relevant CKD stage and use this to decide on whether to include an additional sample, for example, which is likely to improve the accuracy of the parameter estimates. Such changes to the LSS are not possible in the case of multiple linear regression-based methods, where one is restricted to a pre-defined or binned sample space.

For simulation-based studies, it is imperative that the simulated population reflects the underlying research question. While this is implicitly assumed, it is not usually confirmed in simulation-based studies, despite its importance. In this work, we aimed to simulate profiles from a similar population, which was confirmed by evaluating the overlap in parameter densities, in addition to comparisons of weighted mean and median. A disadvantage of the proposed method for semi-parametric simulation is the lack of covariates, given that multiple model parameters were allometrically scaled in the original model. Our strategy for simulation was based on the mechanistic interpretation of the support points representing the discrete population parameter distribution from the NPAG algorithm. However, there is no direct link between the support points and the covariates. For the covariate to be included in the multivariate normal sampling, a sensible mean and variance must be provided. An initial choice would be the observed mean and variance of the covariate, which was attempted during method development, but led to poor overlap between the posterior and simulated parameter densities. Alternate approaches to include covariates in a semi-parametric simulation will be investigated in a future work. Even though the present work utilized a covariate-free version of the original model, we still believe that the proposed simulation method provides an accurate representation of the effect of deviations in LSS sample times on individual pharmacokinetic estimates, as the method for evaluating the robustness of LSS is agnostic to the process for which data is generated.

5. Conclusions

By deviating from the optimally timed sample point(s) of an LSS either empirically or randomly, the robustness of the LSS to such shifts can be approximated. Additionally, empirical optimal sample windows may be obtained for a more flexible sampling schedule. It was further revealed that despite model population parameter estimates being within 10% across all evaluated deviations, individual model parameter estimates were prone to misidentification. These findings provide additional insight into the necessary diligence required during sample collection of optimally timed samples and provide a method for evaluating LSS robustness with respect to both pharmacokinetic (i.e., AUC) and model estimated parameters. We propose the present method be applied during the development and validation of LSS for clinical use.

Supplementary Materials: The following supporting information can be downloaded at: https://www.mdpi.com/article/10.3390/pharmaceutics15041073/s1. Figure S1: Population pharmacokinetic model performance plots for the covariate-free model, including (A) observed-predicted plot, (B) weighted error across observed concentrations, and (C) weighted error across sample time. Solid black lines represent the unity line, and the solid blue lines in (B,C) indicate the loess line. Table S1: Population pharmacokinetic performance metrics for the covariate-free model. Supplementary Code S1: Implementation of the population pharmacokinetic model in mrgsolve for R.

Author Contributions: Conceptualization, M.H., I.R. and A.Å.; Methodology, M.H., I.R., J.-B.W. and A.Å.; Software, M.H. and J.-B.W.; Validation, M.H. and A.Å.; Formal Analysis, M.H.; Investigation, M.H.; Resources, I.R. and A.Å.; Data Curation, A.Å.; Writing—Original Draft Preparation, M.H.; Writing—Review & Editing, M.H., I.R., J.-B.W. and A.Å.; Visualization, M.H.; Supervision, I.R. and A.Å.; Project Administration, A.Å.; Funding Acquisition, I.R. and A.Å. All authors have read and agreed to the published version of the manuscript.

Funding: This research received no external funding.

Institutional Review Board Statement: Not applicable.

Informed Consent Statement: Not applicable.

Data Availability Statement: The data presented in this study are available on request from the corresponding author.

Conflicts of Interest: Hovd, Robertsen, Woillard, and Åsberg declare that they have no conflict of interest.

Abbreviations

P15: the proportion of individuals with an error greater than 15%.

References

1. Lim, A.S.; Foo, S.H.W.; Benjamin Seng, J.J.; Magdeline Ng, T.T.; Chng, H.T.; Han, Z. Area-Under-Curve–Guided Versus Trough-Guided Monitoring of Vancomycin and Its Impact on Nephrotoxicity: A Systematic Review and Meta-Analysis. *Ther. Drug Monit.* **2023**. [CrossRef] [PubMed]
2. van den Elsen, S.H.J.; Sturkenboom, M.G.G.; Akkerman, O.W.; Manika, K.; Kioumis, I.P.; van der Werf, T.S.; Johnson, J.L.; Peloquin, C.; Touw, D.J.; Alffenaar, J.-W.C. Limited Sampling Strategies Using Linear Regression and the Bayesian Approach for Therapeutic Drug Monitoring of Moxifloxacin in Tuberculosis Patients. *Antimicrob. Agents Chemother.* **2019**, *63*, e00384-19. [CrossRef] [PubMed]
3. Teitelbaum, Z.; Nassar, L.; Scherb, I.; Fink, D.; Ring, G.; Lurie, Y.; Krivoy, N.; Bentur, Y.; Efrati, E.; Kurnik, D. Limited Sampling Strategies Supporting Individualized Dose Adjustment of Intravenous Busulfan in Children and Young Adults. *Ther. Drug Monit.* **2020**, *42*, 427–434. [CrossRef] [PubMed]
4. van der Meer, A.F.; Marcus, M.A.; Touw, D.J.; Proost, J.H.; Neef, C. Optimal sampling strategy development methodology using maximum a posteriori Bayesian estimation. *Ther. Drug Monit.* **2011**, *33*, 133–146. [CrossRef] [PubMed]
5. Porrini, E.; Ruggenenti, P.; Luis-Lima, S.; Carrara, F.; Jiménez, A.; de Vries, A.P.J.; Torres, A.; Gaspari, F.; Remuzzi, G. Estimated GFR: Time for a critical appraisal. *Nat. Rev. Nephrol.* **2019**, *15*, 177–190. [CrossRef] [PubMed]
6. Dubourg, L.; Lemoine, S.; Joannard, B.; Chardon, L.; de Souza, V.; Cochat, P.; Iwaz, J.; Rabilloud, M.; Selistre, L. Comparison of iohexol plasma clearance formulas vs. inulin urinary clearance for measuring glomerular filtration rate. *Clin. Chem. Lab. Med.* **2021**, *59*, 571–579. [CrossRef] [PubMed]
7. Delanaye, P.; Ebert, N.; Melsom, T.; Gaspari, F.; Mariat, C.; Cavalier, E.; Björk, J.; Christensson, A.; Nyman, U.; Porrini, E.; et al. Iohexol plasma clearance for measuring glomerular filtration rate in clinical practice and research: A review. Part 1: How to measure glomerular filtration rate with iohexol? *Clin. Kidney J.* **2016**, *9*, 682–699. [CrossRef]
8. Destere, A.; Salmon Gandonnière, C.; Åsberg, A.; Loustaud-Ratti, V.; Carrier, P.; Ehrmann, S.; Barin-Le Guellec, C.; Marquet, P.; Woillard, J.B. A single Bayesian estimator for iohexol clearance estimation in ICU, liver failure and renal transplant patients. *Br. J. Clin. Pharmacol.* **2022**, *88*, 2793–2801. [CrossRef]
9. Asberg, A.; Bjerre, A.; Almaas, R.; Luis-Lima, S.; Robertsen, I.; Salvador, C.L.; Porrini, E.; Schwartz, G.J.; Hartmann, A.; Bergan, S. Measured GFR by Utilizing Population Pharmacokinetic Methods to Determine Iohexol Clearance. *Kidney Int. Rep.* **2020**, *5*, 189–198. [CrossRef]
10. Sarem, S.; Nekka, F.; Ahmed, I.S.; Litalien, C.; Li, J. Impact of sampling time deviations on the prediction of the area under the curve using regression limited sampling strategies. *Biopharm. Drug Dispos.* **2015**, *36*, 417–428. [CrossRef] [PubMed]
11. Neely, M.N.; van Guilder, M.G.; Yamada, W.M.; Schumitzky, A.; Jelliffe, R.W. Accurate detection of outliers and subpopulations with Pmetrics, a nonparametric and parametric pharmacometric modeling and simulation package for R. *Ther. Drug Monit.* **2012**, *34*, 467–476. [CrossRef] [PubMed]
12. R Core Team. *R: A Language and Environment for Statistical Computing*; R Foundation for Statistical Computing: Vienna, Austria, 2020.
13. Yamada, W.M.; Neely, M.N.; Bartroff, J.; Bayard, D.S.; Burke, J.V.; Guilder, M.V.; Jelliffe, R.W.; Kryshchenko, A.; Leary, R.; Tatarinova, T.; et al. An Algorithm for Nonparametric Estimation of a Multivariate Mixing Distribution with Applications to Population Pharmacokinetics. *Pharmaceutics* **2020**, *13*, 42. [CrossRef] [PubMed]

14. Wilhelm, S.; Manjunath, B.G. tmvtnorm: A Package for the Truncated Multivariate Normal Distribution. *R J.* **2010**, *2*, 25–29. [CrossRef]
15. Pastore, M.; Calcagni, A. Measuring Distribution Similarities Between Samples: A Distribution-Free Overlapping Index. *Front. Psychol.* **2019**, *10*, 1089. [CrossRef] [PubMed]
16. Baron, K.T. Mrgsolve: Simulate from ODE-Based Models. R package version 1.0.6. 2022. Available online: https://CRAN.R-project.org/package=mrgsolve (accessed on 1 February 2023).
17. Bayard, D.S.; Jelliffe, R.W. A Bayesian Approach to Tracking Patients Having Changing Pharmacokinetic Parameters. *J. Pharmacokinet. Pharmacodyn.* **2004**, *31*, 75–107. [CrossRef] [PubMed]
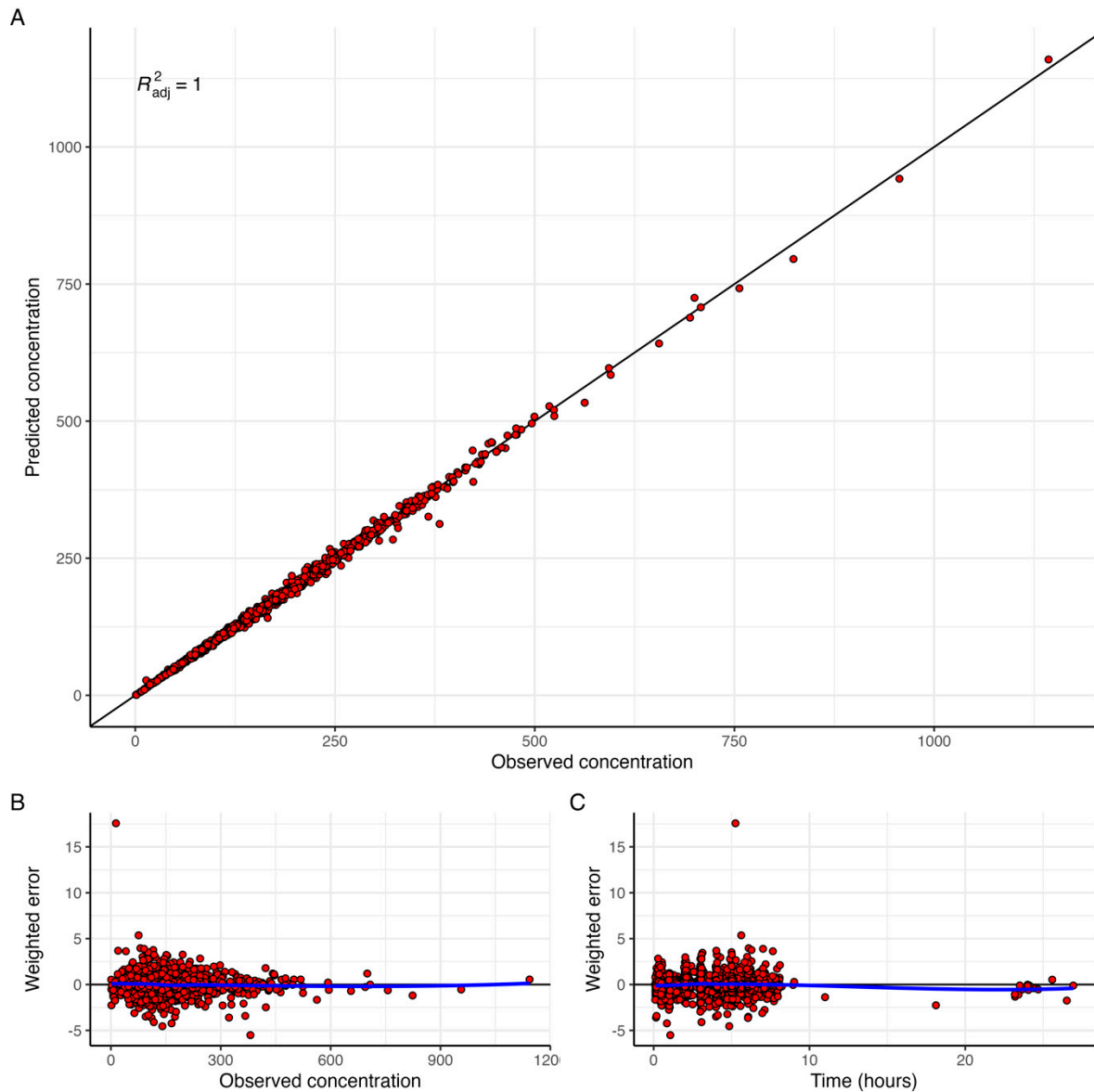
Supplementary Material for Paper III

SUPPLEMENTARY MATERIAL

Population pharmacokinetic model

A covariate free version of the original model [9] was developed, as the present method for simulation does not allow for covariates. The model achieved a mean prediction error -0.28 mg/mL and a relative root mean squared error of 3.7%.

Figure S1. Population pharmacokinetic model performance plots for the covariate-free model, including A) observed-predicted plot, B) weighted error across observed concentrations, and C) weighted error across sample time. Solid black lines represent the unity line, and the solid blue lines in B) and C) indicate the loess line.

Supplementary Table 1. Population pharmacokinetic performance metrics for the covariate-free model.

Metric	Value
Mean prediction error	-0.28
Mean weighted prediction error	0.03
Mean squared prediction error	30.67
Root-mean squared error (RMSE)	5.54
% RMSE	3.66
Mean weighted squared prediction error	1.49
Bias-adjusted mean squared prediction error	30.59
Bias-adjusted mean weighted squared prediction error	1.49

126

Supplementary Code S1

Implementation of the population pharmacokinetic model in mrgsolve for R.

```
$PROB

Population pharmacokinetic model of iohexol

$SET

delta = 0.1

end = 24

$PLUGIN Rcpp mrgx

$PARAM @annotated

TVCL : 2.89 : Typical value of clearance

TVV1 : 10.36 : Volume of central compartment

TVV2 : 9.2 : Volume of peripheral compartment

TVQ : 10.65 : Inter-compartment bloodflow

$MAIN

double WT = TVWT;

double CL = TVCL;

double V1 = TVV1;

double V2 = TVV2;

double Q = TVQ;

double KCP = Q / V1;

double KPC = Q / V2;

$PKMODEL

ncmt=2

depot = FALSE

$CMT @annotated

CENT : Central compartment

PERI : Peripheral compartment

$TABLE

capture CP = CENT/V1;

capture CLi = CL;

$SIGMA @annotated

ADD : 0 : Additive residual

PROP: 0 : Proportional residual error
```